1996

The role of magnesium in concrete deterioration

Guoliang Gan
Iowa State University

INFORMATION TO USERS

This manuscript has been reproduced from the microfilm master. UMI films the text directly from the original or copy submitted. Thus, some thesis and dissertation copies are in typewriter face, while others may be from any type of computer printer.

The quality of this reproduction is dependent upon the quality of the copy submitted. Broken or indistinct print, colored or poor quality illustrations and photographs, print bleedthrough, substandard margins, and improper alignment can adversely affect reproduction.

In the unlikely event that the author did not send UMI a complete manuscript and there are missing pages, these will be noted. Also, if unauthorized copyright material had to be removed, a note will indicate the deletion.

Oversize materials (e.g., maps, drawings, charts) are reproduced by sectioning the original, beginning at the upper left-hand corner and continuing from left to right in equal sections with small overlaps. Each original is also photographed in one exposure and is included in reduced form at the back of the book.

Photographs included in the original manuscript have been reproduced xerographically in this copy. Higher quality 6" x 9" black and white photographic prints are available for any photographs or illustrations appearing in this copy for an additional charge. Contact UMI directly to order.

UMI

A Bell & Howell Information Company
300 North Zeeb Road, Ann Arbor MI 48106-1346 USA
313/761-4700 800/521-0600

The role of magnesium in concrete deterioration

by

Guoliang Gan

A Dissertation Submitted to the

Graduate Faculty in Partial Fulfillment of the

Requirements for the Degree of

DOCTOR OF PHILOSOPHY

Department: Geological and Atmospheric Sciences
Major: Geology

Approved:

Signature was redacted for privacy.

In Charge of Major Work

Signature was redacted for privacy.

In Charge of Major Work

Signature was redacted for privacy.

For the Major Department

Signature was redacted for privacy.

For the Graduate College

Members of the Committee:

Signature was redacted for privacy.

Signature was redacted for privacy.

Signature was redacted for privacy.

Iowa State University
Ames, Iowa

1996

TABLE OF CONTENTS

NOMENCLATURE

In this dissertation, the term concrete refers to the mixture of Portland cement paste, coarse aggregate and fine aggregate; Paste or cement paste will be used to indicate the Portland cement hydration product, as distinguished from the fine and coarse aggregates which occur within the paste; Aggregate, coarse aggregate or dolomite aggregate will be used for the coarse dolomite aggregate used in the concretes; Interface refers to the coarse dolomite aggregate - cement paste interface.

In appendix A (photographs) and B (electron microprobe traverses and SEM-EDAX element maps), the following abbreviations are used:

ce	=	cement;
dol	=	dolomite aggregate;
A	=	dolomite aggregate interior;
B	=	dark dolomite reaction rim;
C	=	thin light-colored dolomite reaction rim;
D	=	light-colored cement reaction rim;
E	=	cement paste interior;
No	=	no experimental treatment;
MgWD	=	freeze/thaw cycling with 3M $MgCl_2$ solution, 60°C immersion and 90°C drying;
CaWD	=	freeze/thaw cycling with 3M $CaCl_2$ solution, 60°C immersion and 90°C drying;
NaWD	=	freeze/thaw cycling with 3M NaCl solution, 60°C immersion and 90°C drying;
H_2OWD	=	freeze/thaw treatment with distilled water, 60°C immersion and 90°C drying ;
MgFT	=	freeze/thaw, with freezing at -70°C in 3M $MgCl_2$ solution, thawing at 25°C in air, and immersion in 3M $MgCl_2$ solution;
CaFT	=	freeze/thaw, with freezing at -70°C in 3M $CaCl_2$ solution, thawing at 25°C in air, and immersion in 3M $CaCl_2$ solution;
NaFT	=	freeze/thaw, with freezing at -70°C in 3M NaCl solution, thawing at 25°C in air, and immersion in 3M NaCl solution;

In experimentally treated concretes, zones with the subscript 'e' refers to the same zones after experimental treatments, except for the $CaCl_2$-solution-treated concretes in which zones Be and Ce appear to be new dark dolomite reaction rim and new light-colored dolomite reaction rim, respectively.

Ae = dolomite aggregate after experiments;

Be = dark dolomite rim after experiments;

Ce = thin light-colored dolomite rim after experiments;

De = light-colored cement rim after experiments;

Ee = cement paste interior after experiments.

GENERAL INTRODUCTION

Deterioration of Iowa Concretes

Premature failures of concrete in highways are due predominantly to deterioration of joints and cracks. This deterioration is generally referred to as D-cracking, which was defined as "cracking in a slab surface in a pattern that appears first in an orientation parallel to transverse and longitudinal joints and cracks, continues around corners, and may progress into the central area of the slab" by Girard et al. (1982), and as "a form of PCC deterioration associated primarily with the use of coarse aggregates in the concrete that disintegrate when they become saturated and are subjected to repetitive cycles of freezing and thawing" by Schwartz (1987). This type of PCC pavement deterioration was first recognized on Iowa's primary road system in the late 1930s. Since 1960, extensive research into the mechanism of D-cracking, and methods of preventing and reducing D-cracking, has been conducted. Marks and Dubberke's (1982) research revealed that most D-cracking in Iowa is a distress that results predominantly from freeze/thaw failure in the coarse aggregate. Based on this finding, Iowa began using ASTM C666 Method B, "Freezing in Air -- Thawing in Water" to evaluate the durability of concrete. The basic tests currently used in Iowa to evaluate the quality of coarse aggregate for concrete, are abrasion by AASHTO T96 and a 16-cycle water-alcohol freeze/thaw test (Marks & Dubberke, 1982). These tests effectively exclude argillaceous (shales) materials and have been a part of the standard specifications for 40 years (Dubberke & Marks, 1987a).

Since 1978, research at the Iowa DOT has focused on the pore system of limestones used as coarse aggregate in PCC concrete and its relationship to freeze/thaw failure (Marks & Dubberke, 1982; Dubberke, 1983). The results of these studies showed that most nondurable aggregate exhibit a predominance of pore sizes in the 0.04-0.2 μm range, and aggregates that do not exhibit a predominance of these pore sizes are generally not prone to freeze/thaw deterioration. Pitt et al.'s (1989) research revealed similar results -- concretes exhibiting the best performance tend to have the fewest pores in the size range of 0.05 - 0.5 μm. In 1978, the Iowa Pore Index Test was adapted as a standard test (Marks & Dubberke, 1982). The Iowa Pore Index Test is a very simple test utilizing a modified pressure meter as a test apparatus. A known volume of oven-dried coarse aggregate is immersed in water in the base of the pressure meter. The volume of water injected into the aggregate under a constant 35 psi pressure during the period between 1 and 15 minutes after the application of this pressure is referred as the pore index. The available test results show that limestones

with pore indexes of ≥ 27 ml are susceptible to freeze/thaw D-cracking deterioration (Marks & Dubberke, 1982).

Although these tests have been relatively effective in yielding durable PCC, exceptions continue to occur and result in rapid deterioration of recently constructed pavements. This suggests that there should be other factors that contribute to the rapid deterioration of highways.

Aggregate - Paste Reaction as a Potential Cause of Concrete Deterioration

One potential factor is the chemical reactions between the cement paste and aggregate particles, which is called "alkali - aggregate reaction". Three types of alkali - aggregate reaction have been recognized: alkali - carbonate, alkali - silica, and alkali - silicate reactions (Gillott, 1975; Poole, 1992; Rogers, 1993). Among them, the alkali - carbonate reaction is of the most concern in Iowa, because most of the aggregate particles used in Iowa highway construction are carbonate rocks. Reactions between clay-rich carbonate aggregate (in Iowa) and cement paste have been reported to result in reaction rims with increased silica concentrations at the outer margins of the aggregate (Bisque & Lemish, 1958). Concretes containing certain types of dolomite aggregate have undergone reactions that result in dolomite aggregate rims with elevated calcium and reduced magnesium (Poole & Sotiropoulos, 1978, 1980; Poole, 1981).

The Role of Magnesium, Calcium and Sodium in Concrete Deterioration

Another potential factor is the deicers applied to reduced hazards of winter snow and ice. Studies show that sodium and calcium chloride deicers produce corrosion of aggregate (Dubberke & Marks, 1985) and concrete (Boies & Bortz, 1965; Neville, 1969; Sayward, 1984), but two contradictory conclusions have been proposed for the role of magnesium in concrete deterioration. While Neville's (1969) and Gillott's (1978) data indicate corrosive effects of $MgSO_4$ solution on concrete and aggregate, Pitt et al.'s (1989) data show that the addition of magnesium chloride into sodium chloride solution appears to enhance the durability of certain types of concrete.

OBJECTIVES OF RESEARCH

The main objective of the current research is to investigate the role of magnesium, which may be introduced into the paste, either from dedolomitization of coarse dolomite aggregate, or from surface-applied magnesium deicers, in the deterioration of Iowa highway concrete. The second objective is to investigate the effects of deicer salt applications on Iowa highway concretes to determine if magnesium deicers might be less damaging than rock salt, NaCl.

These objectives were accomplished by:

(1) Determining the chemical changes that have occurred during deterioration of selected Iowa highway concretes which contain coarse dolomite aggregate from different quarries and geological formations, and relating these changes to the degree of concrete deterioration.

(2) Comparing the chemical changes and characteristics of durable highway concretes having service lives > 40 years to those of non-durable concretes which deteriorate significantly after < 16 years. Both durable and non-durable types contain coarse aggregates which are primarily dolomite.

(3) Conducting laboratory experiments to investigate the chemical reactions between magnesium chloride and concrete, and the effects of these reactions on the deterioration of Iowa concrete which contain coarse dolomite aggregate.

Corresponding to the two major objectives, this dissertation is divided into two parts: the chemical characteristics of Iowa highway concretes containing coarse dolomite aggregates, and experimental study of deterioration of Iowa highway concretes.

PART I.

THE CHEMICAL CHARACTERISTICS

OF IOWA HIGHWAY CONCRETES CONTAINING

COARSE DOLOMITE AGGREGATE

RESEARCH PROCEDURES

Collection of Highway Concretes

Four-inch diameter cores of Iowa highway concrete with different dolomite aggregate sources, service records, and quarry locations were obtained from Iowa highways 20, 29, 52, 63, 151 and 218 by personnel of Iowa Department of Transportation (Table 1, Figs.A1a-f). The coarse aggregates were derived from the Ames gravel pit, and the Smith, Paralta, Garrison, Sundheim, and Mar-Jo Hills quarries. These concretes show a wide variety of service records which, at least partly, are a result of the different coarse aggregate sources.

General Procedures and Instrumentation

The concrete cores were first cut longitudinally, and the cut surface was visually inspected and photographed (Figs.A1a-f). One-half of the core was then cut into small rectangular blocks, approximately 0.5" x 0.5" x 1". Polished thin-sections were made from these blocks and examined by transmitted light utilizing standard polarizing microscope technique, but the great variety of aggregate particles precluded a detailed mineralogical analysis of coarse aggregates in the samples. Detailed studies emphasized the chemistry of the aggregate - paste interface to determine if compositional variations occur in both dolomite aggregate and cement paste at this interface, because paste-initiated reactions with dolomite aggregate should commence at that location. Most compositions were obtained with an electron microprobe and a scanning electron microscope (SEM) with energy dispersive X-ray (EDAX) capability. X-ray diffraction (XRD) methods were also used to supplement electron microprobe and SEM/EDAX data.

Electron probe microanalysis for Ca, Mg, Si, K, Na, Al and Fe, each reported as oxides, were performed using an automated ARL-SEMQ electron microprobe housed in the Department of Geological and Atmospheric Sciences at Iowa State University. This instrument has wavelength and energy dispersive spectrometers, as well as secondary and backscattered imaging capabilities. Operating conditions included an accelerating voltage of 20 kV and a sample current of 20 mA on a Faraday cup. On-line ZAF corrections employed the PRSUPR program utilizing the method of Donovan et al. (1992). When running profiles across the dolomite aggregate - cement paste interface, relatively wide, 10 - 25 μm, steps were first used.

Table 1. Concrete core locations, service records, and aggregate sources

Sample Number	Location of Core	Aggregate Source	Service Record
1	US 63, just north of Buckingham	Smith quarry (Basal Coralville Member, Cedar Valley Formation, Devonian)	12 years
2	US 151, near intersection with IA 13, NE of Cedar Rapids	Paralta quarry (Otis Member, Wapsipinicon Formation, Devonian)	8 years
3	US 218, near intersection with IA 8, east of Vinton	Garrison quarry (Solon Member, Cedar Valley Formation, Devonian)	15 years
4	US 20, west of Dubuque	Sundheim quarry (Hopkinton Formation, Silurian)	> 40 years
5	E 29, 1/2 mile east of US 65	Ames gravel pit (Skunk River gravels, recent)	8 years
6	E 29 at junction with US 65	Ames gravel pit (Skunk River gravels, recent)	8 years
7	US 52, south of Dubuque	Mar-Jo Hills quarry (Stewartville Member, Galena Formation, Ordovician)	> 40 years

The distance between analysis points was later reduced to 1 - 5 μm in order to minimize the possibility of missing important mineral matter by using step increments that were too large. Over 20,000 data points were obtained by electron microprobe techniques. Most of these data are located in an appendix of Cody et al. (1994). When plotting the traverse using the electron microprobe data, a three-point-moving-average method was used to reduce the random variability in the profile.

Most of the SEM/EDAX studies were conducted using a Hitachi S-2460N instrument, a reduced-vacuum scanning electron microscope located in the Department of Civil Engineering at Iowa State University. An accelerating voltage of 15 kV was used. This instrument has a great advantage compared to conventional SEM in that the reduced vacuum and lack of sample coating reduced the possibility of sample dehydration due to high vacuum. High magnification EDAX area maps were performed for Si, Ca, Mg, Al, O, K, Na, Fe, S, and Cl. A few samples were examined with the Department of Botany Jeol JSM-

35 scanning electron microscope. X-ray diffraction studies were performed with a Philips XRG-3100 power diffractometer (30 kV, 20 mA) in the Department of Geological and Atmospheric Sciences, and a Rigaku D/max-γB diffractometer (45 kV, 50 mA) in Yichang Institute of Geology and Mineral Resources, Chinese Academy of Geological Sciences, China.

GENERAL CHARACTERISTICS OF IOWA HIGHWAY CONCRETES

For the purposes of this study, the seven highway concrete cores are divided into two groups based on their service records. The first group consists of durable concretes which contain coarse aggregate from the Sundheim and Mar-Jo Hills quarries and have service records of > 40 years, and the second group has service records of < 16 years and comprises of non-durable concretes containing coarse aggregate from the Smith, Paralta, and Garrison quarries, and from the Ames gravel pit. Aggregate sources included rocks of Ordovician (Mar-Jo Hills quarry), Silurian (Sundheim quarry), Devonian (Smith, Paralta, and Garrison quarry), and Recent (Ames gravel pit) ages.

With the exception of the Ames gravel, most of the coarse aggregate is dolomite with minor amounts of limestone particles present in several of the concretes. The Ames gravel consists of shale, granite, dolomite and limestone particles reflecting diverse source rocks. After an initial study, the Ames quarry aggregate was eliminated from further consideration because it was not possible to determine whether visible color zoning of the aggregate particle formed before or after deposition of the gravel, or as a result of chemical reactions with the paste (Fig.A1d).

Crystallinity and Crystal Size of the Dolomite Aggregates

Both petrographic and SEM studies revealed significant differences in the nature of the coarse dolomite aggregate used in durable and non-durable concretes. The marked differences in crystal size and porosity between dolomite in durable and non-durable concretes are shown in Figures A2a-f. In non-durable concrete, > 90 % of aggregate particles consist of fine-grained dolomite, with abundant void spaces between poorly-formed dolomite crystals, and dolomite crystals typically fall within the diameter of 5 -50 μm (Figs.A2a-b). Figure A2e clearly shows the abundance of small subhedral and euhedral dolomite crystals and void spaces, and the scarcity of tightly interlocking crystals. In durable concrete, by contrast, dolomite crystals are coarser, extremely well-crystallized and more tightly intergrown (Figs.A2c-d and A2f). Typically these large crystals are anhedral because of the interlocking fabric. Individual dolomite crystals commonly exhibit diameters between about 50 - 450 μm.

Chemical Composition of Dolomite Aggregates

Electron microprobe analysis indicated that dolomite aggregates in durable and non-durable concretes contain approximately 30 wt.% CaO and 20 wt.% MgO (Table 2), close to the theoretical composition of dolomite, 30.41 wt.% CaO and 21.86 wt.% MgO. Bulk analyses by the Iowa Department of Transportation (Table 3) show similar results. Their values were consistently higher in Al_2O_3, SiO_2 and K_2O. Very possibly, this is because their analyses are of whole rocks which include impurity minerals such as quartz and clay minerals, whereas the electron microprobe data are more selective and can usually avoid these impurities, although very tiny mineral inclusions may be, occasionally, encountered by the electron beam.

Because the SiO_2, Al_2O_3 and K_2O contents in both durable and non-durable concrete aggregate show strong positive correlation with each other, they indicate the presence of a mineral (or minerals) containing these elements in abundance. Clay minerals, and particularly K-rich illite, are the most probable minerals because of their common occurrence in Paleozoic carbonate rocks.

Physical Characteristics of Cement Paste

Micro-cracks and larger fractures are consistently more common in the paste of non-durable concretes than in the durable concretes (Figs.A2a-d). Often the fractures are parallel to aggregate - paste boundaries, however, many fractures and micro-cracks are also randomly oriented (Figs.A2a-b). Although less common than in the non-durable concretes, micro-cracks also occur in durable concretes, as shown in Figures A2c-d. Cement paste shows some major textural differences between durable and non-durable concretes. Small concentric-laminated, spherical bodies are common in the durable concrete paste (Fig.A3a), whereas they are almost lacking in the non-durable pastes. In the non-durable concrete paste, abundant highly-fractured spherical to subspherical mineral grains without concentric structures occur (Fig.A3b).

Table 2. Chemical Composition of Dolomite Aggregate (Electron Microprobe Data)

Aggregate source	No. Analyses		FeO	K2O	CaO	SiO2	Al2O3	MgO	SrO	BaO	MnO	Na2O	CO2	TOTAL
		Min	0.24	0.10	25.12	0.11	0.04	16.93	0.07	0.10	0.13	0.09	46.80	99.49
Smith	168	Max	2.55	0.41	34.29	3.79	1.01	23.09	0.22	0.33	0.33	0.35	48.47	100.89
		Ave	0.48	0.15	31.04	0.66	0.21	19.57	0.13	0.23	0.20	0.17	47.37	100.21
		Stds	0.28	0.05	1.26	0.59	0.15	0.78	0.03	0.05	0.04	0.05	0.27	0.36
		Min	0.26	0.09	25.69	0.08	0.03	15.69	0.07	0.12	0.14	0.10	46.54	99.02
Paralta	172	Max	3.17	0.24	35.56	2.94	1.57	20.92	0.20	0.44	0.80	0.25	48.25	100.86
		Ave	0.59	0.12	31.01	0.61	0.16	19.10	0.13	0.24	0.21	0.16	47.41	99.76
		Stds	0.45	0.03	1.52	0.60	0.23	1.01	0.03	0.05	0.07	0.03	0.31	0.49
		Min	0.09	0.00	27.90	0.00	0.00	17.56	0.00	0.00	0.00	0.00	45.86	99.00
Garrison	20	Max	2.35	0.20	35.12	2.77	0.67	21.21	0.00	0.00	0.26	0.13	47.53	100.92
		Ave	0.40	0.02	33.30	0.43	0.06	18.76	0.00	0.00	0.02	0.04	46.86	99.89
		Stds	0.48	0.05	1.59	0.73	0.15	0.86	0.00	0.00	0.06	0.04	0.38	0.57
		Min	0.00	0.00	29.97	0.00	0.00	19.32	0.00	0.00	0.00	0.00	45.74	99.58
Mar-Jo Hills	64	Max	0.64	0.18	32.23	2.87	0.56	21.35	0.00	0.03	0.07	0.10	47.86	100.77
		Ave	0.15	0.01	31.56	0.26	0.03	20.67	0.00	0.00	0.01	0.01	47.42	100.10
		Stds	0.10	0.04	0.37	0.55	0.09	0.26	0.00	0.00	0.01	0.02	0.35	0.36
		Min	0.23	0.09	27.16	0.07	0.03	18.17	0.07	0.11	0.11	0.09	47.20	99.07
Sundheim	218	Max	0.56	0.64	31.58	3.55	1.05	21.76	0.21	0.39	0.26	0.33	48.61	100.91
		Ave	0.32	0.13	30.20	0.38	0.12	20.37	0.13	0.24	0.18	0.14	47.56	99.76
		Stds	0.05	0.06	0.61	0.45	0.12	0.53	0.02	0.05	0.02	0.03	0.16	0.41

Table 3. Chemical composition of dolomite aggregate

(Iowa DOT chemical analysis data, average)

Aggregate Source	No. Analyses	FeO**	K2O	CaO	SiO2	Al2O3	MgO	SrO	P2O5	MnO	S	CO2	TiO2	TOTAL
Sundheim	3	0.15	0.20	30.41	2.56	0.49	20.11	0.01	0.01	0.02	0.03	45.82	0.03	99.84
Mar-Jo Hills	13	0.33	0.28	30.75	2.73	0.41	19.48	0.01	0.09	0.05	0.04	45.40	0.00	99.57
Smith	5	0.34	0.14	32.72	1.74	0.40	18.24	0.00	0.02	0.00	0.35	45.59	0.02	99.56
Paralta	8	0.23	0.06	29.47	0.59	0.11	22.01	0.01	0.01	0.03	0.04	47.15	0.01	99.72
Garrison	9	0.62	0.13	32.13	1.57	0.36	18.38	0.01	0.01	0.03	0.66	45.28	0.01	99.19

** FeO is converted from Fe_2O_3.

REACTION RIM DEVELOPMENT IN NON-DURABLE CONCRETES

Physical Characteristics of Reaction Rims

In non-durable concretes, the concretes containing coarse dolomite aggregate from Smith, Paralta, and Garrison quarries, both the coarse aggregate particles and the cement paste adjacent to the aggregate particles often exhibit discolored rims along the interface. Five zones can be distinguished: (1) unaltered dolomite aggregate interior (zone A), (2) and (3) two reaction rims along the dolomite aggregate margins (zone B and C), (4) a reaction rim in the cement paste adjacent to a dolomite aggregate particle (zone D), and (5) unaltered Portland cement paste (zone E). The boundaries between different zones in both dolomite aggregate and cement paste are generally gradational. Depending on rim development, zones B, C and D could be absent.

Zone B is a *dark dolomite rim* (Figs.A3c-f, A4a-f, and A5a-d). It is a relatively thick, typically 100 - 300 μm wide, dark-colored, dirty-appearing rim which occurs at or near the outer margin of the coarse aggregate particles. This rim is much darker and is more porous than the interior, presumably unaltered, dolomite (Figs.A3c-f and A4a-b). It seems to contain smaller and fewer dolomite crystals than the dolomite interior (Figs. A4a-b), possibly suggesting that some dolomite crystals or some part of the dolomite crystals have been dissolved during rim development. In concretes where this rim is directly in contact with the paste, the inner part of this rim is more porous than the outer (i.e. outermost) part, and micro-fractures, parallel to the aggregate - paste interface, may occur between the more porous inner part and the less porous outer part (Figs. A4e-f).

Zone C is a *light-colored dolomite rim* (Figs.A3c-f and A4a-b). It is very narrow, typically 20 - 50 μm wide, unstained and clean-appearing. It is located outside the dark dolomite rim, and is in contact with the cement paste. This rim is much lighter in color, less porous, and exhibits fewer and smaller inter-crystalline voids than the unaltered dolomite, zone A, and the dark dolomite rim, zone B.

Zone D is a *light-colored paste rim* (Figs.A3c-f, A4a-f and A5a-d). It occurs in the Portland cement paste adjacent to the outer margin of the dolomite aggregate. It is relatively thick, usually 50 - 400 μm wide, and typically much lighter in color than the darker, dirtier-appearing, presumably unaltered, paste which occurs farther away from the dolomite aggregate. Although small micro-cracks may occasionally occur within this light-colored paste rim, most fractures occur in zone E.

Zones B and C are best observed with a petrographic microscope in plane-polarized light, and are difficult to distinguish when viewed between cross-polarizer. In SEM images, these zones can be distinguished from each other, and from the dolomite interior by differences in porosity. The light-colored paste rim, zone D, can be best seen when observed between crossed polarizer, and with SEM images.

Aggregate - Paste Interface Patterns

Within the same concrete core, each of the rims may vary in thickness, and one or more rims may be missing depending on the specified aggregate particle. Basically, three types of interface patterns can be distinguished:

Type I interface: Although less common than Type II interface, this type of interface shows the best-developed pattern in which both the dark and light dolomite rims, and the light paste rim occur (Fig.A3c-d and A4a-b). As shown in Figures A3e-f, the dark dolomite rim is more porous, and the light-colored dolomite rim less porous compared to the dolomite interior.

Type II interface: This is the most common type of interface. The light-colored dolomite rim, zone C, is absent, and the dark dolomite rim, zone B, is in contact with the light-colored paste rim, zone D (Figs.A4c-f and A5a-d). As shown in Figures A4e-f, the outer part of the dark dolomite rim is less porous relative to the inner part.

Type III interface: This is the least common type of interface. It exhibits no reaction rims in either dolomite aggregate or cement paste (Figs.A5e-f).

Chemical Characteristics of the Aggregate - Paste Interface

An electron microprobe traverse across a non-durable concrete containing Smith quarry aggregate illustrates a chemical profile across the five zones of the type I interface (Fig.B1). In this traverse, CaO remains essentially constant, with minor irregularly spaced peaks and valleys, throughout zones A and B. MgO shows an antithetic relationship with CaO (Fig.B1a). Variations in CaO and MgO contents typically occur only in the light-colored dolomite rim where there is a distinct increase in CaO and a corresponding decrease in MgO compared to zone A and B. The common association between SiO_2, Al_2O_3 and K_2O at irregular intervals across dolomite aggregate (including interior and rims) shows the presence of small inclusions of potassium alumino-silicate phases, probably illite clay (Figs.B1b-c).

Within the cement paste, CaO, SiO_2, and MgO show great variability. The light-colored paste rim, zone D, is characterized by an enrichment in CaO and a depletion in SiO_2 and MgO (Fig.B1a). MgO content typically decreases across the aggregate - paste interface, and is depleted in the paste rim. There seems to be no clearly defined difference in MgO between the light colored paste rim (zone D) and the presumably unaltered cement paste (zone E) which is located farther from the dolomite - paste interface. Within zone D and zone E, MgO may increase locally, and is due, in part, to the formation of brucite, $Mg(OH)_2$. It should be stressed here that the compositional traverse into the cement paste is markedly variable and highlights the anticipated complex mineralogy. Note that marked variations in FeO, Al_2O_3, Na_2O, and K_2O occur across the boundary of zones D and E. While the specific minerals were not identified, there are strong correlations between K_2O and K_2O, as well as between Al_2O_3 and FeO (Figs.B1b-c).

Figure B2 shows EDAX elemental maps of the type I interface in non-durable Smith quarry concrete. The dark dolomite rim shows relatively uniform element distribution, and contains a few small pyrite and illite clay inclusions, as shown by the Fe- and S-rich, and the Si-, Al- and K-rich dots, respectively. Zones C and D exhibit Ca-enrichment. The Mg- and O-rich dots in dolomite rims and cement paste probably indicate the presence of brucite.

Similar overall compositional pattern and elemental correlations are found for most compositional profiles even in the absence of some rim(s). For the most common type of interface, in which the light-colored dolomite rim, zone C, is absent, electron microprobe data reveal a significant increase in CaO with a corresponding decrease in MgO within the dark dolomite rim compared to the unaltered interior dolomite (Fig.B4a). The light-colored paste rim is enriched in CaO and depleted in SiO_2, MgO. Adjacent to the dark dolomite rim, zone B, the light paste rim becomes calcitic (CaO > 50 wt.%) (Fig.B4a). Zone E is rich in CaO and SiO_2, and depleted in other elements (Figs.B4a-c).

From EDAX elemental maps, it is evident that voids and micro-cracks in dark dolomite rim are filled by some Ca- and O-rich, as well as Mg- and O-rich materials, probably calcite and brucite (Fig.B3). The light-colored paste rim is rich in Ca, and sometime is rich in K (Fig.B5).

REACTION RIM DEVELOPMENT IN DURABLE CONCRETES

Durable concretes typically show considerable differences in reaction rim development and abundance when compared to non-durable concretes. The most common type of interface exhibits no apparent reaction rim in either dolomite aggregate or cement paste (Figs.A6a-f). Electron microprobe traverses indicate that CaO and MgO typically are more uniform and exhibit smaller, localized compositional irregularities than is typical in non-durable concretes (Fig.B6; cf. Figs.B1 and B3). Within dolomite aggregate, the concentrations of minor elements, FeO and Na_2O, show almost no variation along the traverse, and the SiO_2, Al_2O_3 and K_2O concentrations are uniformly low unless a quartz or an illite clay grain is encountered. The paste itself is chemically very similar to that of the unaltered paste in non-durable concretes (Fig.B6; cf. Figs. B1 and B3). Minor amounts of brucite may occur in the cement paste (Fig.B7).

The least common type of interface exhibits discolored reaction rims in both dolomite aggregate and cement paste. The dolomite reaction rim could be either dark dolomite rim which is dirty-appearing and wider and is associated wider cement paste rim (Figs.A7a-b), or light-colored dolomite rim which is clean-appearing and narrower and is associated with narrower light paste rim (Figs.A7c-d). The dark dolomite rim and the light-colored dolomite rim typically do not occur together.

For dolomite aggregates with reaction rim development, compositions from electron microprobe traverses are quite uniform throughout the dolomite interior. The dark dolomite rim normally shows much more variation in CaO, MgO, SiO_2, FeO, Al_2O_3, K_2O and Na_2O than the dolomite interior. Irregular increases in CaO may be associated with corresponding decreases in MgO. The light-colored dolomite rim shows a pronounced increase in CaO with a decrease in MgO (Fig.B8a). As in non-durable concretes, the unaltered paste is rich in CaO and SiO_2 and depleted in other elements, and the light-colored paste rim is very rich in CaO, and depleted in other elements (Figs.B8a-c). Occasionally, there may be a slight enrichment in K_2O and Na_2O in the light paste rim.

DISCUSSION

Reactive vs. Non-reactive Dolomite Aggregates

The fact that most durable Iowa highway concretes exhibit no reaction rim at the aggregate - paste interface suggest that the dolomite aggregates in durable concretes are essentially non-reactive. By contrast, non-durable Iowa highway concretes show abundant and well-developed dolomite and paste reaction rims, and are likely reactive. As mentioned earlier, coarse dolomite aggregates used in durable and non-durable concretes show significant differences in the crystal size and crystallinity: Dolomite crystals typically fall within the diameter of 5 - 50 μm in non-durable concretes and 50 - 450 μm in durable concretes. As shown in Figures A7e-f and B9-B10, clay particles in durable concretes are also coarser than those in non-durable concretes. It is significant to note that: (1) Gillott & Swenson's (1969) experimental data indicated the aggregate - paste reaction became negligibly slow when dolomite crystals exceeded about 75 μm in size; (2) As shown by Deng et al.'s (1994) data, the reaction rate of dolomite and KOH solution increased considerably when the dolomite grain size decreased from 40 - 90 μm to < 40 μm; (3) Among the dolomitic rocks selected by Deng et al. (1993) and Milanesi & Batic (1994) to test the alkali-reactivity, the dolomitic rocks with well-developed coarse dolomite crystals and grain sizes of > 500 μm and 100 - 200 μm, respectively, are non-reactive, whereas the dolomitic rocks with grain sizes of 5 - 50 μm and 10 - 30 μm, respectively, are reactive; (4) Mark & Dubberke's (1982) scanning electron microscopy study showed that "coarse aggregate associated with D-cracking are normally fine-grained whereas durable aggregate is either coarse grained or extremely fine-grained"; and (5) According to Hudec (1989), finer-grained carbonate rocks showed faster absorption rate and higher penetration of water and salt solutions. Therefore, it seems that 50 - 70 μm crystal sizes can be used as a simple dolomite-grain-size criterion to distinguish reactive and non-reactive dolomite aggregates. Fine-grained dolomite aggregates, due to their great surface area, poor crystallinity, and rapid water and solution intake from alkaline cement paste, would show greater potential reactivity than coarse-grained dolomite aggregates.

Rim Development Sequence

Based on the study on Iowa highway concretes containing carbonate (limestone and calcitic dolomite) aggregates, Bisque (1959) and Lemish et al.(1958) identified a reaction rim sequence consisting

of two rims at aggregate - paste interface: a darker inner rim occurring within the aggregate and outlining its outer edge, and an outer rim of light gray material occurring in the cement paste surrounding the affected aggregates. The inner dark (aggregate) rim shows a concentration of opaque materials and interstitial silica or silicate materials, and the material in the outer light (cement-paste) rim was believed to be calcium hydroxide (it could be calcite instead of calcium hydroxide). Bisque & Lemish (1958) found that the inner dark reaction rim was silicified and selectively formed on aggregate containing clay. It contained a high percent of insoluble residue, a high magnesium content, and a higher concentration of silica. The inner rim material from affected concrete was marked by a decrease in magnesium content, a marked increase in insoluble residue (with 85-90 % SiO_2), and a slight increase in calcium content. Hydrochloric acid leaching of the distressed concretes left the inner rim zone standing high in relief. The outer rim of cement paste adjacent to the rimmed aggregate was more rapidly attacked by hydrochloric acid than the paste adjacent to the unrimmed aggregate particle or the paste beyond the outer rim. It was also found that the effective porosity of the aggregate rim zone was markedly decreased as compared to the unaffected aggregate, and aggregates which lack clay did not grow siliceous rims in the laboratory. Based on above observations and experimental results, Bisque, 1959 and Bisque & Lemish (1960a,b) postulated that the siliceous aggregate rim was possibly formed due to "tying together" of clay-size particles in the (amorphous) calcitic matrix by silicon ions.

Buck & Dolch (1966) considered that siliceous rims were formed by reactions between alkaline components in the cement paste and limestone, however, Hadley (1964a,b) argued that there was no apparent contribution of silica from cement paste in the rims described by Bisque & Lemish (1958) and Lemish et al.(1958), and that silica was derived from "argillaceous and siliceous materials" within the carbonate aggregate particle that subsequently reacted with brucite. Hadley identified reactive dolomitic limestones of appropriate composition from Indiana, Illinois, Minnesota, Iowa, Missouri, and Wisconsin, U.S.A., and Ontario, Canada.

Poole (1981) and Poole & Sotiropoulos (1978, 1980) observed a sequence of three reaction rim zones at dolomite aggregate - cement paste interface: zone A, a dark colored zone in the aggregate extending inward from the margin of the aggregate with an irregular and gradational inner margin; zone B, a light colored zone in the cement paste immediately adjacent to the aggregate which is only present around some of the grains; and zone C, a dark colored zone in the cement paste with a gradational margin beyond zone B. The total width of these reaction rims increased slightly with time, and zone C diminished with time as the width of zone B increased. Their electron microprobe analyses data showed that zone A

was Mg-poor, and Ca- and Si-rich compared with the unaltered interior part of dolomite aggregate. The overall composition of zone B was Si-poor, Ca-rich and, possibly Mg-rich, when compared to the cement paste beyond zone C. Zone C sometimes had a higher SiO_2 content.

The present research has revealed a similar, but somewhat different, sequence of reaction rims associated with coarse dolomite aggregate in non-durable Iowa highway concretes. The best-developed interface pattern is: unaltered dolomite aggregate interior (zone A) → dark-colored dolomite reaction rim (zone B) → light-colored dolomite reaction rim (zone C) → light-colored paste reaction rim (zone D) → dark, presumably unaltered, cement paste (zone E). In comparing this rim sequence with those described by Bisque (1959), Bisque & Lemish (1958, 1960), Lemish et al.(1958), Poole (1981), and Poole & Sotiropoulos (1978, 1980), it is very likely that the dark dolomite rim corresponds to the darker inner aggregate rim observed by Lemish et al.(1958) and to zone A in Poole's (1981) observations. The light-colored paste reaction rim seems to correspond to the light outer paste rim in Lemish et al.'s (1958) rim sequence, and to zone B of Poole's (1981) rim sequence. Zone C described by Poole (1981) is missing from the concretes studied in the present research. A reasonable explanation for the absence of this zone is that it has diminished with time, because Poole (1981) found that this zone slowly disappeared over time, and the Iowa concretes we studied have been in service for many years. The light-colored dolomite reaction rim that was observed in the present research was not described by either Lemish et al.(1958) or Poole (1981). A possible reason for this is that this light-colored Ca-rich, Mg-poor dolomite rim represents the end product of a reaction between dolomite aggregate and the cement paste.

Mechanism of Dedolomitization-Induced Concrete Deterioration

Alkali - carbonate reaction and expansion

It is widely accepted that the cement - carbonate aggregate reaction, which represents the alkali - carbonate reaction, is essentially a dedolomitization process: the dolomite constituent of the (reactive) carbonate rock is attacked by the alkali derived from the cement, resulting in the formation of brucite, calcite and alkali carbonate (Carles-Gibergues et al., 1989; Deng & Tang, 1993; Deng et al., 1993, 1994; Gillott, 1964, 1978; Gillott & Swenson, 1969; Hadley, 1961, 1964a,b; Lemish & Moore, 1964; Sherwood & Newlon, 1964; Swenson & Gillott, 1964, 1967; Tang et al., 1986, 1989, 1991, 1994)

$$CaMg(CO_3)_2 + 2\,MOH \rightarrow CaCO_3 + Mg(OH)_2 + M_2CO_3 \qquad [1]$$

where M represents alkalies (K or Na). In concrete, the alkali carbonate produced in reaction [1] would react with the hydration products of portland cement, regenerating alkali. For example:

$$M_2CO_3 + Ca(OH)_2 - 2\,MOH + CaCO_3 \qquad [2]$$

In spite of a small volume decrease accompanying reaction [1], there seems little doubt that dedolomitization actually results in a volume increase. Two contradictory hypotheses have been proposed to explain the observed expansion associated with the alkali - carbonate reactivity: the indirect mechanism which assigns a trigger role to dedolomitization and invokes other factors as primary in producing the expansion (Gillott, 1964, 1978; Gillott & Swenson, 1969; Swenson & Gillott, 1964, 1967), and the direct mechanism which attributes excessive expansion to the attack of the alkali upon the dolomite (Deng & Tang, 1993; Deng et al., 1993; Hadley, 1961, 1964b; Sherwood & Newlon, 1964; Tang et al., 1986, 1989, 1991, 1994).

Because the sum of the volume of solid products in reaction [1] is less than that of the reactants, Gillott and his colleagues, also based on their experimental results, proposed an indirect mechanism in which the alkali - expansitivity of certain dolomitic rocks is due to the development of swelling pressure resulting from wetting of previous unwetted clay-sized minerals, and the wetting is facilitated by dedolomitization reaction which produces access channels for moisture (Gillott, 1964, 1978; Gillott & Swenson, 1969; Swenson & Gillott, 1964, 1967). This proposed mechanism involves two steps: (a) attack by cement alkalies on the dolomite (dedolomitization) which opens micro-cracks allowing water and solution to penetrate into the rock, and (b) moisture uptake by the dry clay with development of expansive forces due to surface hydration and build-up of hydrous double layers surrounding the clay minerals.

In contrast, other researchers considered the alkali - carbonate reaction as the direct cause of the associated expansion. Sherwood & Newlon (1964) suggested that complex hydrated double salts of large unit size caused the increase in solid volume. Hadley (1961) postulated a different cause. His measurements on a single crystal of dolomite during the dedolomitization process disclosed an expansion of 0.15 % after 100 days. In addition to the expansion of the individual dolomite crystals during dedolomitization, Hadley (1964b) postulated that expansion may also result from osmotic forces, because the alkali - carbonate solution at the reacting dolomite crystals may differ in concentration and nature from the solution in the pores, and the differences in flow tendencies of the two solutions through interstitial clay may lead to the build-up of a swelling pressure.

Tang and his colleagues proposed an alternative mechanism, which is opposite to the mechanism proposed by Gillott and his colleagues. This alternative mechanism hypothesized that the network of clay

disseminated throughout impure carbonate rocks furnishes channels, through which the H_2O, K^+, Na^+ and OH^- can migrate into the interior of the reactive rock, and the dedolomitization reaction can directly bring about expansion (Deng & Tang, 1993; Deng et al., 1993, 1994; Tang et al., 1986, 1989, 1991, 1994). Tang and his colleagues concurred that dedolomitization causes a reduction in solid volume, but they pointed out that the reaction products, calcite and brucite, were fine-grained and enclosed many voids. By including the void volume (porosity), their calculation revealed an increase in the overall volume of solid skeleton plus voids during dedolomitization.

Alkali - dolomite reaction as primary cause of Iowa concrete deterioration

In order to understand the possible deterioration mechanism of Iowa highway concretes, the following characteristics are summarized:

(1) Non-durable Iowa highway concretes exhibit much more abundant and better developed reaction rims than durable concretes at dolomite aggregate - cement paste interface. In agreement with Bisque & Lemish's (1958) observation, coarse limestone aggregate, which occurs in few concretes, do not exhibit reaction rims, indicating the reactions responsible for deterioration of highway concretes studied in this research are dolomite-specific. In addition, non-durable concretes are far more deteriorated and contain more cracks or micro-cracks than durable concretes.

(2) The most complete rim sequence includes an inner dark dolomite rim (zone B), an outer light-colored dolomite rim (zone C), and an light-colored cement paste rim (zone D). An increase in Ca and a concomitant decrease in Mg are observed near the edge of dolomite aggregate, either in the light-colored dolomite rim, or in the outer part of the dark dolomite rim when the light dolomite rim is absent.

(3) The light-colored paste rim is very rich in Ca, but poor in Si, Mg and alkali element. The overall composition of this paste rim is more calcitic in non-durable concretes than in durable concretes. In some non-durable concretes, the overall composition of this rim becomes calcitic.

(4) The light-colored dolomite rim, or the outer part of the dark dolomite rim when the light rim is missing, has a lower porosity than the dolomite aggregate interior. Some interstitial spaces have been filled with Ca- and O-rich materials (calcite) and Mg- and O-rich materials (brucite).

(5) Brucite occurs in the dark dolomite reaction rim, throughout the light dolomite rim and light paste rim, and into the dark cement paste. Its abundance is slightly higher in the dark cement paste than in the light paste rim.

(6) Alkalies, potassium and sodium, are often concentrated in the dark cement paste. Sometimes they are enriched in the light paste rim.

Because the only major and consistent differences between durable and non-durable concretes apparently are the coarse aggregates used in making the concretes, the primary cause of deterioration of Iowa highway concretes is almost certainly the reaction between coarse dolomite aggregate and cement paste, which results in rim development. It is essentially a dedolomitization reaction, as described in equation [1].

Reaction rims developed after pouring of the concrete as a result of chemical reactions between the calcium-rich, highly alkaline, cement paste, and the dolomite crystals occurring at or near the dolomite aggregate - paste interface. Dedolomitization of reactive dolomite aggregate has occurred abundantly in non-durable Iowa highway concretes, and to a minor extent in durable concretes, by reaction [1]. Dolomite in reactive dolomite aggregates reacts with alkali derived from the cement, with formation of calcite, brucite, and alkali carbonate. Clay minerals or other clay-size minerals in dolomite aggregate may provide channels for the migration of alkali- and OH^--bearing solution, promoting the reaction. Most of the neo-formed calcite is precipitated along the interface, forming the light-colored paste reaction rim. Some of the neo-formed calcite fills the interstitial space, near the edge of dolomite aggregate, between dolomite crystals, or within voids created by dissolution of dolomite crystals. It thereby reduces the porosity of the dolomite reaction rim. Magnesium ions released by dedolomitization diffuse outward into the cement paste, where they precipitate as brucite in the light paste rim and the dark paste, and inward into the interstitial spaces in dolomite aggregate, where they are deposited as brucite, along with neo-formed calcite. Alkali elements may accumulate in the light paste rim, probably representing regeneration of alkali according to equation [2]. The build-up of strains due to crystal growth at the interface may lead to the cracking, causing concrete deterioration.

The current research extends the work of Gillott & Swenson (1969) who concluded that alkali - carbonate reactions were very common in argillaceous dolomitic limestones or argillaceous calcitic dolomites, in which isolated dolomite rhombohedra are set in a fine-grained calcite and clay. Because the reactive rocks were mixtures of dolomite and calcite, the term alkali - carbonate rock reaction was appropriate. In contrast, the Iowa concrete aggregates studied in the present research are considerably different from those implicated by Gillott & Swenson (1969). The reactive coarse aggregates in non-durable Iowa concretes are composed almost entirely of dolomite without much calcite, and do not show

higher clay concentrations than non-reactive dolomite aggregates used in durable concretes. Therefore, *alkali - dolomite reaction* is a better term in the present investigation.

Magnesium and Concrete Deterioration

During dedolomitization, newly-released magnesium undoubtedly leads to brucite precipitation in the concrete paste and in dolomite reaction rims. Winkler & Singer (1972) concluded that growing gypsum and halite crystals may exert pressures in excess of 2000 atm., so that analogous pressures may be expected to develop from growth of brucite and calcite in concrete voids and interstitial spaces in dolomite reaction rims. The high pressures generated by this growth may lead to expansion and deterioration. In addition, there may be deleterious chemical reactions between magnesium and the paste. At this time, an understanding of effects of magnesium on concrete is especially pertinent because magnesium chloride and/or calcium magnesium acetate have been proposed as road deicers and substitutes for rock salt. The next section of this dissertation, Part II, will explore these effects utilizing an experimental approach.

PART II.

EXPERIMENTAL STUDY OF DETERIORATION

OF IOWA HIGHWAY CONCRETES

INTRODUCTION

The primary objective of the experiments was to evaluate the effects of magnesium-rich solutions on concrete deterioration under different physical and chemical conditions, and determine if magnesium contributes to highway concrete deterioration. The second objective was to evaluate the relative effects of the common deicer salts sodium chloride, calcium chloride, and magnesium chloride on concrete durability, to determine if magnesium deicers might be less damaging than sodium and calcium chlorides, and are acceptable long-term substitutes for rock salt, NaCl.

STARTING MATERIALS, AND EXPERIMENTAL METHODS

Starting Materials

The concrete cores No. 1-7, as listed in Table 1 in the previous section, were used for experiments. Each core was sliced in half longitudinally, and cut into small rectangular blocks about 0.5" * 0.5" * 1".

Distilled water (for control) and 0.75M and 3M $MgCl_2$, $CaCl_2$, and NaCl solutions were used to immerse concrete blocks in cleaned polymethypentene (PMP) containers. These chloride solutions were made with double-distilled water and ACS certified chemicals, $CaCl_2 \cdot 2H_2O$, $MgCl_2 \cdot 6H_2O$, and NaCl. To control the mold and bacteria growth in the solutions during the extended experiments, all the solutions contained 0.01 % sodium azide. A concrete block from each core was immersed in 100 ml of each solution.

Experimental Methods

Three sets of experiments were performed: wet/dry, freeze/thaw, and continuous soaking. Prior to wet/dry, freeze/thaw, and soaking treatment, concrete blocks were immersed in distilled water or chloride solutions at 60°C. Experiments were discontinued when some concrete samples showed obvious deterioration under specific conditions for each set of experiments.

Wet/Dry (WD) experiments

This set of experiments involved cycles alternating between total immersion in solutions and complete drying of the concrete blocks. Two different drying temperatures, 60°C and 90°C, were used. On the upper surfaces of Iowa highways, 60°C temperature might well develop during very hot, sunny summer days. A temperature of 90°C was used to determine if higher temperatures would enhance concrete deterioration.

Concrete blocks were immersed in solutions at 60°C for 132 hours, removed from the solutions, dried at 90°C or 60°C for 24 hours, air-cooled to 25°C, rinsed for 1 minute in distilled water to remove surface salts, returned to their immersion solutions at 25°C, and again stored at 60°C for 132 hours. Cycles

continued until some samples developed significant deterioration. Longer term experiments would have caused severe crumbling of the materials, and difficulty in making sections for analysis.

Freeze/Thaw (FT) experiments

Experiments involved cycles alternating between total immersion in solutions and freezing in air. Two different temperatures, 0°C and -70°C, were tested. The lower temperature (-70°C) was far colder than any Iowa winter temperature and used to insure freezing of all deicer solutions, whereas the higher freezing temperature (0°C) was used to more closely simulate winter highway temperatures at some depth within the concrete slab where concentrated salt solutions would not completely freeze.

Samples were removed from solutions after immersion at 60°C for 132 hours, air-cooled to 25°C, frozen for 24 hours at either 0°C or -70°C, air-warmed to 25°C, returned to the 25°C solutions, and stored at 60°C for 132 hours. Cycling was continued until concrete blocks developed some deterioration.

Continuous immersion experiments

For comparison, this set of experiments involved continuous immersion of concrete samples in solutions. Concrete blocks were constantly immersed in solutions at 60°C for 222 days.

End of experiment procedures

After experiments were terminated, the solution-treated samples were rinsed for 1 minute in distilled water, dried at room temperature, and visually inspected to determine patterns of deterioration. Representative samples were then photographed, thin-sections and polished sections were made and studied by petrographic microscopy, SEM, EDAX elemental mapping, and electron microprobe. It should be noted that photographs and electron microprobe traverses were obtained with cut and polished concrete blocks, so that the horizontal surfaces used for views and analyses were never directly in contact with salt solutions during experiments. Any observed features of concrete deterioration that are different from those in untreated concrete samples must have been developed due to the reaction between relatively porous and permeable concrete blocks and penetrating salt solutions.

EXPERIMENTAL RESULTS

General Observations

The experimental results are summarized in Table 4. General observations include:

(1) Essentially no deterioration was evident in concrete sample treated with distilled water, regardless of concrete source and experimental type (wet/dry, freeze/thaw, or continuous soaking) (Fig.A9a).

(2) Calcium or magnesium chloride solutions produced much more severe deterioration than sodium chloride, regardless of solution concentration and concrete source (durable vs. non-durable) (Figs.A8a-f).

Table 4 A summary of concrete experiments

Experiment Type	NaCl	$MgCl_2$	$CaCl_2$	H_2O
F/T, 3 M, -70°C/25°C/60°C, 9 cycles	NC	NC	NC	NC
W/D, 3 M, 60°C/90°C, 4 cycles	NC	Paste: brown color and decomposes Aggr.: NC	Paste: cracks at paste/aggr. interface Aggr.: NC	NC
W/D, 3 M, 60°C/60°C, 6 cycles	NC	Paste: brown color and severe decomposition Aggr.: NC	Paste: cracks at paste/ aggr. interface Aggr.: NC	NC
Soak only, 3 M, 60°C, 222 days	Paste: slight brown color Aggr.: NC	Paste: dark brown color and cracks at paste/aggr. interface Aggr.: NC	Paste: brown color and cracking or initial cracking Aggr.: NC	NC
W/D, 0.75 M, 60°C/60°C, 16 cycles	NC	Paste: brown rim in paste around aggr. Aggr.: cracking	Paste: decomposition at paste/aggr. interface, some cracks Aggr.: cracking	NC
F/T, 0.75 M, 0°C/25°C/60°C, 16 cycles	Paste: pale brown color Aggr.: NC	Paste: slightly brownish and slight crumbling Aggr.: NC	Paste: corners crumble, some cracks Aggr.: NC	NC

Aggr. = aggregate; NC = no change

(3) Concrete deterioration in magnesium or calcium chloride solutions, regardless of solution concentration and concrete source, was wet/dry condition > continuous soaking condition > freeze/thaw condition (Figs.A9b-f and A10a). Furthermore, wet/dry deterioration was more pronounced when samples were dried at 90°C than at 60°C (Table 4).

(4) Magnesium chloride solutions typically caused severe paste decomposition and dark brownish paste discoloration, whereas calcium chloride solutions produced deterioration which was characterized by crack development and brownish paste discoloration (Figs.A8a-f, A9b-f, and A10a). There was no distinct difference in deterioration of non-durable concretes and durable concretes.

(5) Regardless of concrete durability, $Ca(OH)_2$ in cement paste disappeared after $CaCl_2$, $MgCl_2$, and NaCl solution treatment.

Effects of Magnesium Chloride Solutions

Concrete deterioration was especially severe with magnesium chloride treatment (Figs. A8a-f). The most severe paste decomposition and dark brownish paste discoloration occurred during wet/dry cycling, with cement paste in both durable and non-durable concretes being equally affected (Figs.A9e-f and A10a). After solution treatment, the cement paste became very loose and porous, and some parts have been totally dissolved, leaving the coarse aggregate exposed (Figs. A8a-e).

In durable concrete, it seems that no "new" reaction rim has been formed in either dolomite aggregate or cement paste during magnesium chloride solution treatment (Figs.A12e-f). However, dolomite aggregates in treated concrete show a very uniform composition pattern (Fig.B18), and dolomite aggregates in both treated and untreated concretes exhibit almost identical XRD patterns, suggesting that dolomite aggregates underwent essentially no chemical change. Near the aggregate - paste interface, dolomite aggregate may develop minor cracking. These micro-cracks are filled with late-formed grey Mg-, O-rich (brucite) and dark-grey Mg-, Cl-rich materials (magnesium chloride or magnesium chloride hydrates), and sometimes a very thin film of white Ca-rich materials (calcite) exists along the crack wall (Figs.A13a and B19), implying calcite was precipitated before brucite and Mg-, Cl-rich phases.

However, as shown in Figs.A12e-f, A13a-b and B18, cement paste has undergone substantial chemical and physical changes during experimental treatment: (1) The treated cement paste became much richer in MgO (10-30 %) and poorer in CaO and SiO_2 (generally < 20 %) than the untreated paste (generally 25-45 % CaO, 15-35 % SiO_2, and 1-5 % MgO); (2) MgO and SiO_2 became strongly positively correlated

(refer to Figs.B18, B21 and B6 for comparison); (3) The "original" untreated cement paste has been dissolved away or replaced by Ca-, O-rich (calcite), Mg-, O-rich (brucite) and Mg-, Si-, Cl-bearing phases; (4) Some new phases have been precipitated, partially or completely filling cracks and voids, which were originally occupied by cement paste before experimental treatment. As shown in Figures A13a-b and B19-B20, these crack-filling materials exhibit zonation. A white calcite film precipitated immediately adjacent to the walls of the openings. Farther away from the crack walls, a later-stage intermediate layer of brucite, magnesium chloride or magnesium chloride hydrate, Mg-, O-, and Cl-rich minerals and alumina, precipitated on the calcite film, and finally was covered by the latest precipitates consisting of very fine-grained, poorly consolidated minerals containing Mg, Si, Cl, Fe, S and showing very complicated mineralogy. This zonation suggests that calcite began to precipitate before brucite and magnesium chlorides, magnesium chloride hydrates, alumina, and other products formed during the interaction between magnesium chloride solution and concrete.

Unlike in durable concretes, reaction rims in both dolomite aggregate and paste were observed in non-durable concretes after experimental treatment (Figs.A13c-f and A14a-b). It seems that these reaction rims represent the "original" rims, because the aggregate - paste interface pattern and the composition pattern of dolomite aggregate (electron microprobe traverses) look identical to those in untreated concrete (cf. Figs.A13c-f, A14a-b and A3c-f, A4a-b for comparison). Minor effects of magnesium chloride treatment appear to be superimposed on the "original" dolomite rims, as interstitial void-filling materials include Mg- and Cl-rich phases (magnesium chloride or magnesium chloride hydrates) as well as Mg-, O-rich (brucite) and Ca-rich (calcite) phases (Fig.A13e-f and B22). The light cement paste rim seems to have survived during experimental cycling: Similar to the paste reaction rim in untreated non-durable concretes, it is still CaO-rich and SiO_2-poor, and looks white under SEM view. The minor effects of magnesium chloride solutions on the paste rim may include the development of few micro-cracks and the slightly elevated Cl and Mg concentrations, compared to its counterpart in untreated concrete (Figs.A13e-f and B21 - B22). As in treated durable concrete, the dark cement paste in non-durable concretes, zone Ee, has undergone major chemical and physical changes during experiments, which include severe crack development (Figs.A13c-f), paste dissolution/decomposition (Figs.A13e-f), formation of new Mg-, O-rich (brucite), Mg-, Cl-rich phases (Figs.A13e and B22), and development of strongly positive correlation between MgO and SiO_2 contents (Fig.B21). Also, the treated dark cement paste, as expected, exhibit elevated Mg and Cl concentration in relative to the untreated dark paste (cf. Figs.B21 - B22 and B1 - B2 for comparison).

Effects of Calcium Chloride Solutions

With $CaCl_2$-solution treatment, both durable and non-durable concretes showed severe deterioration mainly by crack development and brownish paste discoloration. Both cement paste and dolomite aggregate appear to show reduced porosity after $CaCl_2$-solution treatment. These effects were especially evident during wet/dry cycling (Figs.A8a-f, A9a-d, and A10e). In general, cracks were much better developed in the paste than in the coarse dolomite aggregate. Many of the cracks occurred adjacent to the outside of aggregate boundaries, and were chiefly oriented parallel or sub-parallel to the aggregate - paste interface (Figs. A8a-f, A9b-d, and A10e). Only a few cracks occurred precisely at the interface. As revealed by SEM micrograph and EDAX elemental maps, neo-formed crack-filling materials are Ca-rich (calcite) and sometimes Al-, O-rich (alumina), and void-filling materials appear to exhibit zonation: A very thin Ca-rich (calcite) film precipitated immediately adjacent to the void-wall, and Ca-, Cl-rich and Al-bearing phases and Ca-, S-rich and O-bearing phases precipitated on the calcite film (Figs.A10e and B11).

Unlike with magnesium chloride treatment, experiments with calcium chloride solution produced new, highly visible, reaction rims at margins of coarse aggregates in non-durable concretes under wet/dry and freeze/thaw conditions (Figs.A9f, A11a-e). Concretes containing Paralta quarry aggregate were especially susceptible to new rim development. These reaction rims are continuous along the edge of dolomite aggregate, even along the edge which was directly contacted with $CaCl_2$ solution instead of cement paste during experimental treatment, suggesting these rims are "new" reaction rims and were formed due to the interaction between concrete (or aggregate) and $CaCl_2$ solution. The "new" dolomite rims look very similar to older dolomite rims (i.e. the dolomite rims at the best-developed interface in untreated non-durable concretes) in that (1) they both include a wide, dark rim and a narrow, light-colored rim (cf. Figs.A10f, A11a-b, A11e, and A3c-d, A4a-b), and (2) the light-colored rim is less porous than the dark rim (cf. Figs. A11c-d and A3e-f). However, there are some critical differences between the "new" rims and the older ones: (1) The new rims are much wide than the older rims (cf. Figs.A10f, A11a-b, A11e and A3c-d, A4a-b for comparison); (2) The outermost region of "new" rims shows an increase in MgO and a corresponding decrease in CaO whereas the old rims exhibit reverse chemical changes (cf. Figs.B12, B14 and B1 for comparison).

Some older dolomite reaction rims in non-durable concretes seem to have survived during $CaCl_2$-solution treatment, and only minor effects have been superimposed. The dolomite rims Be and Ce shown in Figure A11f resemble zone B and zone C in Figures A3c-d and A4a-b. Also, the composition pattern

shown in Figure B15 is very similar to that in Figure B1, and no obvious depletion in CaO and enrichment in MgO occur at the outermost margin of dolomite aggregate.

It appears that, at least, the "original" cement reaction rim has not been seriously altered during CaWD and CaFT cycling, because the paste rim in solution-treated concretes and untreated concretes show very similar composition -- rich in CaO, poor in SiO_2 and MgO. Sometimes the "original" cement reaction rim appears to have become wider after $CaCl_2$-solution treatment, maybe more calcitic materials were precipitated around this cement reaction rim. As expected, the cement reaction rim in treated concrete contains minor amount of Cl (Fig.B13).

Unlike non-durable concretes, durable concretes subjected to continuous immersion, wet/dry, and freeze/thaw cycling in $CaCl_2$ solution exhibit no "new" reaction rims in either coarse aggregate or cement paste (Figs.A12a-d). As in the untreated durable concrete, dolomite aggregates in treated durable concretes exhibit uniform composition patterns. Relative to the untreated dark paste, the treated dark cement paste shows a much higher CaO/SiO_2 ratio (Figs.B16 and B17), indicating the calcium uptake of cement paste from solution during experimental treatments.

Effects of Sodium Chloride Solutions

Under the same experimental conditions in which $MgCl_2$ and $CaCl_2$ solutions were highly destructive, NaCl solutions proved to have little deleterious effects on both durable and non-durable concretes (Figs.A10b-d). NaCl brine (3M) was nearly non-destructive under 60°C and 90°C wet/dry conditions and -70°C freeze/thaw condition. Cement paste showed a slightly brownish discoloration under 60°C continuous soaking condition in 3 M NaCl solution, and moderate crumbling and slightly brownish discoloration in 0.75 M NaCl solution under 0°C freeze/thaw condition.

It appears that dolomite reaction rim(s) and paste reaction rim survived during experimental treatment, and no "new" reaction rims are visible in either dolomite aggregate or cement paste (Figs.A14c-f). Electron microprobe traverses were essentially identical to those of untreated concretes (cf. Figs.B23 and B4 for comparison). Sometimes, a few micro-cracks developed in dark cement paste and at the contact between dolomite aggregate and cement paste (Figs.A14e-f). As expected, the experimental treated cement paste contains some Cl (chloride) (Fig.B24), which was shown by XRD analysis to exist as halite.

DISCUSSION

Mechanism of Magnesium Chloride Attack on Concrete

A brief review of the effects of magnesium chloride vs. magnesium sulphate on concrete

The effects of magnesium chloride on concrete have been studied by several researchers, but the mechanism of the attack of magnesium chloride on concrete is still poorly understood, possibly due to the lack of detailed study on the interaction between magnesium chloride solution and cement paste. The results of the most significant studies on magnesium chloride can be summarized as follows:

(1) Magnesium chloride may cause concrete expansion and cracking (Heller & Ben-Yair, 1966; Lambert et al., 1992; Oberste-Padtberg, 1985);

(2) Magnesium chloride partially leaches (Oberste-Padtberg, 1985; Sayward, 1984; Smolczyk, 1969) or totally leaches out $Ca(OH)_2$ from cement paste (Smolczyk, 1969);

(3) Brucite, $Mg(OH)_2$, is the most common product (Ftikos & Parissakis, 1985; Heller & Ben-Yair, 1966; Kurdowski et al., 1990, 1994; Lambert et al., 1992; Oberste-Padtberg, 1985; Sayward, 1984). It plays an important role in causing the porous cement paste to be denser (Kurdowski et al., 1990, 1994), plugging pores and therefore reducing or preventing further salt penetration/attack (Sayward, 1984);

(4) Other products observed include $CaSO_4 \cdot 2H_2O$ (*gypsum*) (Kurdowski et al., 1990, 1994; Lambert et al., 1992; Smolczyk, 1969), $3CaO \cdot Al_2O_3 \cdot CaCl_2 \cdot 10H_2O$ (*Friedel's salt, Ca-chloroaluminate*) (Heller & Ben-Yair, 1966; Kurdowski et al., 1990, 1994; Lambert et al., 1992), $3CaO \cdot Al_2O_3 \cdot 3CaSO_4 \cdot 31H_2O$ (*ettringite*), $Mg_2(OH)_3Cl \cdot 4H_2O$ (Lambert et al., 1992), $MgO \cdot Mg(OH)Cl \cdot 5H_2O$ (Smolczyk, 1969), $Al(OH)_3$ gel, $Mg_3Cl_2(OH)_4 \cdot 2H_2O$, and $Mg_3Cl(OH)_5 \cdot 4H_2O$ (Kurdowski et al., 1990, 1994);

(5) Al-, Fe-, and Si-rich cement shows less deterioration than Al-, Fe-, and Si-poor cement (Ftikos & Parissakis, 1985).

In contrast, the effects of magnesium sulphate on concrete have been extensively studied, and the mechanism of magnesium sulphate attack on concrete is relatively well understood (Al-Amoudi et al., 1995; Cole & Hueber, 1957; Gjorv, 1971; Mather, 1966; Neville, 1969; Rasheeduzzafar et al., 1994). Deterioration due to sulphate attack may manifest itself in two forms. The first type of deterioration is acidic in nature and is associated with the formation of gypsum. It is characterized by disintegration of hydrated cement paste and progressive reduction to noncohesive granular mass, leaving aggregates exposed. The

second type of sulphate attack is normally characterized by expansion and cracking, and takes place when the reactive hydrated aluminate phases present in sufficient quantities are attacked by sulphate ions in the presence of $Ca(OH)_2$, therefore forming ettringite, leading to disruptive expansion and cracking.

Magnesium sulphate attacks most of the constituents of hydrated cement paste via a variety of reactions (Mather, 1966; Neville, 1969; Al-Amoudi et al., 1995). It reacts with calcium aluminate hydrates to form ettringite, brucite, and aluminum hydroxide

$$3MgSO_4 \cdot 7H_2O + 2\,(3CaO \cdot Al_2O_3 \cdot 12H_2O) \rightarrow 3CaO \cdot Al_2O_3 \cdot 3CaSO_4 \cdot 31H_2O + 3Mg(OH)_2 + 2Al(OH)_3 + H_2O \quad [3]$$

Magnesium sulphate also reacts with calcium hydroxide to form calcium sulphate, which, in turn, reacts with calcium aluminate hydrate to form additional ettringite

$$MgSO_4 \cdot 7H_2O + Ca(OH)_2 \rightarrow CaSO_4 \cdot 2H_2O + Mg(OH)_2 + 5H_2O \quad [4]$$

$$3\,(CaSO_4 \cdot 2H_2O) + 3CaO \cdot Al_2O_3 \cdot 12H_2O + 13H_2O \rightarrow 3CaO \cdot Al_2O_3 \cdot 3CaSO_4 \cdot 31H_2O \quad [5]$$

Unlike other sulphates, magnesium sulphate reacts also with calcium silicate hydrates (C-S-H), for example $3CaO \cdot 2SiO_2 \cdot nH_2O$, to form calcium sulphate, brucite, and silica gel ($SiO_2 \cdot nH_2O$)

$$MgSO_4 \cdot 7H_2O + 3CaO \cdot 2SiO_2 \cdot nH_2O \rightarrow CaSO_4 \cdot 2H_2O + Mg(OH)_2 + SiO_2 \cdot nH_2O \quad [6]$$

Finally, brucite produced from the above reactions can react with silica gel to form non-cementitious, porous magnesium silicate hydrate (M-S-H)

$$4Mg(OH)_2 + SiO_2 \cdot nH_2O \rightarrow 4MgO \cdot SiO_2 \cdot 8.5H_2O + (n - 4.5)H_2O \quad [7]$$

It was suggested by Cohen & Bentur (1988) that the decomposition of C-S-H gel to non-cementitious M-S-H can take place either indirectly by conversion of C-S-H to brucite to M-S-H, as shown by equations [6]-[7], or directly by substitution of Ca^{2+} ions in C-S-H gel with Mg^{2+} ions.

As pointed out by Al-Amoudi et al. (1995), even if ettringite succeeds to form during exposure to magnesium sulphate solution, it would become unstable under the low-alkalinity condition provided by $Mg(OH)_2$ and will eventually decompose to gypsum, alumina, and brucite.

It is apparent that both magnesium-chloride-attack and magnesium-sulphate-attack leach out $Ca(OH)_2$, produce brucite and, possibly, gypsum and alumina gel. Whereas magnesium-chloride-attack also produces Ca-chloroaluminate, magnesium chloride hydrate or other Mg-, Cl-bearing complex phase, magnesium-sulphate-attack is characterized by the conversion of C-S-H into noncohesive, porous M-S-H.

Possible mechanism of magnesium chloride attack on Iowa highway concrete

The following observations may be important in understanding the possible deterioration mechanism due to $MgCl_2$ solution attack of Iowa highway concretes:

(1) In both durable and non-durable concretes, coarse aggregate underwent little or no change, but cement paste underwent substantial chemical and physical changes during magnesium chloride treatment.

(2) The $MgCl_2$-treated cement is characterized by severe paste decomposition, disintegration, dark brownish discoloration, enrichment in MgO, Cl, and depletion in CaO, suggesting major changes in mineralogy. The strong positive correlation between MgO and SiO_2 apparently indicates magnesium silicate hydrate.

(3) During experiments, as shown by XRD studies, brucite was formed, whereas $Ca(OH)_2$ was consumed.

(4)The neo-formed calcite along with the survival of the Ca-rich (calcite-rich) cement rim in non-durable concrete during experiments indicates that calcite is a stable phase.

(5) The positive correlative between Al_2O_3 and FeO in both untreated and $MgCl_2$-solution-treated cement paste implies that Al- and Fe-rich cement phases are resistant to magnesium chloride attack. This is supported by the experiments of Ftikos & Parissakis' (1985) who showed that Fe- and Al-richer cement showed less deterioration in solutions containing Mg^{2+} and Cl^-.

(6) A tentative precipitation sequence of neo-formed phases is calcite → brucite, magnesium chloride and/or magnesium chloride hydrates → aluminum hydroxide, silica, and possibly other complex Fe-, S-, Cl-bearing phases.

By comparing these observations with the effects of magnesium chloride and magnesium sulphate listed on the previous page, it is apparent that the effects of magnesium chloride on Iowa highway concretes are very similar to these of magnesium sulphate except for the absence of abundant SO_4^{2-}-containing phases such as gypsum and ettringite. Several reactions may have been involved during magnesium chloride attack:

(1) Magnesium chloride leaches out $Ca(OH)_2$ in cement paste to form calcite and brucite

$$MgCl_2 + Ca(OH)_2 + CO_3^{2-}(aq.) \rightarrow Mg(OH)_2 + CaCO_3 + 2\,Cl^- \qquad [8]$$

where CO_3^{2-} would be derived from dissolved CO_2 in solution or the decomposition of dolomite aggregate. Brucite, calcite, along with magnesium chloride hydrate which may precipitate especially during drying condition, fill air-voids and micro-cracks, and may cause further micro-cracking, as shown in Figs.A13a-e. These micro-cracks can serve as new pathways for solution attack.

(2) In the absence of $Ca(OH)_2$ (e.g. when $Ca(OH)_2$ has been leached out), Mg^{2+} in solution would react more directly and extensively with the cementitious calcium silicate hydrate to non-cementitious magnesium silicate hydrate. Due to the very limited availability of SO_4^{2-}, the released Ca^{2+} may precipitate as calcite instead of gypsum.

(3) Magnesium chloride may react with calcium aluminate hydrate to form brucite and aluminum hydroxide. Furthermore, magnesium chloride may react with calcium silicate hydrate to form brucite and silica gel, which, in turn, react to form magnesium silicate hydrates.

Mechanism of Calcium Chloride Attack on Concrete

Calcium chloride has been found to be aggressive to concrete (Smolczyk, 1969; Neville, 1969) and particularly at higher temperatures (Browne & Cady, 1975). Concrete deterioration is associated with expansion and cracking (Heller & Ben-Yair, 1966; Lawrence & Vivian, 1960; Moriconi et al., 1989; Neville, 1969; Sayward, 1984), leaching of $Ca(OH)_2$ (Amin et al., 1994; Berntsson & Chandra, 1982; Collepardi & Monosi, 1992; Monosi et al., 1989; Smolczyk, 1969; Ushiyama & Goto, 1974; Yang et al., 1992), and the formation of *gypsum* (Smolczyk, 1969), *Freidel's salt* (Berntsson & Chandra, 1982; Bonen & Sarkar, 1994; Collepardi & Monosi, 1992; Heller & Ben-Yair, 1966; Lawrence & Vivian, 1960; Monosi et al., 1989; Yang et al., 1992), *$CaO{\cdot}CaCl_2{\cdot}2H_2O$* (Smolczyk, 1969), *$3CaO{\cdot}CaCl_2{\cdot}15H_2O$* (Collepardi & Monosi, 1992; Monosi et al., 1989), *$CaCl_2{\cdot}Ca(OH)_2{\cdot}H_2O$* (Yang et al., 1992), as well as *calcium chloride hydrate and monochlorohydrate* (Bonen & Sarkar, 1994). It is generally accepted that Freidel's salt forms due to the interaction between $CaCl_2$ solution and Al-bearing compounds in cement paste (such as tricalcium aluminate). Whether Freidel's salt is the real cause of concrete deterioration is still controversial. Chatterji (1978) suggested that concrete deterioration was not caused by $3CaO{\cdot}Al_2O_3{\cdot}CaCl_2{\cdot}xH_2O$ or by leaching out $Ca(OH)_2$, but by expansive complex salt containing $CaCl_2$, $Ca(OH)_2$ and/or $CaCO_3$. Collepardi & Monosi (1992) and Yang et al. (1992) attributed concrete deterioration to $3CaO{\cdot}CaCl_2{\cdot}15H_2O$ and $CaCl_2{\cdot}Ca(OH)_2{\cdot}H_2O$, respectively.

As mentioned in the previous section, $CaCl_2$ attack on both durable and non-durable concretes is characterized by crack development, presumably due to concrete expansion. It is important to note that: (1) The $CaCl_2$-solution-treatment cement paste showed reduced porosity; (2) Air-voids and micro-cracks are partially or completely filled with neo-formed Ca-, Cl-rich and O-, Al-bearing (Freidel's salt), Ca-, S-rich, O-bearing and, sometimes, Al-bearing (ettringite and gypsum), Ca-rich (calcite), and Al-, O-rich (alumina)

materials; (3) At least some micro-cracks obviously originated from air-voids or "major" cracks developed during experimental treatment; (4) The Ca-rich (calcite-rich) cement reaction rim in non-durable concrete survived; (5) The treated cement paste in both durable and non-durable concrete exhibited a higher CaO/SiO_2 ratio than the untreated cement paste; and (6) $Ca(OH)_2$ in cement paste disappeared after $CaCl_2$ treatment. These observations apparently indicate that the precipitation of neo-formed materials (calcite, Freidel's salt, ettringite, gypsum, etc.), due to the reaction between $CaCl_2$ solution and cement paste, and the stress associated with crystal growth caused concrete expansion and led to crack development.

Dolomite aggregates in non-durable concretes, that were characterized by reaction rim development, were also considerably more reactive during $CaCl_2$-solution treatment than those in durable concretes. Contrary to the "old" reaction rims developed under highway conditions, the "new" dolomite reaction rims developed in our experiments are rich in MgO and relatively poor in CaO. The mechanism of "new" rim development is not well understood. As shown by Figure B13, the enrichment in MgO in the "new" dolomite rim is caused by the existence of abundant brucite. One possible explanation for the enrichment in MgO and depletion in CaO is that $CaCl_2$ solution enhances dedolomitization, causing dolomite decomposition. Mg^{2+} was precipitated in-situ as brucite at aggregate edges, whereas Ca^{2+} diffused outward into cement paste and precipitated as calcite (calcite in the Ca-rich zone De may act as crystal nuclei).

Mechanism of Sodium Chloride Attack on Concrete

Sodium chloride has been found to cause concrete scaling under certain conditions (Yang et al., 1992) or cause minor or no damage to concrete (Cantor & Kneeter, 1976; Moriconi et al., 1989; Smolczyk, 1969). However, like calcium chloride attack, sodium chloride attack is also associated with the leaching of $Ca(OH)_2$ (Kawadkar & Krishnamoorthy, 1981; Locher, 1969; Smolczyk, 1969; Ushiyama & Goto, 1974), and the formation of Freidel's salt (Heller & Ben-Yair, 1966; Hoffermann, 1984; Kawadkar & Krishnamoorthy, 1981; Locher, 1969; Pitt et al., 1987).

Our experiments disclosed that sodium chloride is relatively benign in terms of concrete deterioration, and the most damage to concrete, moderate crumbling and brownish paste discoloration, was produced by 0.75 M NaCl solution under 0°C freeze/thaw conditions instead of 3 M NaCl solution under -70°C/25°C freeze/thaw conditions (Table 4). This seems to be consistent with the experimental results of Yang et al.'s (1992) who showed that under -20°C/20°C freeze/thaw condition, concrete scaling reached the maximum at deicer concentration of about 4% NaCl.

Role of Magnesium in Concrete Deterioration

In order to help determine the role of magnesium in concrete deterioration, one group of wet/dry experiments was conducted using magnesium-acetate and magnesium nitrate solutions. Both solutions were found to produce concrete deterioration very similar to that caused by magnesium chloride (i.e., paste decomposition and brownish discoloration). As discussed in the previous section, the effects of magnesium chloride on concrete (cement paste) are also very similar to the effects of magnesium sulphate. Therefore, it appears that magnesium of any source is deleterious to concrete and would cause paste decomposition, disintegration and, directly or indirectly, convert calcium silicate hydrates in cement paste into non-cementitious magnesium silicate hydrates.

GENERAL CONCLUSIONS AND RECOMMENDATIONS

General Conclusions

Two groups of Iowa highway concretes studied here can be differentiated: durable concretes with extended service lives of > 40 years containing coarse dolomite aggregates from Sundheim and Mar-Jo Hills quarries, and non-durable concretes with short service lives of 8-12 years that contain coarse dolomite aggregates from the Garrison, Paralta, and Smith quarries, and Ames gravel pit. Non-durable concretes are far more deteriorated and contain more cracks or micro-cracks than durable concretes. In addition, non-durable concretes exhibit more abundant and better developed reaction rims than durable concretes at dolomite aggregate - cement paste interfaces. The only major and consistent differences between durable and non-durable concretes are the coarse aggregates used in making the concretes, so that the aggregate source determines aggregate reactivity. Less abundant coarse limestone aggregate which occurs in some of the concretes does not exhibit reaction rims, indicating that the reactions responsible for reaction rim development are dolomite-specific. Both petrographic and SEM studies revealed that reactive dolomite aggregates exhibit higher porosity and consist of fine-grained dolomite crystals with a diameter of 5 - 50 μm, whereas non-reactive dolomite aggregates exhibit lower porosity and consist of coarse, extremely well-crystallized, and tightly inter-grown dolomite crystals with a diameter of 50 - 450 μm.

The best-developed interface pattern is: unaltered dolomite aggregate interior (zone A) → inner dark dolomite reaction rim (zone B) → outer light-colored dolomite reaction rim (zone C) → light-colored paste reaction rim (zone D) → dark, presumably unaltered, cement paste (zone E). Regardless of the presence or absence of zone C, there is an increase in Ca and a concomitant decrease in Mg near the edge of dolomite aggregate close to the aggregate - paste interface, along with the formation of calcite and brucite near the interface. Zone D is Ca-rich with compositions approaching calcite. The compositional variations and mineralogy strongly suggest these reaction rims were formed as a result of dedolomitization reactions between reactive dolomite aggregate and alkaline cement paste. The alkali - dolomite reaction is a significant cause of Iowa highway concrete deterioration.

Both durable and non-durable Iowa concretes were subject to wet/dry, freeze/thaw, and continuous soaking treatment with magnesium chloride, calcium chloride, sodium chloride solutions, and water. No deterioration was evident in concrete samples treated with water, regardless of the experimental condition. Sodium chloride solution was found to be relatively benign in terms of concrete deterioration, and the most

damage to concrete, moderate crumbling and brownish paste discoloration, was produced by 0.75 M NaCl solution under 0°C freeze/thaw conditions instead of 3 M NaCl solution under -70°C/25°C freeze/thaw conditions. However, magnesium and calcium chloride solutions were found to be deleterious, regardless of solution concentration and concrete source (durable vs. non-durable), and the associated concrete deterioration was wet/dry condition > continuous soaking condition > freeze/thaw condition. In addition, wet/dry deterioration was more pronounced when samples were dried at higher temperatures.

Magnesium chloride solution typically caused severe paste decomposition, disintegration and dark brownish paste discoloration. The reactions between magnesium chloride and cement paste may involve $Ca(OH)_2$ leaching out, replacement of Ca^{2+} in calcium silicate hydrate by Mg^{2+}, and the decomposition of calcium aluminate hydrate, to form non-cementitious magnesium silicate hydrate, brucite, and calcite, causing paste disintegration and discoloration. Since magnesium chloride attack showed similar deleterious effects on concrete to that shown by magnesium sulphate, magnesium acetate, and magnesium nitrate, any magnesium source, either from magnesium road deicers or from reactive dolomite aggregate, is thought to play a major role in highway concrete deterioration.

Calcium chloride attack on concrete is characterized by crack development and brownish paste discoloration. Our observations indicate that the precipitation of neo-formed materials (calcite, Freidel's salt, ettringite, gypsum, etc.), due to the reaction between $CaCl_2$ solution and cement paste, and the stress associated with crystal growth caused concrete expansion and led to crack development. The interaction between calcium chloride solution and reactive dolomite aggregate would release Mg^{2+} from dolomite. Most of the released Mg^{2+} would precipitate in-situ as brucite, and some Mg^{2+} would diffuse into cement and eventually react with calcium silicate hydrates to form magnesium silicate hydrates, causing paste discoloration.

Recommendations

Upon consideration of the results of this study, several recommendations are made. The first is that dolomite aggregate source rocks should be screened for average crystal size, porosity and texture. These can be accomplished by petrographic microscopic study and, possibly, SEM study. Those with relatively high porosity and fine crystal size (< 50 μm) should be eliminated for concrete use.

The second recommendation is that magnesium chloride, calcium magnesium acetate (CMA) and calcium chloride deicers should be used with caution, and long-term testing should be implemented to

determine if they accelerate highway concrete deterioration. This study concluded that magnesium plays a major role in concrete deterioration, either by converting cement paste into brucite and non-cementitious magnesium silicate hydrate, or by promoting concrete expansion due to its involvement in the reaction between reactive dolomite and cement paste (i.e. alkali-dolomite reaction).

The final recommendation is that further experiments should be performed to determine the reactivity of Iowa dolomite aggregates by treating concretes in concentrated calcium chloride solutions. This study disclosed that reactive and poorly-performing dolomite aggregates were more susceptible to reaction rim development than non-reactive dolomites when concretes were subject to wet/dry and freeze/thaw cycling in calcium chloride brine. Treating dolomite aggregate or dolomite-aggregate-containing concretes in calcium chloride solutions may be a easy way to test aggregate reactivity.

REFERENCES

Al-Amoudi O. S. B., Maslehuddin M., Saadi M. M., 1995, Effect of magnesium sulfate and sodium sulfate on the durability performance of plain and blended cements. *ACI Materials Journal*, **92** [1] 15-24.

Amin A. M. Ali A. H., Sharara A. M., El-Didamony H., 1994, Resistivity of an artificial Pozzolanic cement to chloride solutions. *Silicates Industriels*, **LIX** [11-12] 307-312.

Berntsson L. & Chandra S., 1982, Damage of concrete sleepers by calcium chloride. *Cement & Concrete Research*, **12** [1] 87-92.

Bisque R. E., 1959, Silicification of argillaceous carbonate rocks. Ph.D. dissertation, Iowa State University, 64pp.

Bisque R. E. & Lemish J., 1958, Chemical characteristics of some carbonate aggregates as related to durability of concrete. *Highway Research Board Bull.*, [196] (Air Voids in Concrete and Characteristics of Aggregates), 29-45.

Bisque R. E. & Lemish J., 1960a, Effect of illitic clay on chemical stability of carbonate aggregates. *Highway Research Board Bull.*, [275] (Concrete Quality Control, Aggregate Characteristics, and the Cement - Aggregate Reaction), 32-38.

Bisque R. E. & Lemish J., 1960b, Silicification of carbonate aggregates in concrete. *Highway Research Board Bull.*, [239] (Physical and Chemical Properties of Cement and Aggregate in Concrete), 41-57.

Boies D. G. & Bortz S., 1965, Economical and effective deicing agents for use on highway structures. *Natl. Coop. Highw. Res. Prog. Rep.*, **19**, 1-19.

Bonen D. & Sarkar S. L., 1994, Environmental Attack on Concrete. In: Proc. of the 16th International Conf. on Cement Microscopy (Eds. Gouda G. R., Nisperos A., Bayles J.), International Cement Microscopy Association, Texas, 11-23.

Browne F. P. & Cady P. D., 1975, Deicer scaling mechanism in concrete. *Am. Concr. Inst.*, **SP-47** (Durability of Concrete) 101-119.

Buck A. D. & Dolch W. L., 1966, Investigation of a reaction involving non-dolomitic limestone aggregate in concrete: *J. Amer. Con. Inst. Proceedings*, **63** 755-765.

Cantor T. R. & Kneeter C. P., 1977, Influence of salt on the freeze - thaw deterioration of concrete. *Materials Performance*, **16** [5] 28-32.

Carles-Gibergues A., Olivier J. P., Fournier B., Berube M. A., 1989, A new approach to the study of alkali - aggregate reaction mechanisms. In: Alkali - Aggregate Reaction (Proc. 8th International Conf. on Alkali-Aggregate Reaction, Kyoto, Japan; Eds. Okada K., Nishibayashi S., Kawamura M.), Elsevier Applied Science, New York, 161-166.

Chatterji S., 1978, Mechanism of the $CaCl_2$ attack on Portland cement concrete. *Cement and Concrete Research*, **8** [4] 461-468.

Cody R. D., Spry P. G., Cody A. M., Gan G. L., 1994, The role of magnesium in concrete deterioration . Final Report for Iowa DOT Project HR-335. 171pp.

Cohen M. D. & Bentur A., 1988, Durability of Portland cement - silica fume pastes in magnesium sulfate and sodium sulfate solutions. *ACI Materials Journal*, **85** [3] 148-157.

Cole W. F. & Hueber H. V., 1957, Hydrated magnesium silicates and aluminates formed synthetically and by the action of sea water on concrete. *Silicates Industriels*, **XXII** [2] 75-85.

Collepardi M. & Monosi S., 1992, Effect of the carbonation process on the concrete deterioration by $CaCl_2$ aggression. In: Proc. 9th International Congress on the Chemistry of Cement, New Delhi, India, V (Performance and Durability of Concrete and Cement Systems), National Council for Cement and Building Materials, New Delhi, India, 389-395.

Crumpton C. F., Smith B. J., Jayaprakash G. P., 1989, Salt weathering of limestone aggregate and concrete without freezing-thaw. *Transportation Research Record*, [1250] (Innovation in Aggregate Testing), 8-16.

Deng M. & Tang M. Sh., 1993, Mechanism of dedolomitization and expansion of dolomitic rocks. *Cement and Concrete Research*, **23** [6] 1397-1408.

Deng M., Han S. F., Lu Y. N., Lan X. H., Hu Y. L., Tang M. S., 1993, Deterioration of concrete structures due to alkali - dolomite reaction in China. *Cement and Concrete Research*, **23** 1040-1046.

Deng M., Wang Q., Mu X. F., Tang M. Sh., 1994, The chemical reaction in dolomite - KOH solution systems autoclaved at high temperatures. *Advances in Cement Research*, **6** [22] 61-65.

Donovan J. J., Rivers M. L., Armstrong J. T., 1992, PRSUPR: Automation and analysis software for wavelength dispersive electron-beam microanalysis of a PC. *American Mineralogist*, 77 [3-4] 444-445.

Dubberke W., 1983, Factors relating to aggregate durability in Portland Cement Concrete. Interim report for Project HR-2022, Iowa Department of Transportation.

Dubberke W. & Marks V. J., 1985, The effects of deicing salt on aggregate durability. *Transportation Research Record*, [1031] (Geotechnical Engineering Research), 27-34.

Dubberke W. & Marks V. J., 1987a, The instability of ferroan dolomite aggregate in concrete (presented at the 66th Annual Meeting of the Transportation Research Board, Washington, D.C.). Final Report for Iowa Highway Research Board Research Project HR-266. 18pp.

Dubberke W. & Marks V. J., 1987b, The relationship of ferroan dolomite aggregate to rapid concrete deterioration. *Transportation Research Record*, [1110] (Concrete and Concrete Construction), 1-10.

Dubberke W. & Marks V. J., 1989, Evaluation of carbonate aggregate using X-ray analysis. *Transportation Research Record*, [1250] (Innovation in Aggregate Testing), 17-24.

Dubberke W. & Marks V. J., 1992, Thermogravimeteric analysis of carbonate aggregate (presented at the 71st Annual Meeting of the Transportation Research Board, Washington, D.C.). Progress Report for Highway Research Advisory Board Research Project HR-336. 27pp.

Ftikos Ch. & Parissakis G., 1985, The combined action of Mg^{2+} and Cl^{-} ions in cement paste. *Cement & Concrete Research*, **15** [4] 593-599.

Gillott J. E., 1964, Mechanism and kinetic of expansion in alkali - carbonate rock reaction. *Canadian J. Earth Sci.*, 1 121-145.

Gillott J. E., 1975, Alkali - aggregate reactions in concrete. *Engineering Geol.*, **9** [4] 303-326.

Gillott J. E., 1978, Effect of deicing agents and sulphate solution on concrete aggregate. *Q. J. Engng Geol.*, **11** 177-192.

Gillott J. E. & Swenson E. G., 1969, Mechanism of the alkali - carbonate rock reaction. *Q. J. Engng Geol.*, **2** [1] 7-23.

Girard R. J., Myers W., Manchester G. D., Trimm W. L., 1982, D-cracking: Pavement design and construction variables. *Transportation Research Record*, [853] (Concrete Analysis and Deterioration), 1-9.

Gjorv O. E., 1971, Long-time durability of concrete in seawater. *ACI Materials Journal*, **68** [1] 60-67.

Hadley D. W., 1961, Alkali reactivity of carbonate rocks -- expansion and dedolomitization. *Highway Research Board*, **40** (Proc. 40th Annual Meeting, Washington D. C.), 463-474.

Hadley D. W., 1964a, Alkali reactive carbonate rocks in Indiana: A pilot regional investigation. *Highway Research Record*, [45] (Symp. Alkali - Carbonate Rock Reactions), 196-221.

Hadley D. W., 1964b, Alkali reactivity of dolomitic carbonate rocks. *Highway Research Record*, [45] (Symp. Alkali - Carbonate Rock Reactions), 1-19.

Heller L. & Ben-Yair M., 1966, Effect of chloride solutions on Portland cement. *J. Appl. Chem.*, **16** [8] 223-226.

Hoffmann D. W., 1984, Changes in structure and chemistry of cement mortars stressed by a sodium chloride solution. *Cement and Concrete Research*, **14** [1] 49-56.

Hudec P. P., 1989, Durability of rocks as function of grain size, pore size, and rate of capillary absorption of water. *J. of Materials in Civil Engineering*, **1** [1] 3-9.

Kawadkar K. G. & Krishnamoorthy S., 1981, Behavior of cement concrete under common salt solution both under hydrostatic and atmospheric pressure. *Cement & Concrete Research*, **11** [1] 103-113.

Kuenning W. H., 1966, Resistance of Portland cement mortar to chemical attack -- A progress report. *Highway Research Record*, [113] (Symposium on Effects of Aggressive Fluids on Concrete), 43-87.

Kurdowski W., Taczuk L., Trybalska B., 1990, Behaviour of high alumina cement in chloride solutions. In: Calcium Aluminate Cement (Proc. of the International Symp. held at London; Ed. Mangabhai R. J.), Chapman & Hall, London, 222-229.

Kurdowski W., Trybalska B., Duszak S., 1994, SEM studies of corrosion of cement paste in chloride solution. In: Proc. of the 16th International Conf. on Cement Microscopy, (Eds. Gouda G. R., Nisperos A., Bayles J.), International Cement Microscopy Association, Texas, 80-89.

Lambert S. J., Nowak E. J., Wakeley L. D., Poole T. S., 1992, Interaction between concrete and brine at the waste isolation pilot plant (WIPP) site, New Mexico. In: Mat. Res. Soc. Symp. Proc., **245** 111-116.

Lawrence M. & Vivian H. E., 1960, The action of calcium chloride on mortar and concrete. *Australian J. of Appl. Sci.*, **11** [4] 490-498.

Lemish J. & Moore W. J., 1964, Carbonate aggregate reactions: Recent studies and an approach to the problem. *Highway Research Record*, [45] (Symp. Alkali - Carbonate Rock Reactions), 57-71.

Lemish J., Rush F. E., Hiltrop C. L., 1958, Relationship of physical properties of some Iowa carbonate aggregates to durability of concrete. *Highway Research Board Bull.*, [196] (Air Voids in Concrete and Characteristics of Aggregates), 1-16.

Locher F. W., 1969, Influence of chloride and hydrocarbonate on the sulphate attack. In: Proc. of the 5th International Symp. on the Chemistry of Cement, 1968. Part III -- Properties of Cement Paste and Concrete, The Cement Association of Japan, 328-335.

Marks V. J, & Dubberke W., 1982, Durability of concrete and the Iowa Pore Index test. *Transportation Research Record*, [853] (Concrete Analysis and Deterioration), 25-30.

Mather B., 1966, Effects of sea-water on concrete. *Highway Research Record*, [113] (Symposium on Effects of Aggressive Fluids on Concrete, 1965), 33-42.

Mather B., 1974, Developments in specification and control. *Highway Research Record*, [525] (Cement - Aggregate Reactions), 38-42.

Milanesi C. A. & Batic O. R., 1994, Alkali reactivity of dolomitic rocks from Agentina. *Cement and Concrete Research*, **24** [6] 1073-1084.

Monosi S., Alvera L, Collepardi M., 1989, Chemical attack of calcium chloride on the Portland cement paste. *Il Cemento*, [2] 97-104.

Moriconi S., Pauri M., Alvera L, Collepardi M., 1989, Damage of concrete by exposure to calcium chloride. In: Materials Engineering (Proc. of the 2nd International Conf. on Engineering Materials, EM'88, Bologna, Italy), 1 [2] (From Research to Application and Design) 491-496.

Nadezhdin A., Mason D. A., Malric B., Lawless D. F., Fedosoff J. P., 1988, Effect of deicing chemicals on reinforced concrete. *Transportation Research Record*, [1157] (Deicing Chemicals and Snow Control), 31-37.

Neville A. M., 1969, Behavior of concrete in saturated and weak solutions of magnesium sulphate and calcium chloride. *J. Mater.*, 4 [4] 781-816.

Oberste-Padtberg R., 1985, Degradation of cements by magnesium brine: A microscopic study. In: Proc. of the 7th International Conf. on Cement Microscopy (Ft. Worth, Texas; Eds. Bayles J., Gouda G. R., Nisperos A.), International Cement Microscopy Association, Duncanville, Texas, 24-36.

Pitt J. M., Schluter M. C., Lee D. Y. Dubberke W., 1987, Sulfate impurities from deicing salt and durability of portland cement mortar. *Transportation Research Record*, [1110] (Concrete and Concrete Construction), 16-23.

Pitt J. M., Carnazzo R. A., Vu J., 1989, Control of concrete deterioration due to trace compounds in deicers. Phase II Report for Iowa DOT Project HR-299, ERI Project 3071 and ISU-ERI-Ames-89419. 45pp.

Poole A. B., 1981, Alkali - carbonate reactions in concrete. In: Alkali - Aggregate Reaction in Concrete (Proc. 5th International Conf.), National Building Research Institute, Council for Scientific and Industrial Research, Pretoria, South Africa, Publication S252/1981, 327-334.

Poole A. B., 1992, Introduction to alkali - aggregate reaction in concrete. In: The Alkali - Silica Reaction in Concrete (ed. Swamy R. N.), Van Nostrand Reinhold, New York, 1-29.

Poole A. B. & Sotiropoulos P., 1978, The interaction of alkalies with dolomite and quartz in experimental concrete systems. In: Effects of Alkalies in Cement and Concrete (Proc. 4th International Conf.), Publication No. CE-MAT-1-78, Purdue University, Indiana, 163-179.

Poole A. B. & Sotiropoulos P., 1980, Reactions between dolomitic aggregate and alkali pore fluids in concrete. *Q. J. Eng. Geol.*, 13 281-287.

Rasheeduzzafar B., Al-Amoudi O. S. B., Abduljauwad S. N., Maslehuddin M., 1994, Magnesium-sodium sulphate attack in plain and blended cements. *J. of Materials in Civil Engineering*, 6 [2] 201-222.

Rogers C. A., 1986, Evaluation of the potential for expansion and cracking of concrete caused by the alkali-carbonate reaction. *Cem. Concr. Aggregates*, 8 [1] 13-23.

Sayward J. M., 1984, Salt action on concrete (Special report CRREL-SR-84-25), Cold Regions Research and Engineering Lab., Hanover, NH, 76 pp.

Schwartz D., 1987, D-cracking of the concrete pavement. National Cooperative Highway Research Program, Synthesis of Highway Practice. Transportation Research Board, National Research Council, Washington, D. C. [134] 1-34 .

Sherwood W. C. & Newlon H. H., 1964, Studies on the mechanisms of alkali - carbonate reaction. Part I -- Chemical reactions. *Highway Research Record*, [45] (Symp. Alkali - Carbonate Rock Reactions), 41-56.

Smolczyk H. G., 1969, Chemical reactions of strong chloride-solutions with concrete. In: Proc. of the 5th International Symp. on the Chemistry of Cement, 1968. Part III -- Properties of Cement Paste and Concrete, The Cement Association of Japan, 274-280.

Swenson E. G. & Gillott J. E., 1964, Alkali - carbonate rock reaction. *Highway Research Record*, [45] (Symp. Alkali - Carbonate Rock Reactions), 21-45.

Swenson E. G. & Gillott J. E., 1967, Alkali reactivity of dolomitic limestone aggregate. *Mag. Concrete Res.*, **19** [59] 95-104.

Tang M. Sh., Liu Zh., Han S. F., 1986, Mechanism of alkali - carbonate reaction. In: Concrete Alkali - Aggregate Reaction (Proc. 7th International Conf.; Ottawa, Canada; Ed. Grattan-Bellew P. E.), Noyes Publications, New Jersey, 275-279.

Tang M. Sh., Lu Y. N., Han S. F., 1989, Kinetics of alkali - carbonate reaction. In: Alkali - Aggregate Reaction (Proc. 8th International Conf., eds. Okada K., Nishibayashi S., Kawamura M.), Elsevier Applied Science, New York, 147-152.

Tang M. Sh., Liu Zh., Lu Y. N., Han S. F., 1991, Alkali - carbonate reaction and pH value. *Il Cemento*, **88** [3] 141-150.

Tang M. Sh., Deng M., Lan X. H., Han S. F., 1994, Studies on alkali - carbonate reaction. *ACI Materials Journal*, **91** [1] 26-29.

Ushiyama H. & Goto S., 1974, In: 6th International Cong. on the Chemistry of Cement, Suppl. Paper, Section II, Moscow, 23pp.

Winkler E. M. & Singer P. C., 1972, Crystallization pressure of salts in stone and concrete. *Bull. Geol. Soc. Am.*, **83** [11] 3509-3514.

Yang Q. B., Wu X. L., Huang S. Y., 1992, Mechanisms of deicer scaling of concrete. In: Proc. 9th International Congress on the Chemistry of Cement. National Council for Cement and Building Materials, New Delhi, India, V (Performance and Durability of Concrete Cement Systems), 282-288.

ACKNOWLEDGEMENTS

I am very grateful to Dr. P. G. Spry and Dr. R. D. Cody for their patient supervision and guidance during the course of my Ph. D. study at Iowa State University. I also acknowledge my graduate committee members Dr. J. Lemish, Dr. R. C. Brown, and Dr. C. S. Oulman for their patience and encouragement throughout my Ph. D. study. Discussion with Dr. J. Lemish is gratefully appreciated.

Special appreciation is extended to Ms. A. M. Cody for her help with the experiments and discussion of the results. Thanks are also due to Messrs. W. Dubberke, V. J. Marks, J. Myers, and Dr. W. Rippie for their advice, support, and providing bulk rock data of dolomite aggregates used in this study. I am especially grateful to Dr. A. Kracher for help with electron microprobe analysis, Mr. S. Thieben and Mr. X. Q. Xiong for assistance with XRD analysis, Dr. J. Amenson and Dr. S. Schlorholtz for their assistance with SEM analyses.

I would like to express my gratitude to the faculty, staff, and students of the Department of Geological and Atmospheric Sciences, Iowa State University for their help during my stay at Iowa State University.

Finally, thanks must go to my wife, Lan Zheng, and my son, Qi Gan, for their dedication over the past several years.

This study was funded primarily by the Iowa Department of Transportation, Project No. HR-355, and partially supported by the Iowa State Mining and Mineral Resources Research Institute program. Their support is gratefully acknowledged.

APPENDIX A:

PHOTOGRAPHS

Figure A1 Core samples of Iowa highway concrete. The concretes contain aggregates from Smith quarry (a), Paralta quarry (b), Garrison quarry (c), Ames gravel-pit quarry (d), Sundheim quarry (e) and Mar-Jo Hills quarry (f). Arrows show representative visible cracks and dolomite reaction rims. Non-durable concretes containing dolomite aggregate from Smith, Garrison, Paralta and Ames pit quarries show more pronounced dolomite reaction rims and cracks than durable Sundheim and Mar-Jo Hills concretes. Bars = 2 cm.

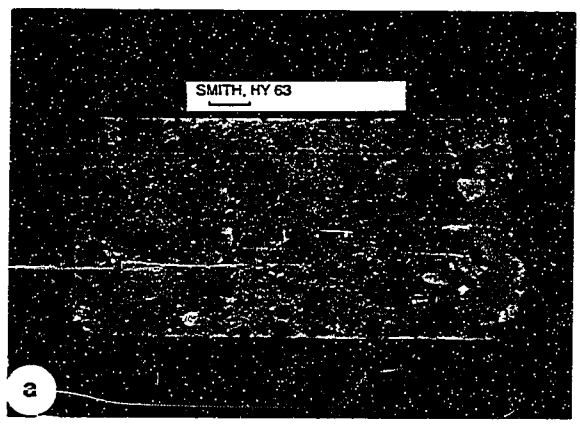
SMITH, HY 63
a

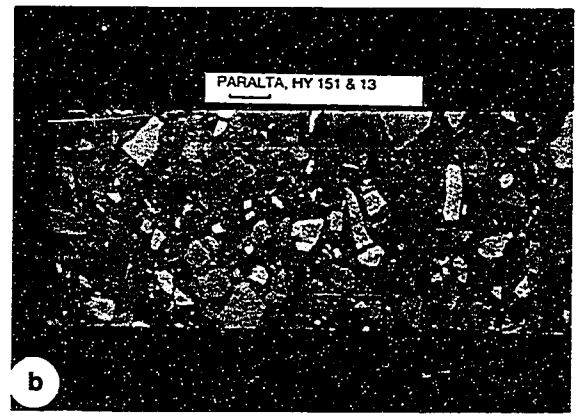
PARALTA, HY 151 & 13
b

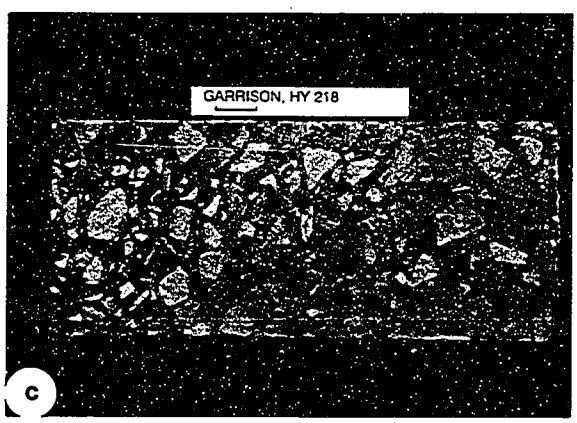
GARRISON, HY 218
c

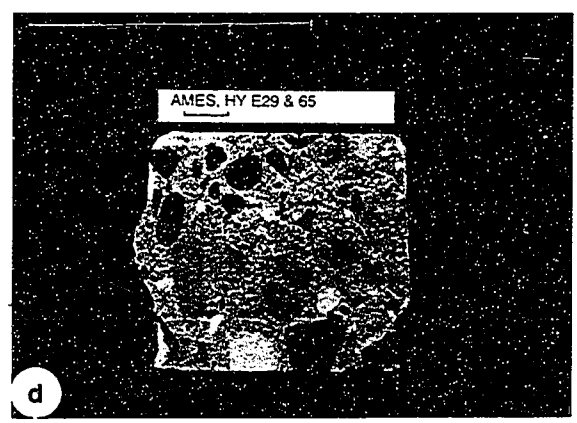
AMES, HY E29 & 65
d

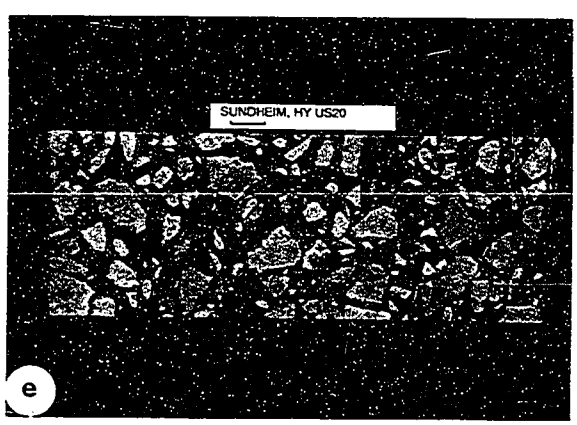
SUNDHEIM, HY US20
e

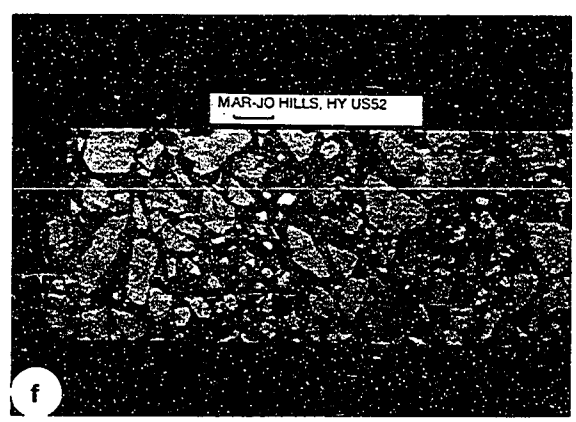
MAR-JO HILLS, HY US52
f

Figure A2 SEM micrographs of non-durable Smith (a) and Paralta (b) quarry concretes, durable Mar-Jo Hills (c) and Sundheim (d) quarry concretes, and dolomite aggregates from Paralta quarry (e) and Sundheim quarry (f).

The Smith and Paralta dolomite aggregates (a and b), which produce concretes with short service lives, are much finer-grained than the Mar-Jo Hills and Sundheim dolomite aggregates (c and d) which produce highly durable concretes.

The magnification of the Paralta dolomite (e) is 3 times that of the Sundheim dolomite (f). The Paralta quarry dolomite is very finely crystalline, with abundant euhedral and subhedral dolomite crystals, is highly porous, and contains small unidentified minerals, possibly clays, in voids. The Sundheim quarry dolomite, in contrast, consists of tightly intergrown dolomite crystals, and has almost no voids between the crystals.

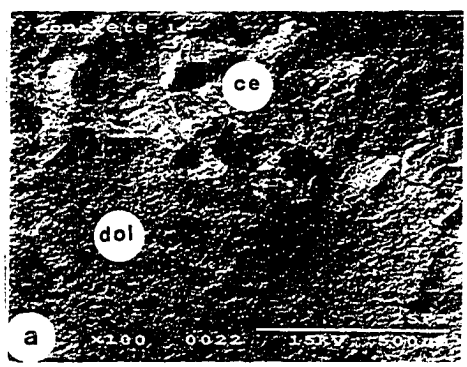
ce
dol
a

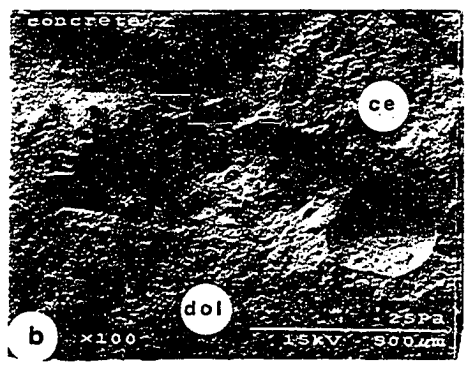
ce
dol
b

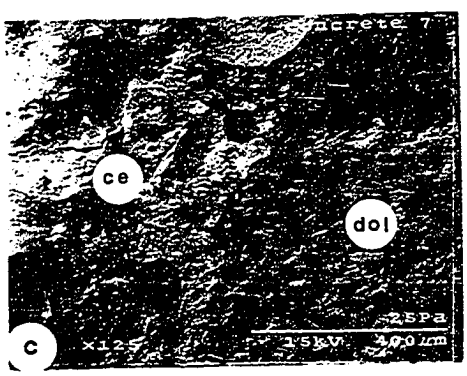
ce
dol
c

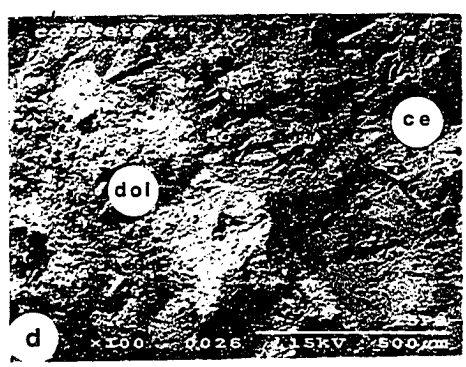
ce
dol
d

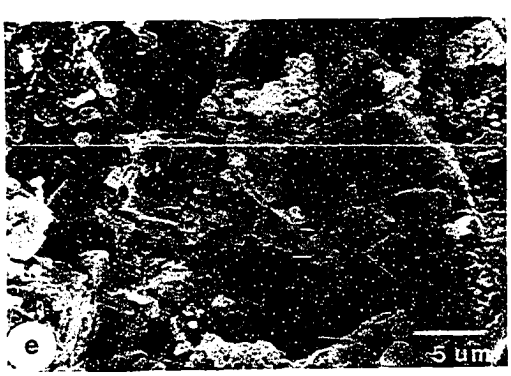
5 um
e

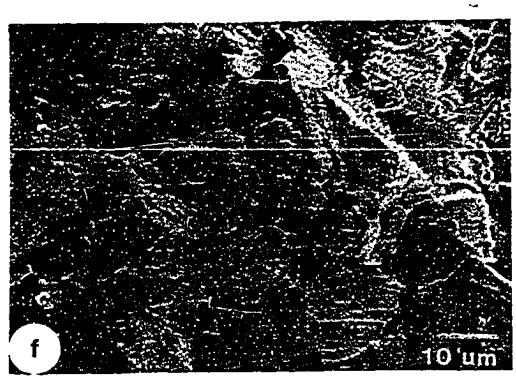
10 um
f

Figure A3 SEM and light micrographs of Sundheim, Paralta and Smith quarry concretes.

a. SEM micrograph of a section through durable Sundheim quarry concrete. Many small spherical to sub-spherical grains with concentric lamination (representatively shown by arrows) are present in the cement paste. The concentric structure is not easy to see here because of low magnification. EDAX data indicate that the major components of these grains are Ca and Si, possibly suggesting that they are calcium silicate hydrates.

b. SEM micrograph of a section through non-durable Paralta quarry concrete. Many small spherical to sub-spherical grains (representatively shown by arrows) with abundant micro-cracks are present in cement paste. These grains are possibly calcium silicate hydrates.

c-d. Light micrographs of the dolomite aggregate - cement paste interface in non-durable Smith quarry concrete, in plane-polarized light and between cross-polarizer, respectively. Boundaries between different zones are gradational except for that between zones C and D. Dark and light-colored dolomite reaction rims are best seen in plane-polarized light, whereas light-colored cement reaction rim is best distinguished from cement paste interior between cross-polarizer. Bar = 250 μm.

e-f. SEM micrographs of dolomite aggregate - paste interface in non-durable Smith quarry concrete. Figures A3e and A3f show the same area as A3c-d and A4a-b, respectively. Boundaries between different zones are gradational except for that between zones C and D. Compared to zone A, zone B is more porous, and zone C is less porous. Zone D is much brighter (whiter) than zone E. Most micro-cracks are visible in zone E rather than zone D, and some air voids are filled with secondary materials.

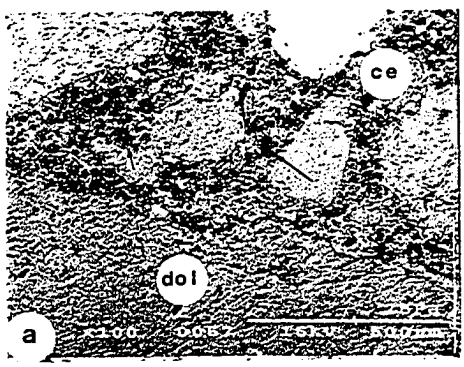
ce
dol
a

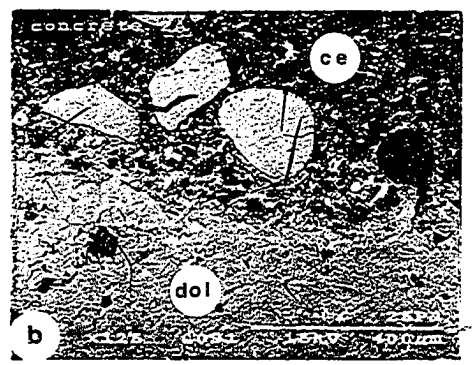
ce
dol
b


A
B
C
D
E
c

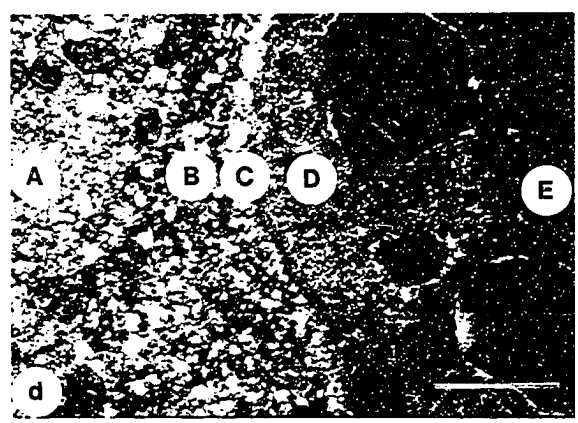
A
B
C
D
E
d

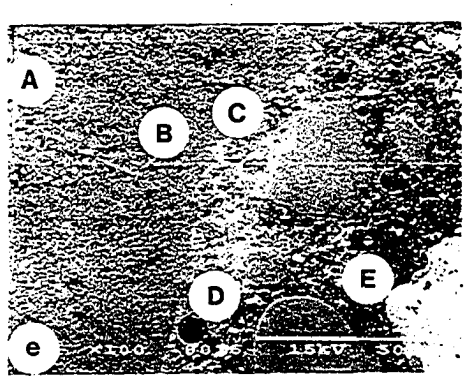
A
B
C
D
E
e

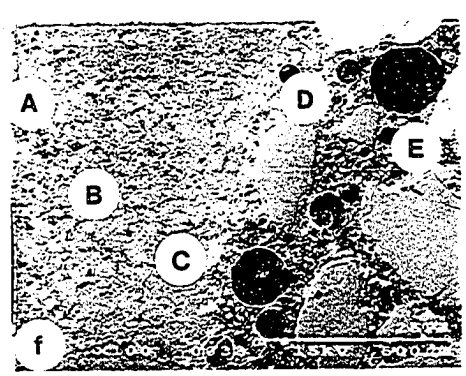
A
B
C
D
E
f

Figure A4 SEM and light micrographs of Smith and Paralta quarry concretes.

a-b. Light micrographs of the dolomite aggregate - cement paste interface in non-durable Smith quarry concrete, in plane-polarized light and between cross-polarizer, respectively. Boundaries between different zones are gradational except for that between zones C and D. Zone B seems to contain smaller and fewer dolomite crystals than zone A. Figure B1 shows an electron microprobe traverse at the interface. Figure B2 shows EDAX elemental maps of the central portion of the above photographs. Bar = 250 μm.

c-d. Light micrographs of the dolomite aggregate - cement paste interface in non-durable Paralta quarry concrete, in plane-polarized light and between cross-polarizer, respectively. Boundary between zones A and B, or between zones C and D is gradational. Zone C is absent at the interface. Bar = 500 μm.

e. SEM micrograph of the central portion of Figures A4c-d. Note the variable width of the light-colored cement paste rim, zone D, the high porosity of the inner region of the dark dolomite reaction rim, zone B, and the reduced porosity of the outer part of zone B.

f. Enlarged SEM view of the left side of Figure A4e. In zone B, interstitial voids have been filled secondary minerals. Between the more porous inner part and less porous outer part of zone B, there is a crack which is parallel to the aggregate - paste interface. The crack is filled with minerals that appear white and gray in SEM views. There are many micro-cracked grains in the cement paste, as indicated by arrows. Refer to Figure B3 for EDAX elemental maps of the area.

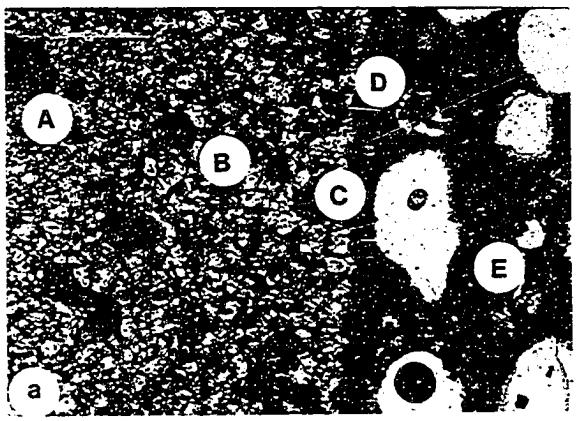
A
B
C
D
E
a

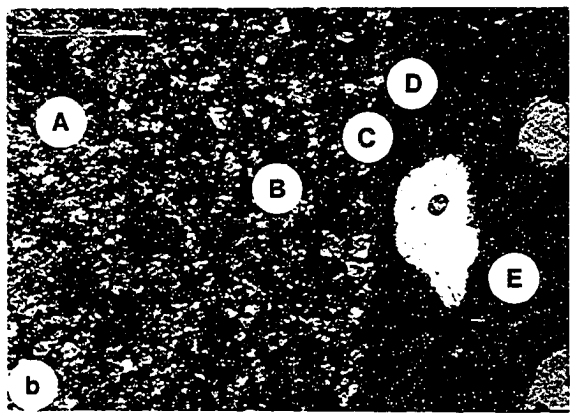
A
B
C
D
E
b

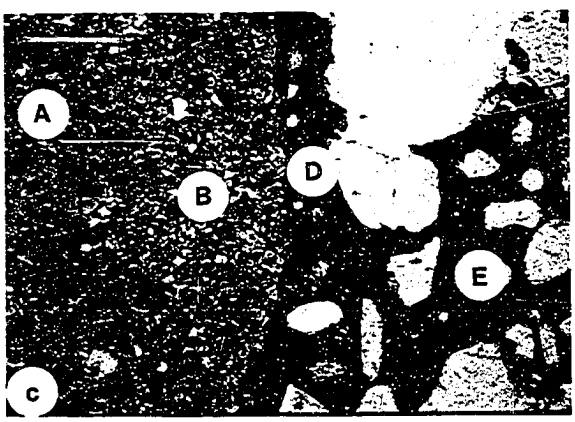
A
B
D
E
c

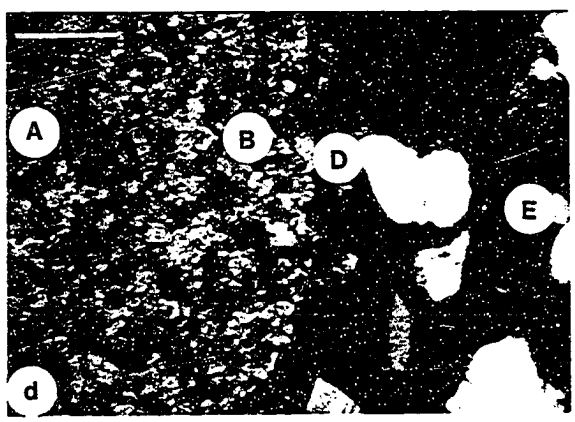
A
B
D
E
d

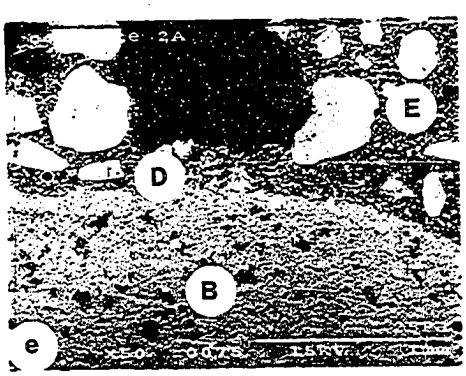
E
D
B
e

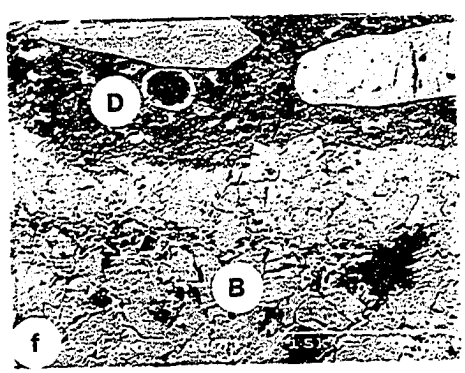
D
B
f

Figure A5 Light and SEM micrographs of Paralta and Smith quarry concretes.

a-b. Light micrographs of the dolomite aggregate - cement paste interface in non-durable Paralta quarry concrete, in plane-polarized light and between cross-polarizer, respectively. Zone C is absent at the interface. Zone B is relatively narrow, and the boundary between zones B and A is difficult to define from the photographs. The horizontal dark straight line across the photographs represents an electron microprobe traverse, which is shown in Figure B4. Bar = 250 μm.

c-d. SEM micrographs of the dolomite aggregate - cement paste interface of non-durable Smith quarry concrete. The light-colored dolomite reaction rim, zone C, is absent. Zone B is very porous and some voids are filled with new minerals. Note the variable width of zone D, and the micro-cracked grains in zone E, as indicated by arrows. The air-void is filled with new minerals.

e-f. Light micrographs of the dolomite aggregate - cement paste interface in non-durable Paralta quarry concrete, in plane-polarized light and between cross-polarizer, respectively. No reaction rims are evident at the interface. Bar = 500 μm.

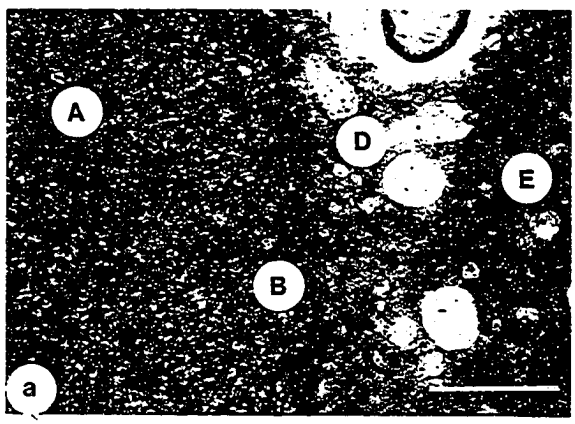
A
D
E
B
a

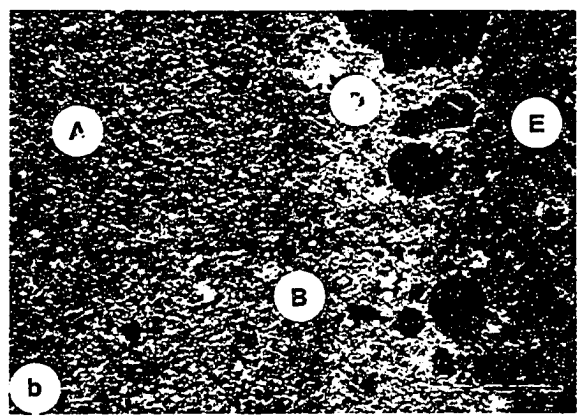
A
E
B
b

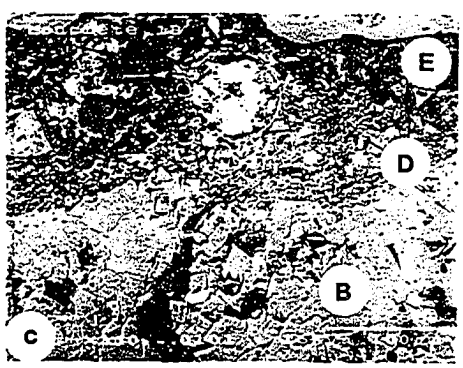
E
D
B
c

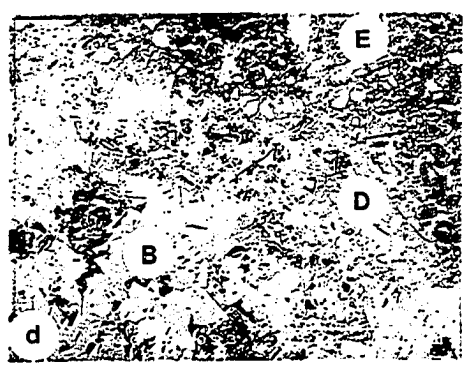
E
D
B
d

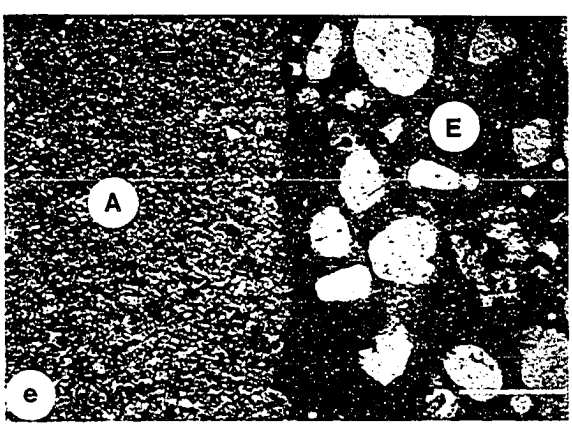
E
A
e

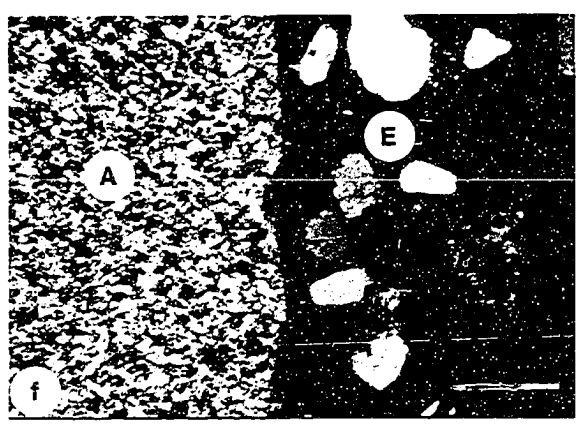
E
A
f

Figure A6 Light and SEM micrographs of durable Mar-Jo Hills and Sundheim quarry concretes.

a-b. Light micrographs of the aggregate - paste interface in durable Mar-Jo Hills quarry concrete with plane-polarized light and cross-polarizer, respectively. No reaction rims are observable in dolomite or paste at the interface. Bar = 250 μm.

c-d. Light micrographs of the aggregate - paste interface in durable Sundheim quarry concrete with plane-polarized light and cross-polarizer, respectively. No reaction rims are observable in dolomite or paste at the interface. Refer to Figure B6 for electron microprobe traverse at the interface. Bar = 500 μm.

e. SEM micrographs of the left side of Figures A6c-d. No reaction rim is visible in dolomite aggregate or cement paste.

f. Enlarged SEM view of the central portion of Figure A6e. No reaction rim is visible in dolomite aggregate or cement paste. A very few micro-cracks are visible in the paste.

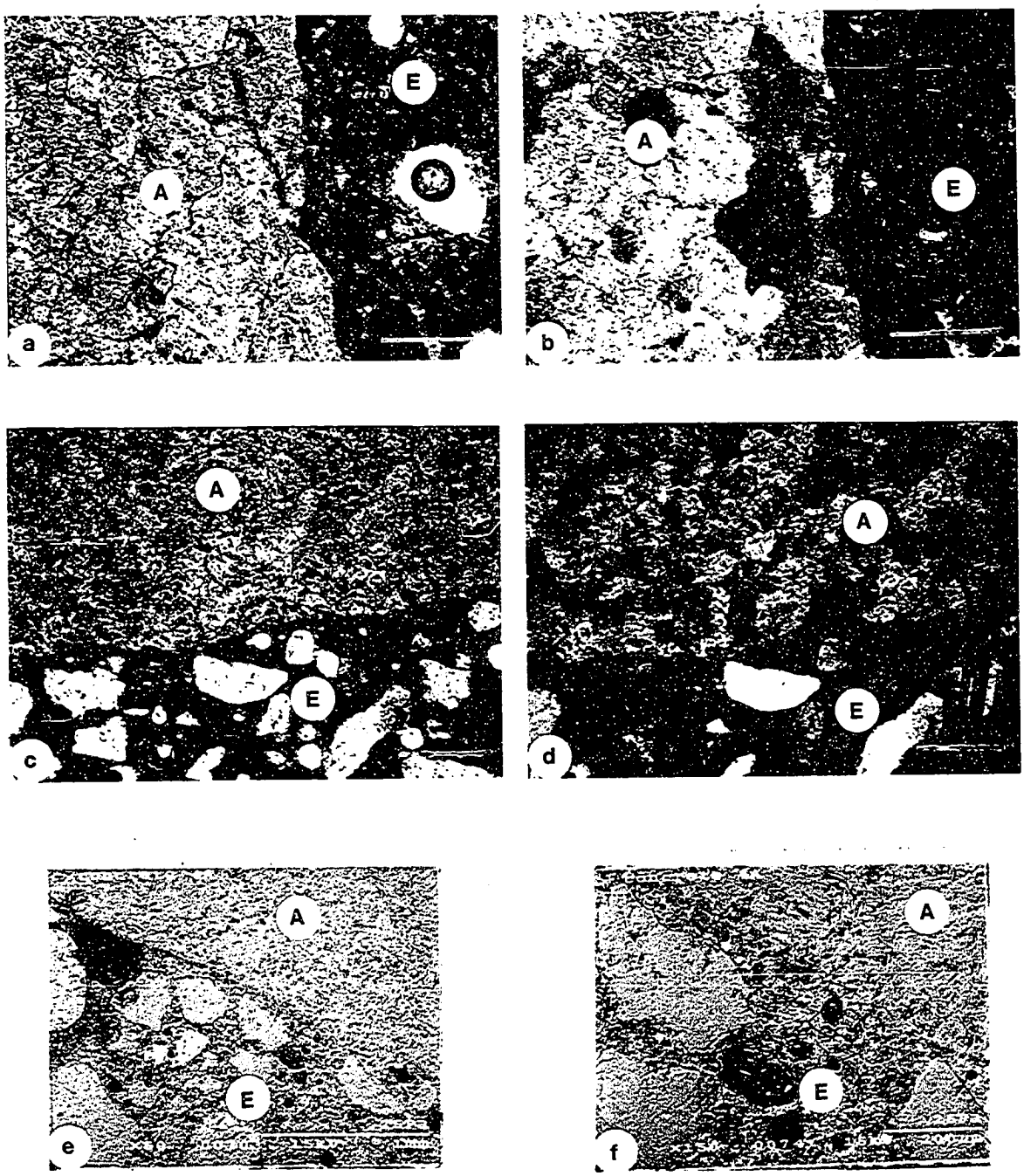
a
A
E
b
A
E
c
A
E
d
A
E
e
A
E
f
A
E

Figure A7 Light and SEM micrographs of durable Mar-Jo Hills and Sundheim and non-durable Smith quarry concretes.

a-b. Light micrographs of the aggregate - paste interface in durable Mar-Jo Hills quarry concrete with plane-polarized light and cross-polarizer, respectively. Boundary between zones A and B, or between zones D and E, is gradational. Bar = 500 μm.

c-d. Light micrographs of the aggregate - paste interface in durable Sundheim quarry concrete with plane-polarized light and cross-polarizer, respectively. Reaction rims, zones C and D, are relatively narrow. See Figure B8 for electron microprobe traverse at the interface. Bar = 500 μm.

e. SEM micrograph of interior part of Mar-Jo Hills dolomite aggregate particle. The dolomite is well-crystallized. Note the bright euhedral clay particle (possibly illite) in the central portion of the photograph. Refer to Figure B9 for corresponding EDAX elemental maps.

f. SEM micrograph of the aggregate - paste interface in non-durable Smith quarry concrete. The left part shows zone B and the right part shows zone D. Note the high porosity of the inner part of zone B and the reduced porosity of the outer part of zone B. Figure B10 gives corresponding EDAX elemental maps. Also note the tiny holes in a row in dolomite aggregate caused by beam damage during electron microprobing.

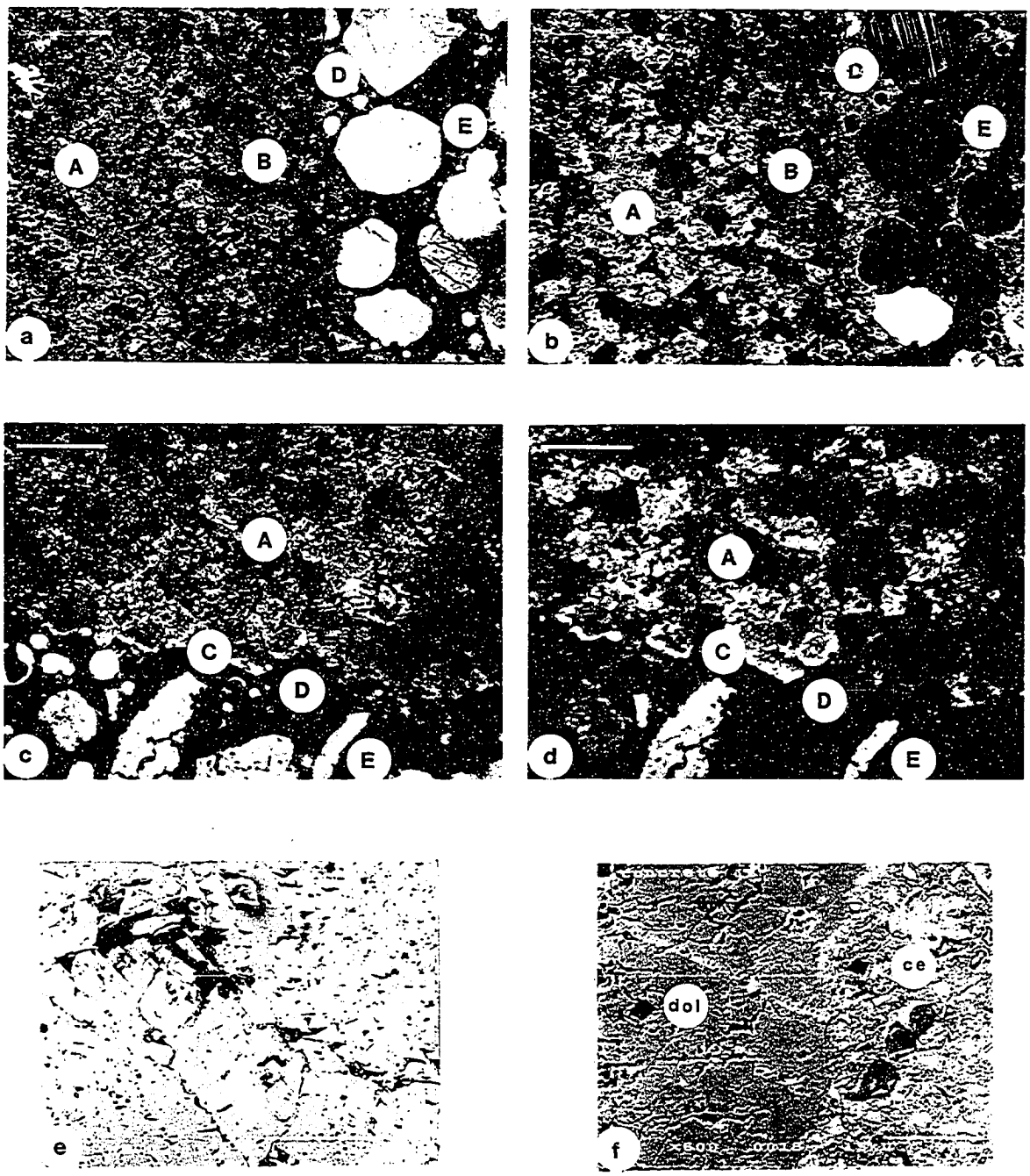
A
B
D
E
a
A
B
D
E
b
A
C
D
E
c
A
C
D
E
d
e
dol
ce
f

Figure A8 Experimentally-produced deterioration of Iowa highway concretes. The concretes contain aggregates from Smith (a), Paralta (b), Garrison (c), Ames gravel pit (d), Sundheim (e), and Mar-Jo Hills (f) quarries.

All of the concretes exhibited marked cracks (shown by arrows) and browning paste discoloration from CaWD cycles. All concretes showed severe crumbling and decomposition, and dark brown paste discoloration from MgWD cycles, whereas concretes exhibited little deterioration from NaWD cycling. Bar scale in cm and mm.

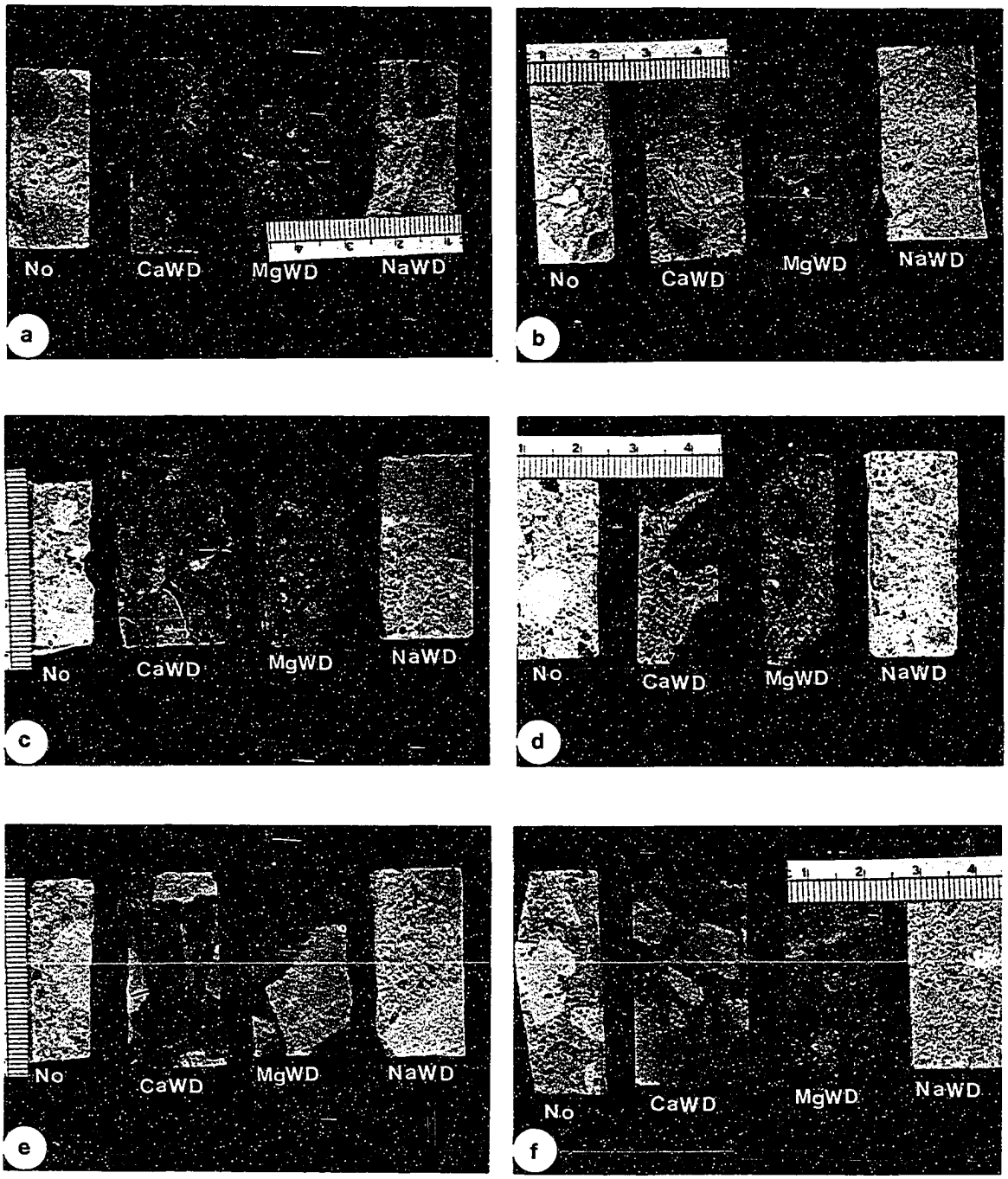
No
CaWD
MgWD
NaWD
a
No
CaWD
MgWD
NaWD
b
No
CaWD
MgWD
NaWD
c
No
CaWD
MgWD
NaWD
d
No
CaWD
MgWD
NaWD
e
No
CaWD
MgWD
NaWD
f

Figure A9 Experimentally-produced deterioration of concretes containing Smith, Garrison, Sundheim, and Mar-Jo Hills dolomite aggregates.

a. Smith quarry concrete
b. Garrison quarry concrete
c. Sundheim quarry concrete
d. Mar-Jo Hills quarry concrete
e. Smith quarry concrete
f. Garrison quarry concrete

Essentially no deterioration was observed from wet/dry cycles in water and NaCl solutions. All concretes exhibited a slightly brown discoloration of cement paste in $CaCl_2$ solution with freeze/thaw cycling, and all exhibited severe crack development and darker brown paste discoloration after wet/dry cycling in $CaCl_2$ solution. Cement paste in concretes showed light brown discoloration during MgFT cycling, and dark brown discoloration and severe decomposition from MgWD cycles. Bar scale in cm and mm.

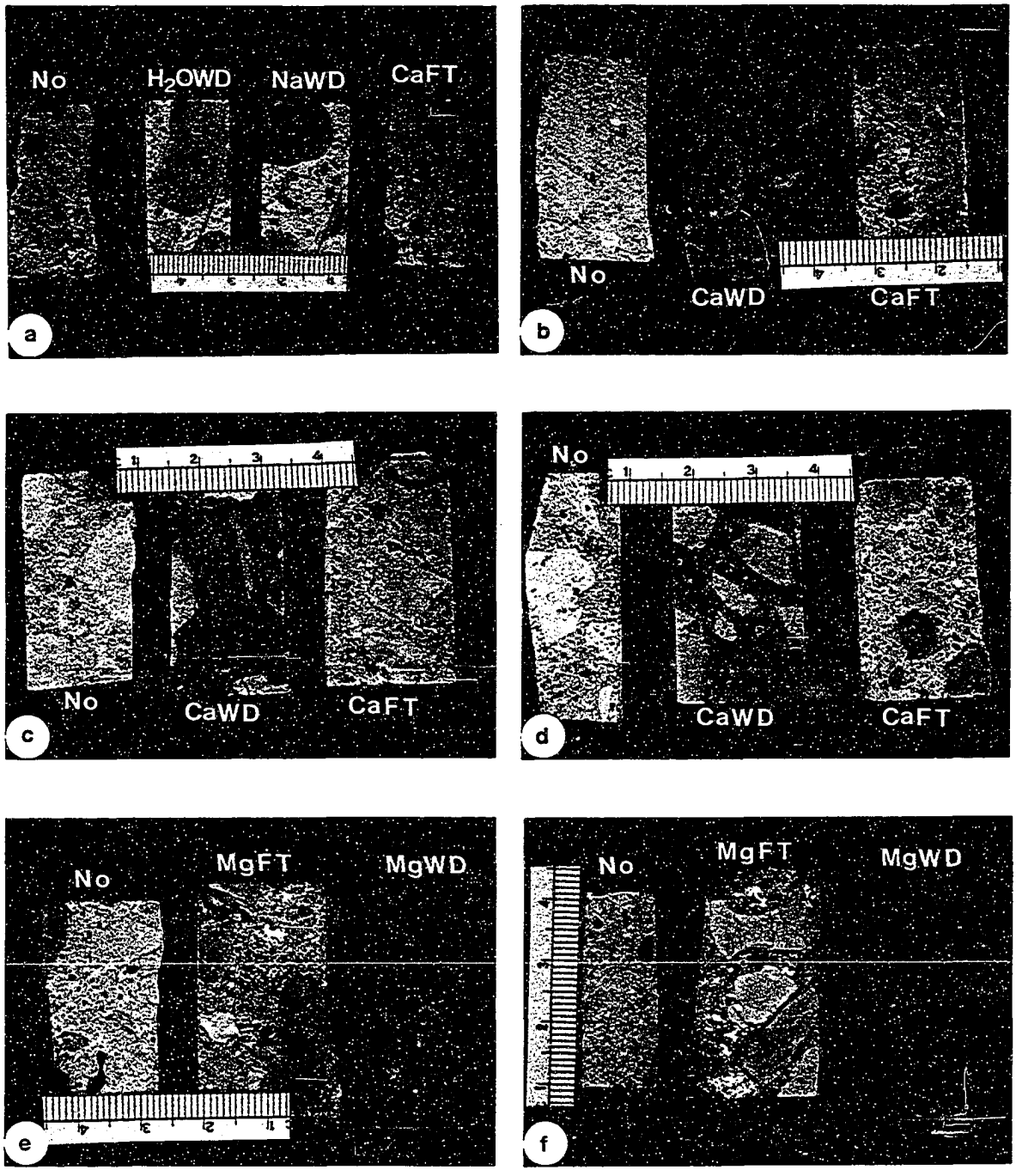
No
H_2OWD
NaWD
CaFT
a
No
CaWD
CaFT
b
No
CaWD
CaFT
c
No
CaWD
CaFT
d
No
MgFT
MgWD
e
No
MgFT
MgWD
f

Figure A10 Experimental deterioration of concretes and micrographs of treated concretes.

a. Experimental deterioration of Mar-Jo Hills quarry concrete in $MgCl_2$ solution. Cement paste in concretes showed light brown discoloration during MgFT cycling, and dark brown discoloration and severe decomposition from MgWD cycles. Bar scale in cm and mm.

b-d. Experimental deterioration of Mar-Jo Hills (**b**), Paralta (**c**), and Ames gravel pit (**d**) quarry concretes in NaCl solution. Almost no paste decomposition and discoloration occurred during wet/dry and freeze/thaw conditions. Bar scale in cm and mm.

e. SEM micrograph of Garrison quarry concrete from CaWD cycling. Cracks are evident in cement paste and at the aggregate / paste interface. Air-voids and cracks are partially or fully filled with late-formed materials. See Figure B11 for the corresponding EDAX elemental maps.

f. Light micrograph, with cross-polarizer, showing experimental deterioration of Paralta quarry concrete from CaWD cycling. Boundaries between zones Ae and Be, and between De and Ee, are gradational. Dark and light dolomite reaction rims, zones Be and Ce respectively, are continuous along the aggregate edge where dolomite aggregate was in contact with $CaCl_2$ solution (lower left) and along the margins of aggregate in contact with paste. Both zones Be and Ce look similar to, but are much wider than, zones B and C in untreated concrete as shown in Figures A3c-d.

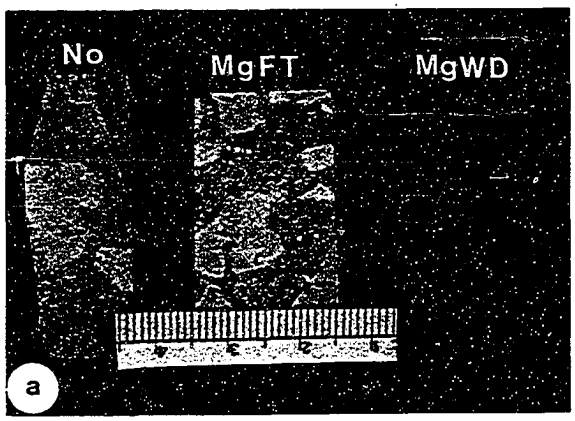
No
MgFT
MgWD
a

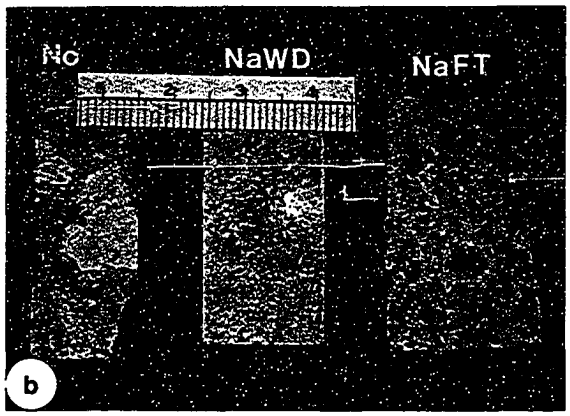
No
NaWD
NaFT
b

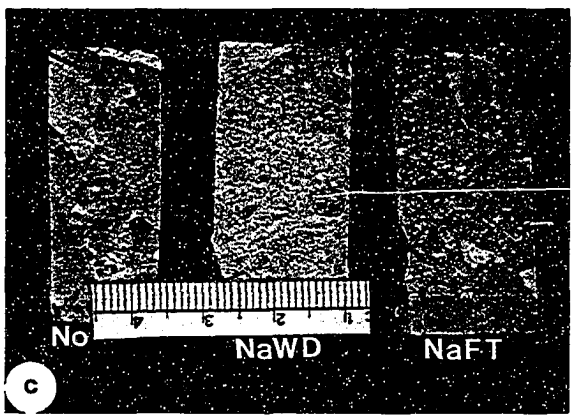
No
NaWD
NaFT
c

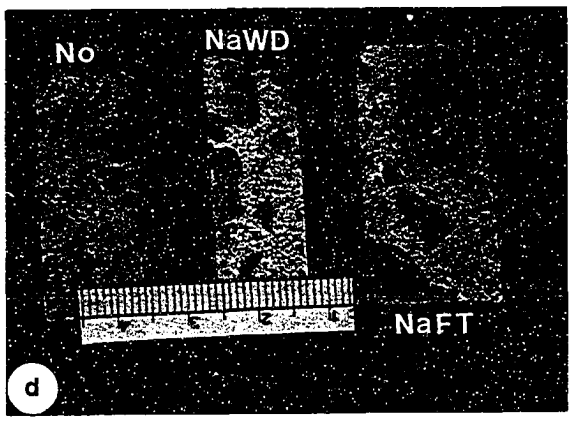
No
NaWD
NaFT
d

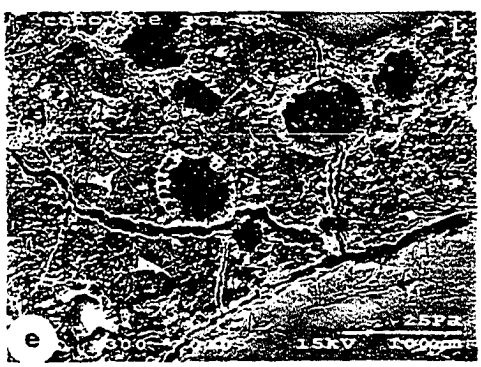
e

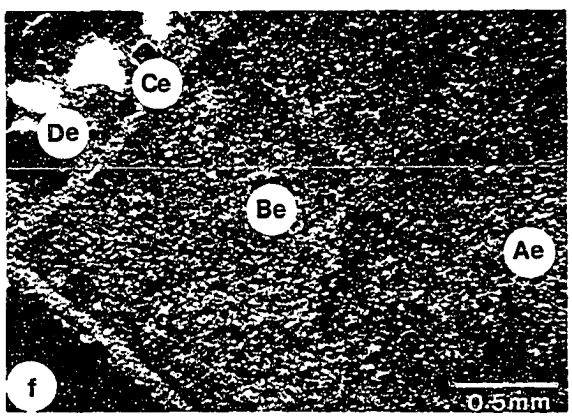
Ce
De
Be
Ae
f
0.5mm

Figure A11 Light and SEM micrographs showing experimental deterioration of Paralta and Smith quarry concretes.

a-b. Light micrographs, with plane-polarized light and cross-polarizer, of the aggregate - paste interface in Paralta quarry concrete after CaWD cycling. Dark and light-colored dolomite rims, zones Be and Ce, are visible at the interface and along the crack within the aggregate interior. These two dolomite rims look similar to, but are much wider than, dolomite rims in untreated concrete, zones B and C, as shown in Figures A3c-d. See Figure B12 for electron microprobe traverse.

c. SEM micrograph of Paralta quarry concrete after CaWD treatment. It shows almost the same area as Figures A11a-b.

d. Enlarged SEM view of the central portion of Figure A11c. Zones Be and, especially, zone Ce, contain abundant void-filling interstitial materials, and the porosity of the light-colored dolomite rim, zone Ce, is less than that of the dark dolomite rim, zone Be. Refer to Figure B13 for corresponding EDAX elemental maps.

e. Light micrograph, with cross-polarizer, of Paralta quarry concrete after CaFT treatment. The aggregate - paste interface is very similar to that in CaWD-treated concrete, as shown in Figures A10f and A11a-b, but zones Be and Ce are much wider than zones B and C in untreated concrete as shown in Figures A3c-d. Refer to Figure B14 for corresponding electron microprobe traverses.

f. Light micrograph, with cross-polarizer, of Smith quarry concrete after CaWD cycling. The aggregate - paste interface resembles that in untreated concrete shown in Figures A3c-d and A4a-b, but looks different from that shown in Fig. A10f and A11a-b in having a thinner light dolomite rim, zone Ce. Figure B15 gives the corresponding electron microprobe traverse.

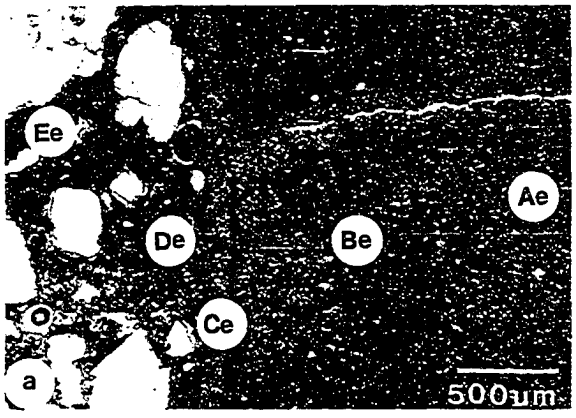
Ee
Ae
De
Be
Ce
a
500um

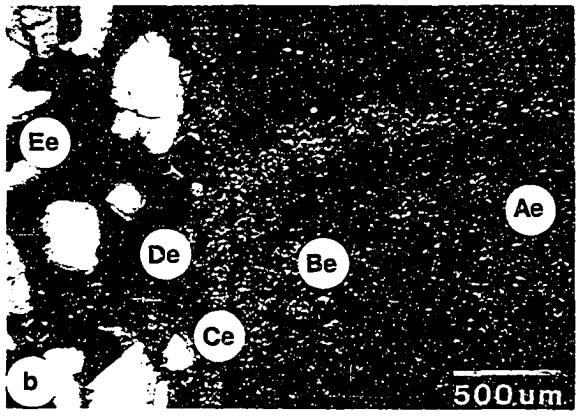
Ee
Ae
De
Be
Ce
b
500um

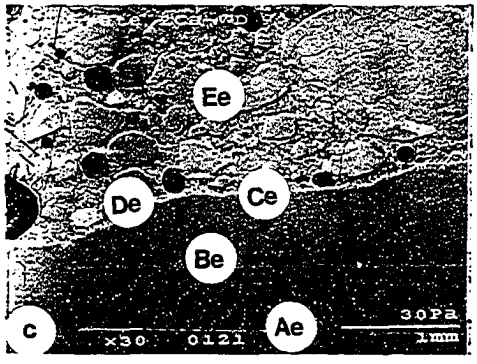
Ee
De
Ce
Be
c
x30
Ae
30Pa
1mm

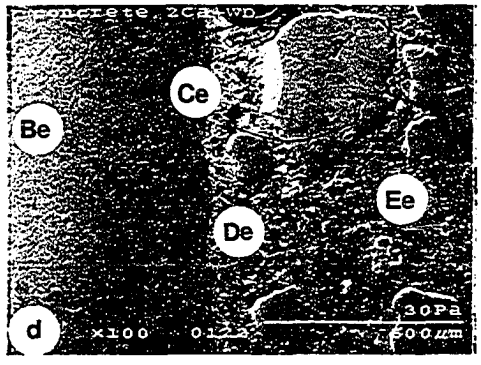
Ce
Be
Ee
De
d
x100
30Pa

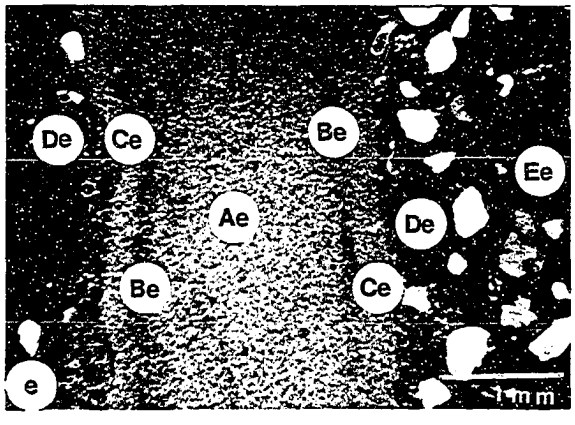
De
Ce
Be
Ee
Ae
De
Be
Ce
e
1mm

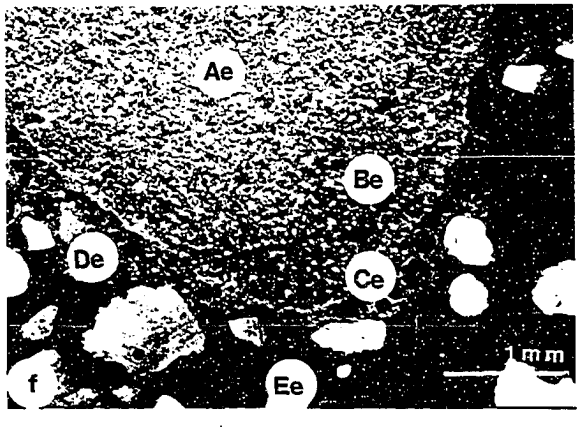
Ae
Be
De
Ce
mm
f
Ee

Figure A12 Experimental deterioration of Mar-Jo Hills quarry concrete.

a-b. Light micrographs, with plane-polarized light and cross-polarizer, of the aggregate - paste interface in Mar-Jo Hills quarry concrete after CaWD cycling. No reaction rims are visible in coarse aggregate or cement paste after wet/dry cycling in $CaCl_2$ solution. Cement paste shows cracks after experimental treatment. The white patch in dolomite aggregate (left-bottom) is due to the removal of carbon-coating. Figure B16 shows electron microprobe traverse at the interface.

c-d. Light micrographs, with plane-polarized light and cross-polarizer, of the aggregate - paste interface in Mar-Jo Hills quarry concrete after CaFT cycling. Experimental treatment did not produce reaction rims at the interface, but led to the cracking of cement paste. Figure B17 gives electron microprobe traverse at the interface.

e-f. Light micrographs, with plane-polarized light and cross-polarizer, of the aggregate - paste interface in Mar-Jo Hills quarry concrete after MgWD cycling. Cement paste underwent severe decomposition and, in some locations, was completely dissolved away. No reaction rim is visible in either dolomite aggregate or cement paste. See Figure B18 for electron microprobe traverse at the interface.

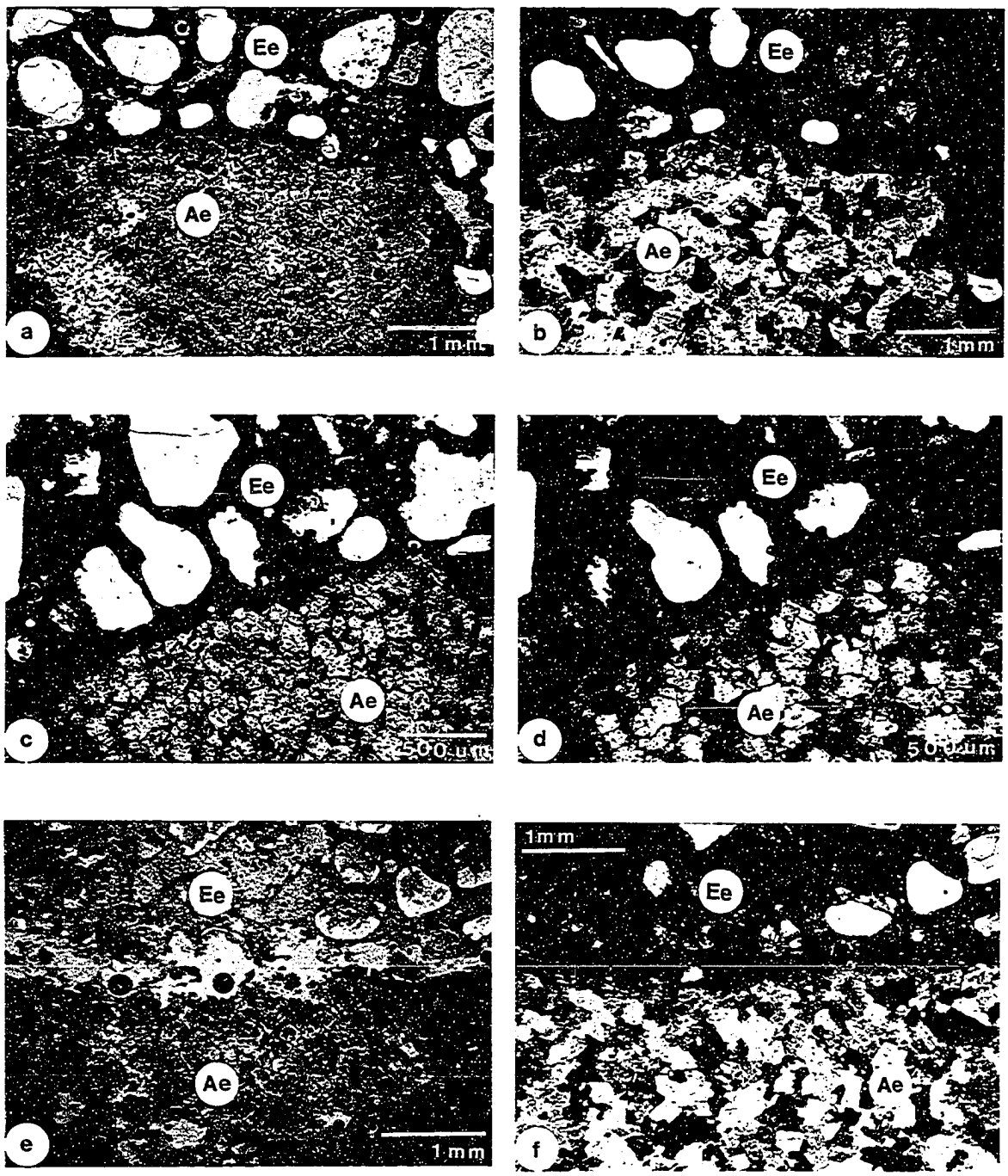
Ee
Ae
a
1 mm
Ee
Ae
b
1 mm
Ee
Ae
c
500 µm
Ee
Ae
d
500 µm
Ee
Ae
e
1 mm
1 mm
Ee
Ae
f

Figure A13 Experimental deterioration of Mar-Jo Hills and Garrison quarry concretes after $MgCl_2$-solution treatment.

a-b. SEM micrographs of aggregate - paste interface of durable Mar-Jo Hills quarry concrete after MgWD cycling. Figure A13b shows the enlarged central portion of A13a. Micro-cracks in dolomite aggregate are filled with abundant materials which appear white, gray and dark gray in SEM views. Cement paste shows severe cracking and decomposition. Cracks and voids are partially or completely filled with white, gray and dark gray materials which exhibit tiny crystal size, and may show very complex mineralogy. These void- and crack-filling materials also show zonation (see text for details). See Figures B19-B20 for corresponding EDAX elemental maps.

c-d. Light micrographs, with plane-polarized and cross-polarized light, of the interface in non-durable Garrison quarry concrete after MgWD treatment. Zone Ee, dark paste region after wet/dry cycling in $MgCl_2$ solution, exhibits severe cracking and decomposition. The aggregate - paste interface resembles that in untreated concrete as shown in Figures A3c-d and A4a-b. Refer to Figure A13f for corresponding SEM view and Figure B21 for electron microprobe traverse of similar interface.

e-f. SEM micrographs of MgWD-treated Garrison quarry concrete. Figure A13e shows the enlarged central portion of A13f which shows the same area as A13c-d. Zone Be, the dark dolomite rim, is very porous, whereas zone Ce, the light dolomite rim, has reduced porosity. Interstitial voids are filled with abundant white and gray minerals. Zone De, the light paste rim, shows little cracking, whereas zone Ee, the dark cement paste exhibits severe cracking and decomposition. Figure B22 shows the corresponding EDAX maps.


ce
dol
a
30Pa
400μm


b
30Pa
100μm

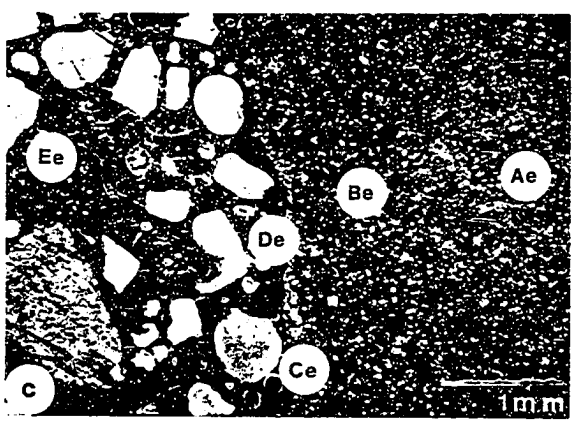
Ee
Be
Ae
De
Ce
c
1mm

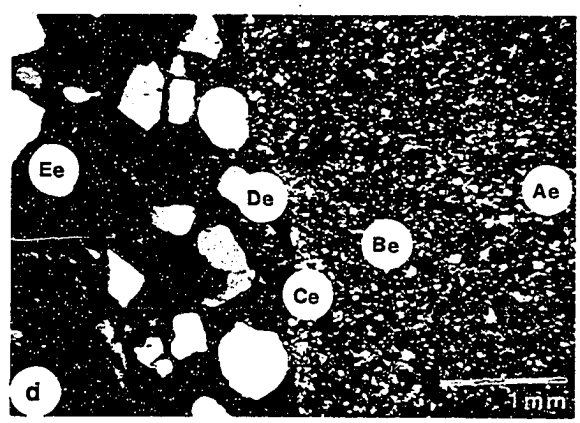
Ee
De
Ae
Be
Ce
d
1mm

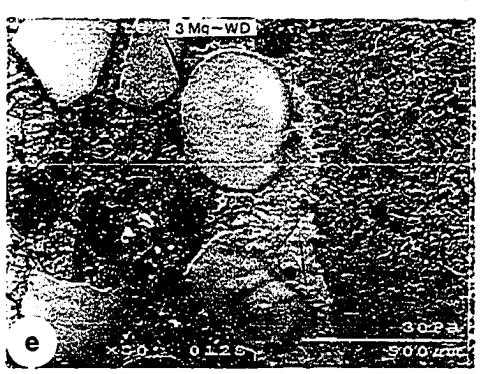
3Mg—WD
e
30Pa

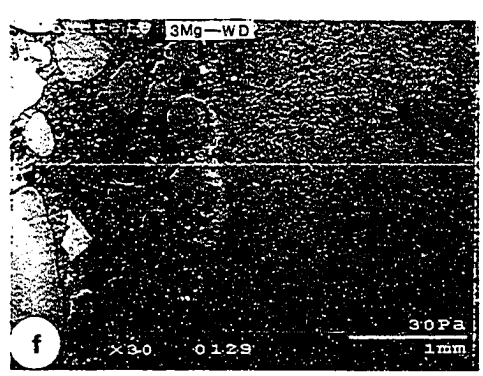
3Mg—WD
f
30Pa
1mm

Figure A14 Experimental deterioration of Paralta quarry concrete after MgWD and NaWD treatments.

a-b. Light micrographs, with plane-polarized light and cross-polarizer, of the interface in non-durable Paralta quarry concrete after MgWD treatment. The interface between aggregate and paste resembles that in untreated concrete as shown in Figures A3c-d and A4a-b. Zone Ee, the dark paste, exhibits severe cracking and decomposition, whereas zone De, the light paste rim, shows little cracking. Refer to Figure B21 for electron microprobe traverse at the interface.

c-d. Light micrographs, with plane-polarized light and cross-polarizer, of the interface in non-durable Paralta quarry concrete after NaWD treatment. Very few effects of experimental treatments are visible. The interface resembles that in untreated concrete as shown in Figures A5a-b. A few cracks developed in the dark cement paste and at the contact between the dark dolomite rim and the light paste rim. Refer to Figure A14f for SEM view and Figure B23 for electron microprobe traverse.

e-f. SEM micrographs of NaWD-treated Paralta quarry concrete. Figure A14f shows the enlarged lower-right portion of A14e which shows almost the same area as A14c-d. Zone Be, the dark dolomite rim, is less porous than porous than zone Ae, dolomite aggregate interior. No severe cracking or decomposition is evident in cement paste after NaCl-solution treatment. See Figure B23 for corresponding electron microprobe traverse, and Figure B24 for EDAX maps.

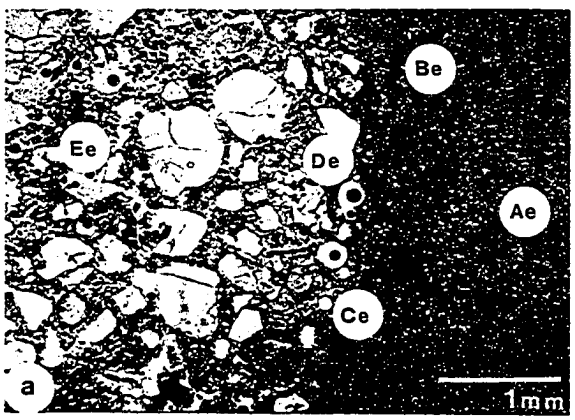
Be
Ee
De
Ae
Ce
a
1mm

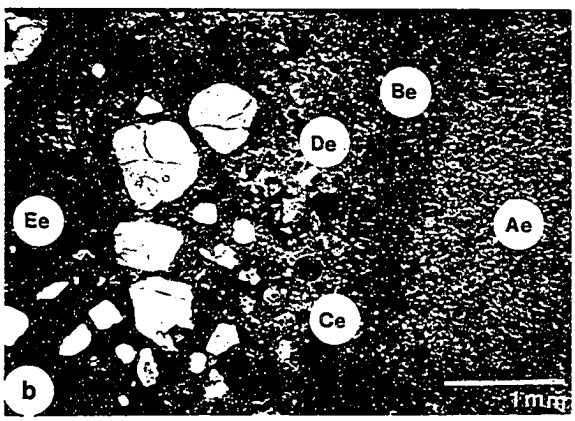
Be
De
Ee
Ae
Ce
b
1mm

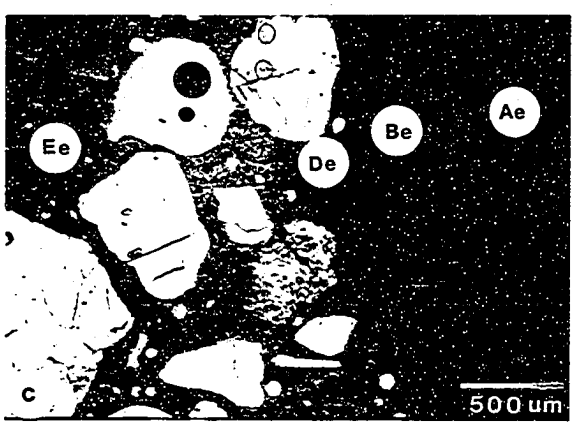
Ae
Be
Ee
De
c
500 um

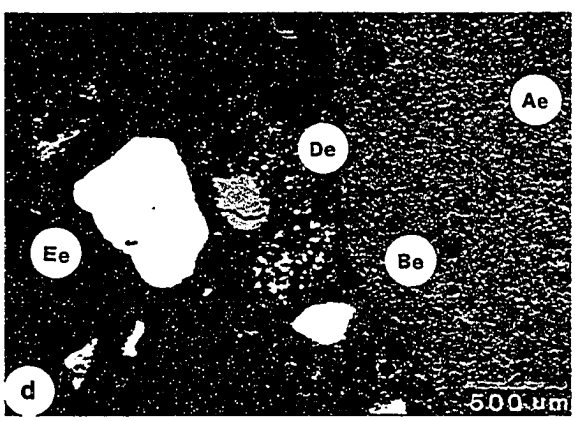
Ae
De
Ee
Be
d
500 um

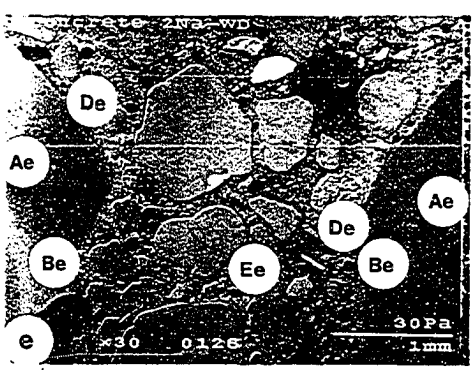
De
Ae
Ae
De
Be
Ee
Be
e
30Pa
1mm

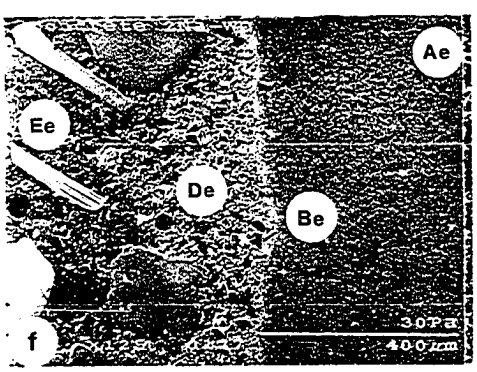
Ae
Ee
De
Be
f
30Pa
400um

APPENDIX B

ELECTRON MICROPROBE TRAVERSES

AND SEM-EDAX ELEMENT MAPS

Figure B1. Electron microprobe traverse across dolomite aggregate - cement paste interface in non-durable Smith quarry concrete.

a. CaO, MgO and SiO_2 traverse.
b. Al_2O_3 and FeO traverse.
c. K_2O and Na_2O traverse.

The light-colored dolomite reaction rim, zone C, shows a significant increase in CaO with a corresponding decrease in MgO, compared to zone A, the "unaffected" dolomite aggregate interior. Zone D is rich in CaO and poor in SiO_2, K_2O and Na_2O, compared to zone E, in which CaO and SiO_2 contents are of the same order. Refer to Figures A3f and A4a-b for SEM and light micrographs and Figure B2 for EDAX element maps of traversed area.

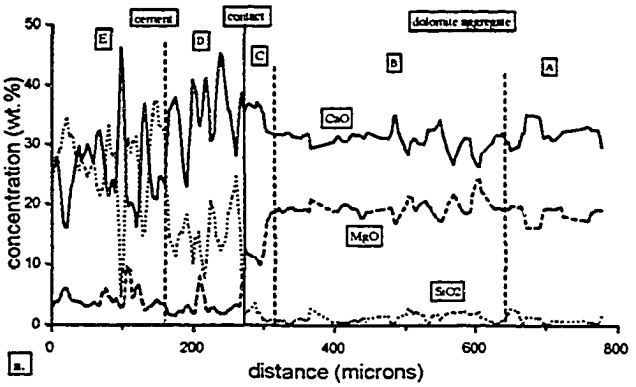
cement
contact
dolomite aggregate
E
D
C
B
A
CaO
MgO
SiO2
concentration (wt.%)
distance (microns)
a.

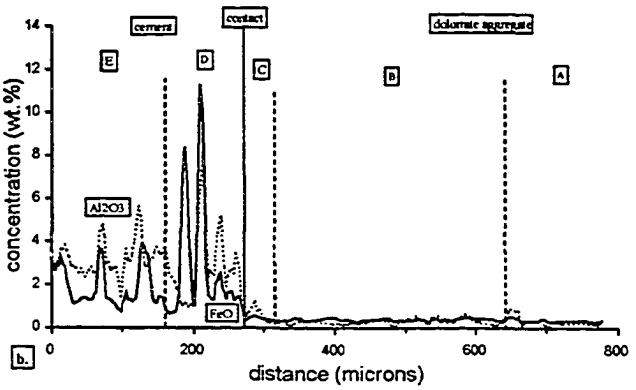
cement
contact
dolomite aggregate
E
D
C
B
A
Al2O3
FeO
concentration (wt.%)
distance (microns)
b.

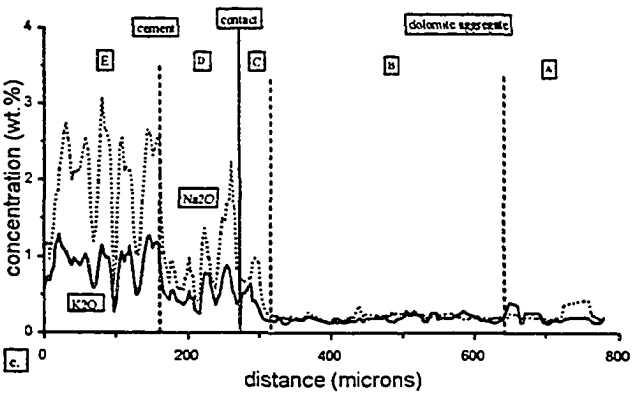
cement
contact
dolomite aggregate
E
D
C
B
A
Na2O
K2O
concentration (wt.%)
distance (microns)
c.

Figure B2. EDAX element maps at dolomite aggregate - cement paste interface in non-durable Smith quarry concrete. The dolomite interior, zone A, is outside of the map, and the right-bottom corner shows a small portion of zone E. Note the S- and Fe-rich spots (possibly pyrite), Si-, Al- and K-rich dots (possibly illite) in dolomite aggregate. Mg- and O-rich dots in dolomite aggregate (rims) and cement paste may indicate brucite. Arrow indicates the evident enrichment of Ca in the light-colored paste reaction rim. Refer to the central part of Figures A3f and A4a-b for corresponding SEM and light micrographs.

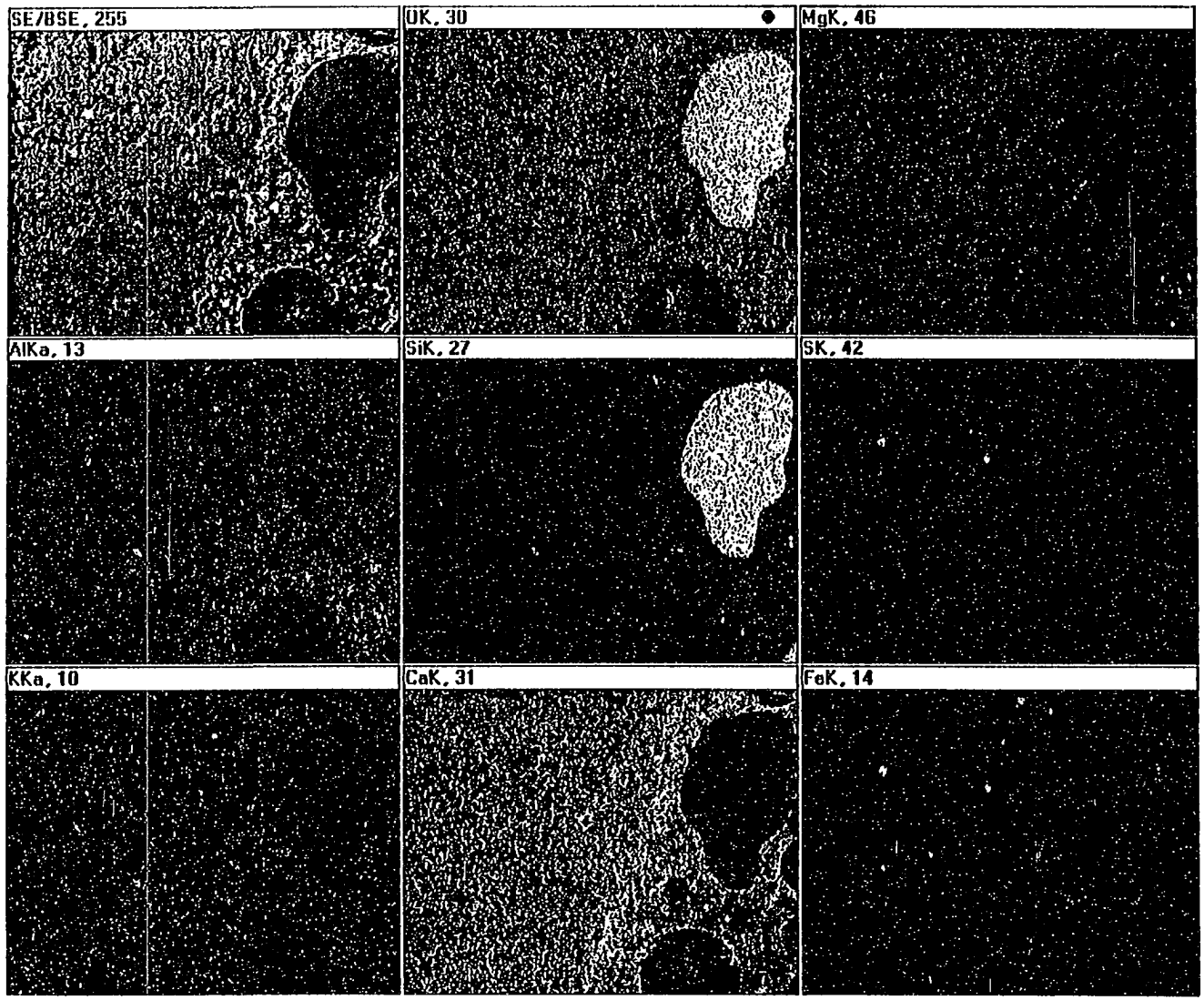
SE/BSE, 255
OK, 30
MgK, 46
AlKa, 13
SiK, 27
SK, 42
KKa, 10
CaK, 31
FeK, 14

Figure B3. EDAX element maps of dolomite reaction rim, zone B, and paste reaction rim, zone D, in non-durable Paralta quarry concrete. Note that voids and cracks in dolomite reaction rim, zone B, are filled with Mg- and O-rich (possibly brucite), and Ca- and O-rich (possibly calcite) materials. Small clay and pyrite inclusions probably are responsible for elevated Al, Si, O, S and Fe in localized concentrations. Small Mg- and O-rich dots in cement paste rim probably indicate brucite. Figure A4f shows the corresponding SEM micrograph.

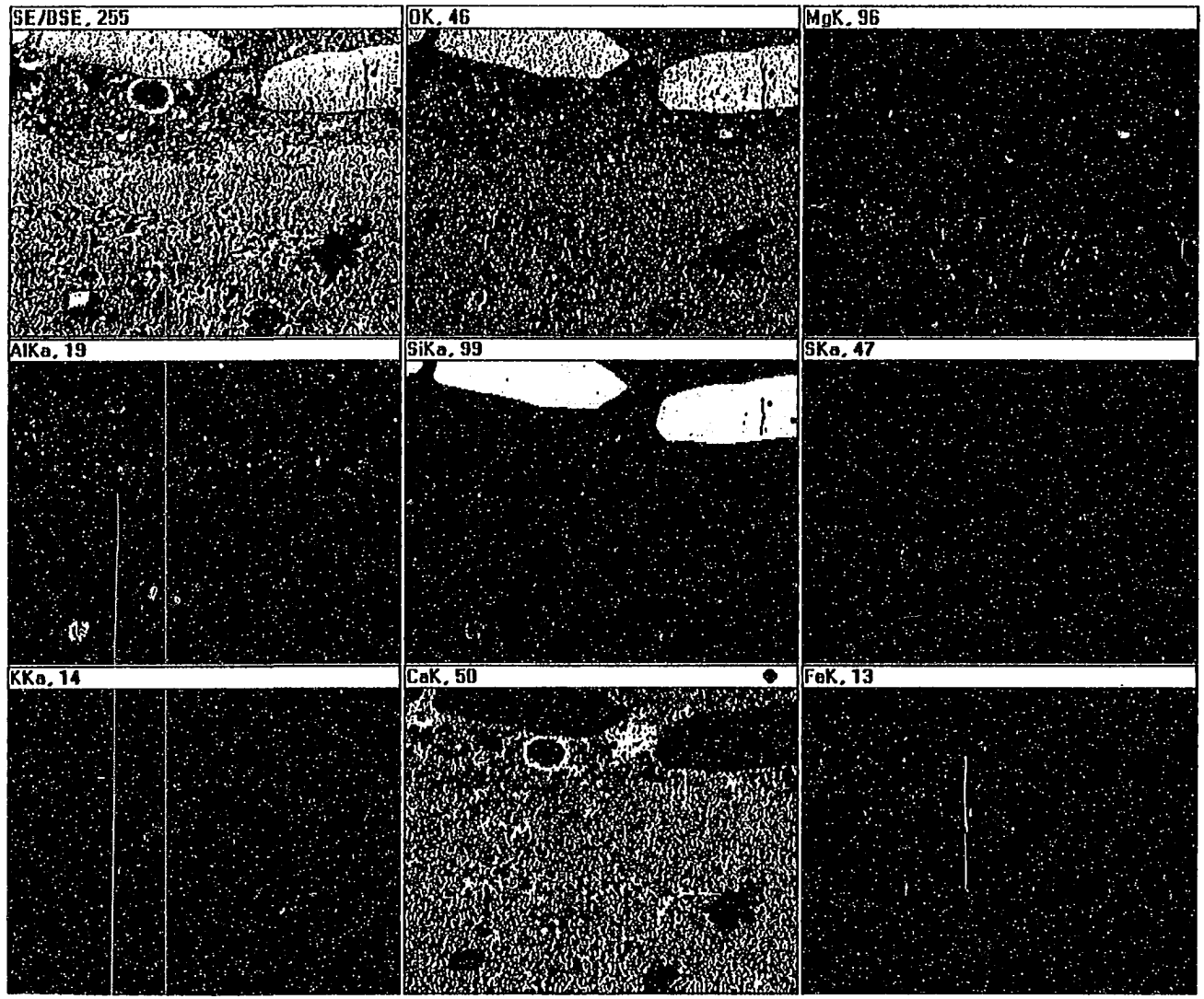
SE/BSE, 255
OK, 46
MgK, 96
AlKa, 19
SiKa, 99
SKa, 47
KKa, 14
CaK, 50
FeK, 13

Figure B4. Electron microprobe traverse across dolomite aggregate - cement paste interface in non-durable Paralta quarry concrete.

a. CaO, MgO and SiO_2 traverse.
b. Al_2O_3 and FeO traverse.
c. K_2O and Na_2O traverse.

Zone C, the light-colored dolomite rim, is absent at the interface, and zone B, the dark dolomite rim, is directly in contact with the paste reaction rim, zone D. CaO is elevated and MgO is significantly reduced in the outer region of zone B. Zone D is extremely enriched in CaO and exhibits a calcitic composition at the aggregate - paste contact. The overall composition of zone E, the cement paste interior, shows almost the same amount of CaO and SiO_2. See Figures A5a-b for light micrographs of corresponding area.

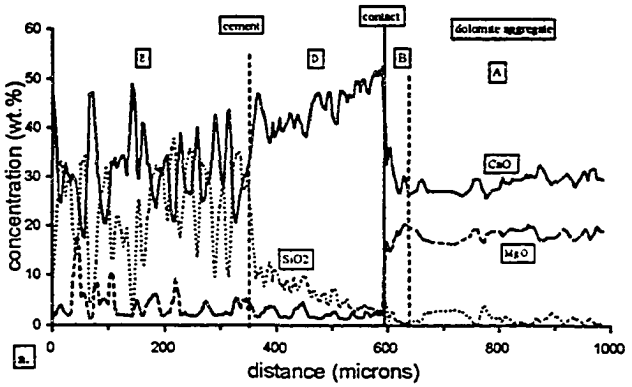
cement
contact
dolomite aggregate
E
D
B
A
CaO
MgO
SiO2
concentration (wt.%)
distance (microns)
a.

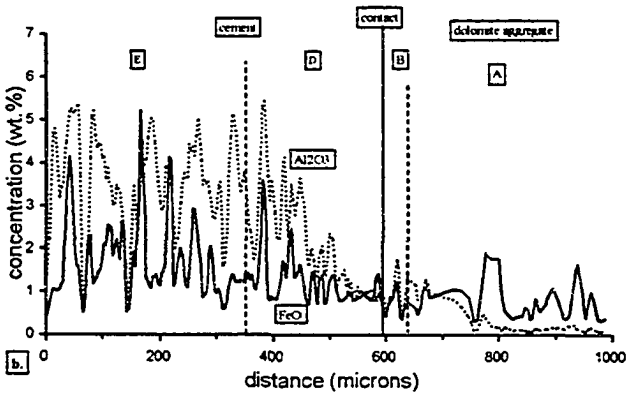
cement
contact
dolomite aggregate
E
D
B
A
Al2O3
FeO
concentration (wt.%)
distance (microns)
b.

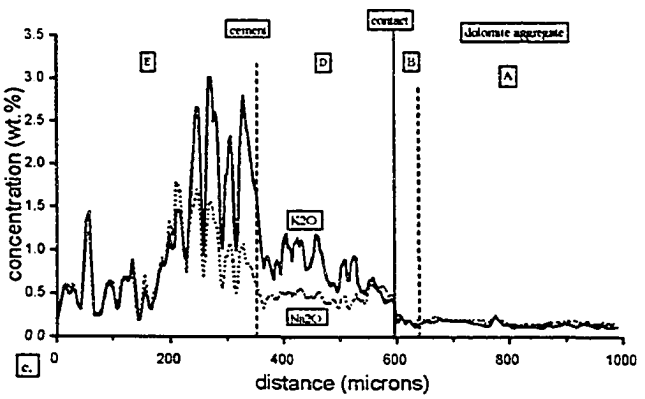
cement
contact
dolomite aggregate
E
D
B
A
K2O
Na2O
concentration (wt.%)
distance (microns)
c.

Figure B5. EDAX element maps for non-durable Smith quarry concrete, showing dolomite aggregate - paste interface corresponding to SEM micrograph in Figure A5c. Voids in porous dolomite reaction rim are filled with Ca-, Mg- and O-rich materials (probably calcite and brucite). Note the Ca- and K-enrichment in cement paste rim, zone D, compared to zone E. The Mg- and O-rich spots in cement paste probably indicate brucite.

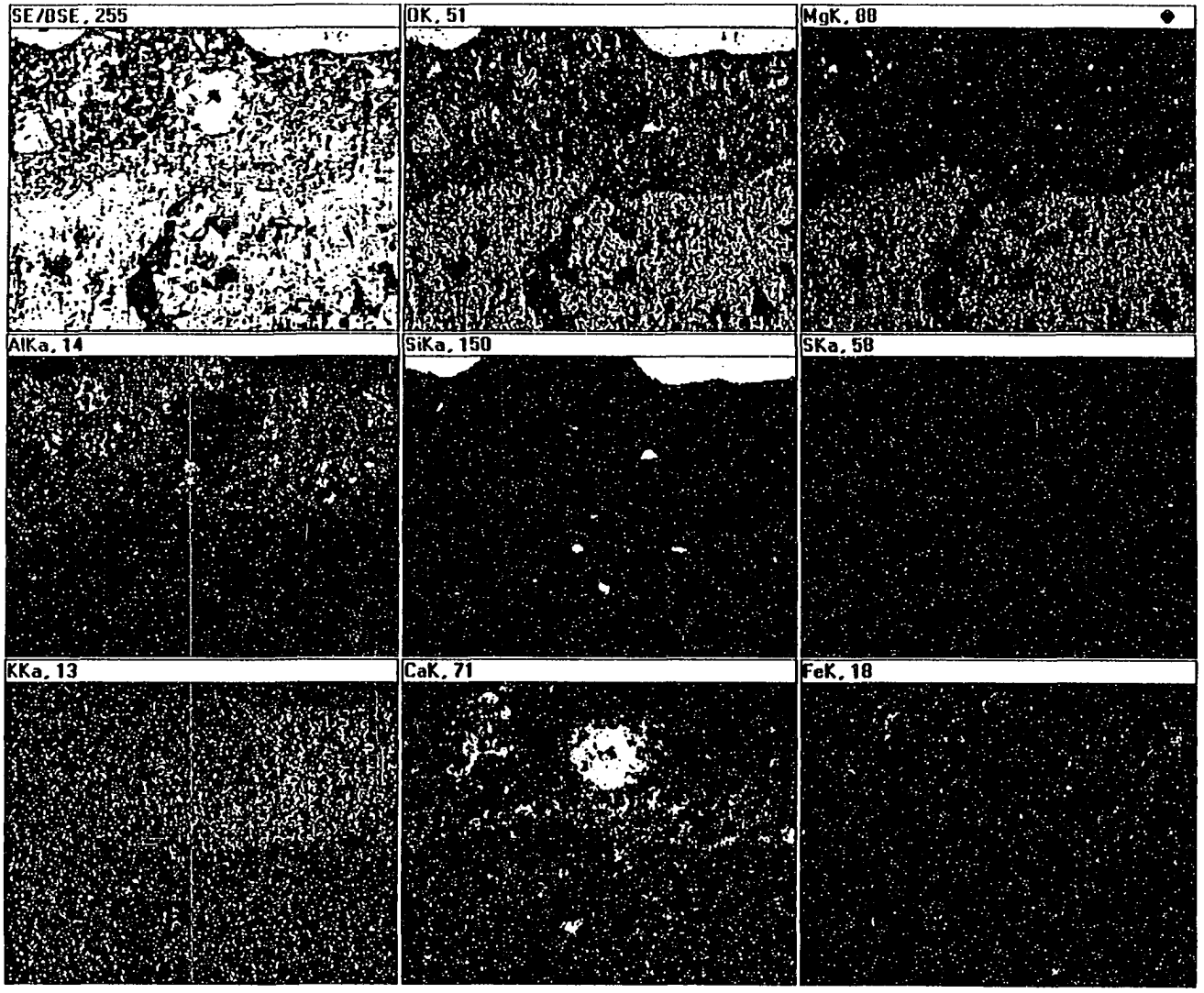
SE/BSE, 255
OK, 51
MgK, 88
AlKa, 14
SiKa, 150
SKa, 58
KKa, 13
CaK, 71
FeK, 18

Figure B6. Electron microprobe traverse through durable Sundheim quarry concrete.

a. CaO, MgO and SiO_2 traverse.
b. Al_2O_3 and FeO traverse.
c. K_2O and Na_2O traverse.

No reaction rims are visible in the dolomite aggregate or cement paste. Dolomite aggregate shows a much more uniform composition than the corresponding aggregate interior in non-durable concretes, as shown in Figures B1 and B4. The sharp enrichment in SiO_2, $Al2O_3$ and K_2O at about 1000 μm site probably indicates illite. Figures A6c-e show corresponding light and SEM micrographs of the traversed area.

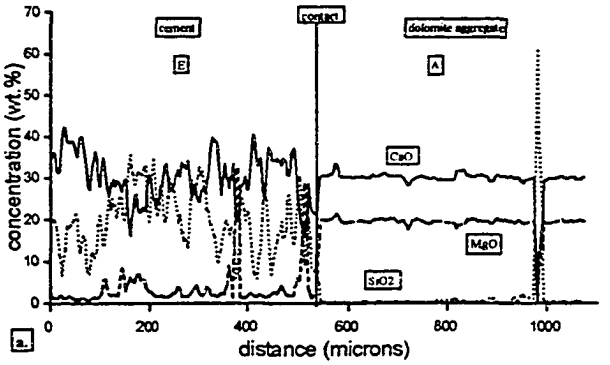
cement
contact
dolomite aggregate
E
A
CaO
MgO
SiO2
concentration (wt.%)
distance (microns)
a.

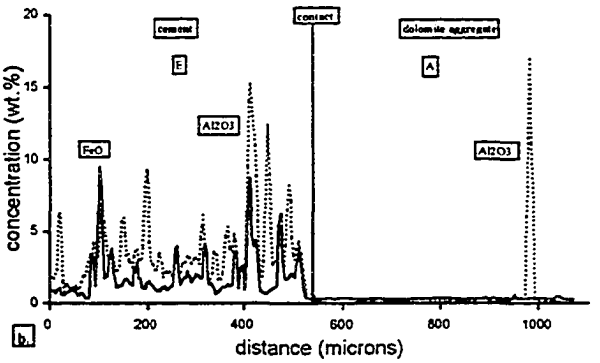
cement
contact
dolomite aggregate
E
A
FeO
Al2O3
Al2O3
concentration (wt.%)
distance (microns)
b.

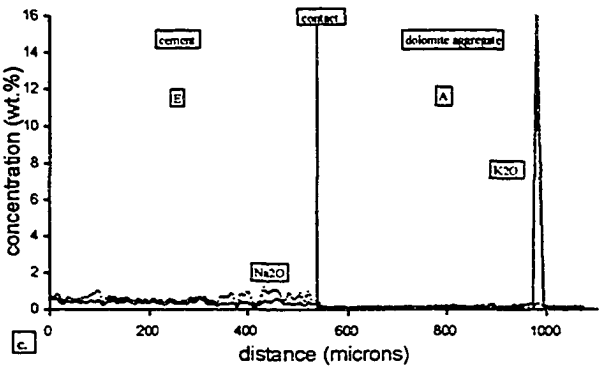
cement
contact
dolomite aggregate
E
A
K2O
Na2O
concentration (wt.%)
distance (microns)
c.

Figure B7. EDAX elemental maps of durable Sundheim quarry concrete. Both dolomite aggregate and cement paste are much more uniform in composition than the corresponding phases in non-durable concretes (such as Figures B2, B3 and B5). Small Si-rich dots in dolomite indicate quartz inclusions, and Mg-rich dots in paste may indicate brucite. Figure A6e shows corresponding SEM view, and Figures A6c-d show light micrographs of area of maps.

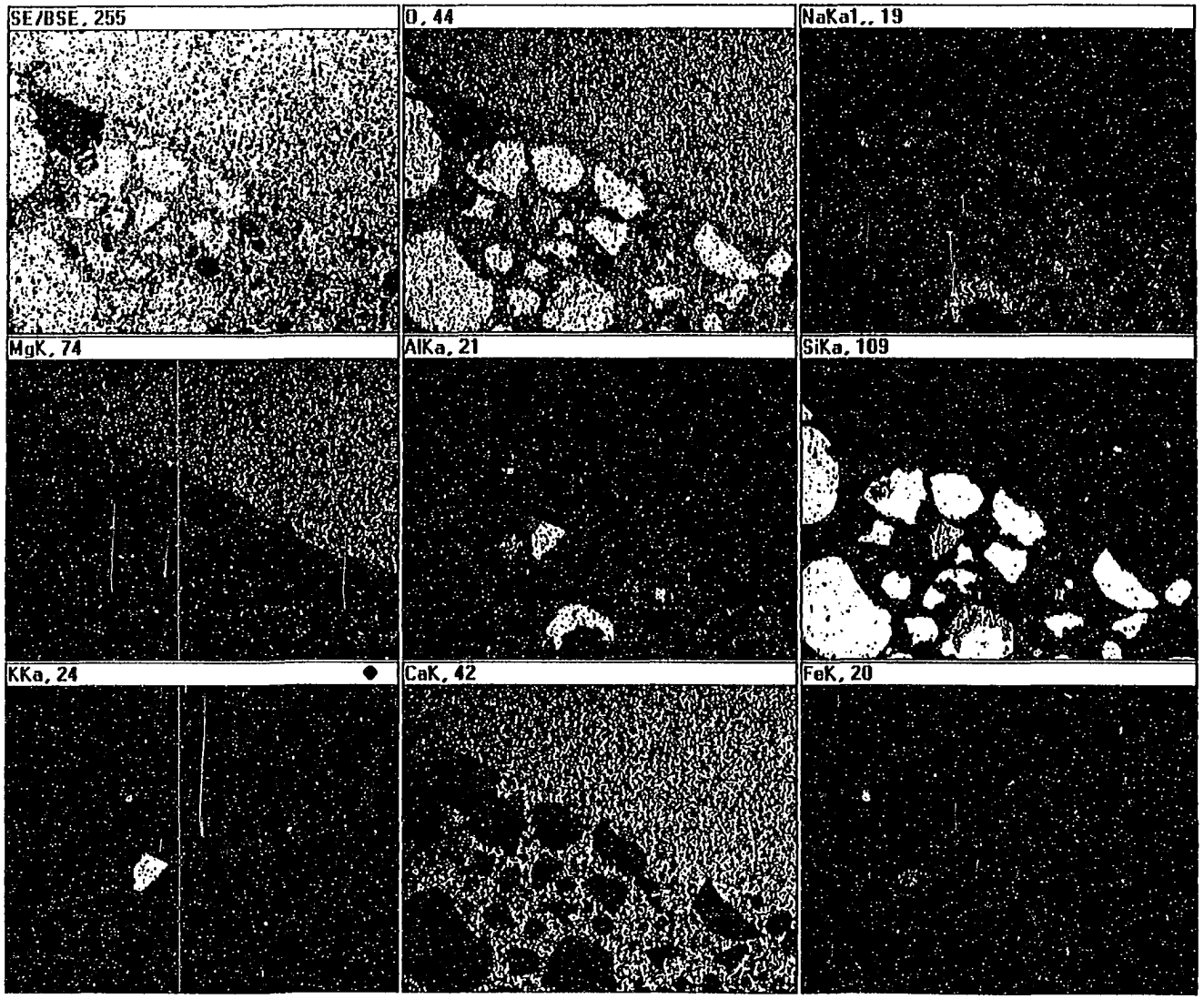
SE/BSE, 255
O, 44
NaKa1,, 19
MgK, 74
AlKa, 21
SiKa, 109
KKa, 24
CaK, 42
FeK, 20

Figure B8. Electron microprobe traverse through durable Sundheim quarry concrete.

a. CaO, MgO and SiO_2 traverse.
b. Al_2O_3 and FeO traverse.
c. K_2O and Na_2O traverse.

The dolomite aggregate interior has a very uniform composition, with a very thin light-colored dolomite rim, zone C. Zone C has an elevated CaO concentration and a reduced MgO concentration. Refer to Figures A7c-d for light micrographs.

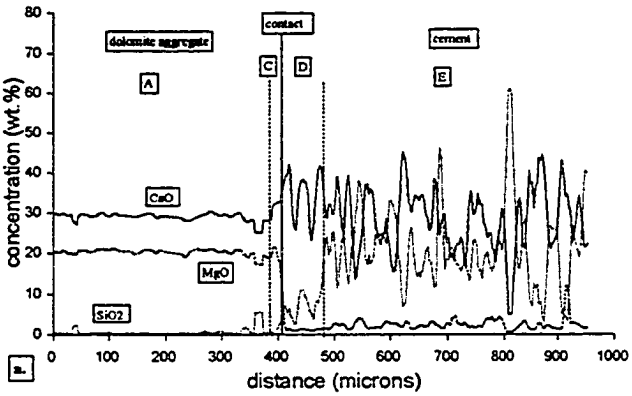
dolomite aggregate
contact
cement
A
C
D
E
CaO
MgO
SiO2
concentration (wt.%)
distance (microns)
0
10
20
30
40
50
60
70
80
0
100
200
300
400
500
600
700
800
900
1000

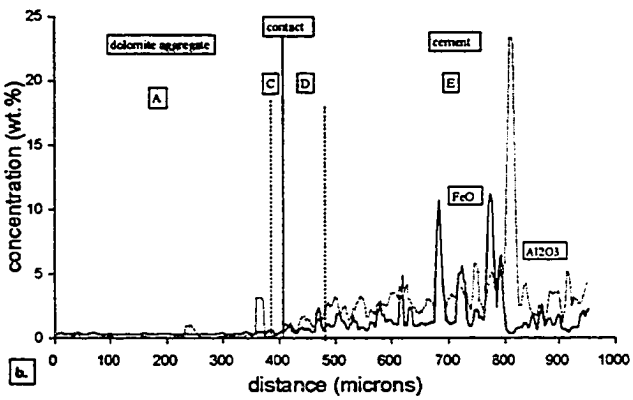
dolomite aggregate
contact
cement
A
C
D
E
FeO
Al2O3
concentration (wt.%)
distance (microns)
0
5
10
15
20
25
0
100
200
300
400
500
600
700
800
900
1000

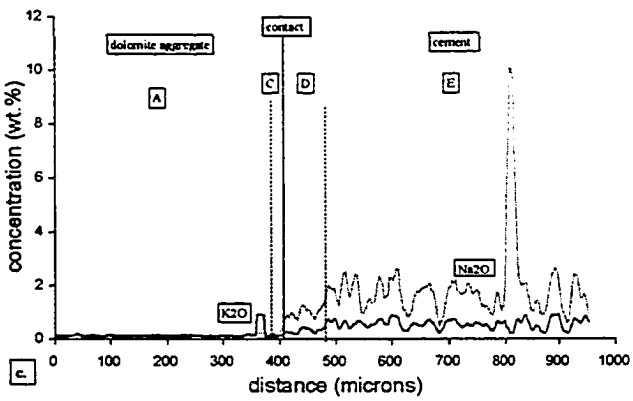
dolomite aggregate
contact
cement
A
C
D
E
Na2O
K2O
concentration (wt.%)
distance (microns)
0
2
4
6
8
10
12
0
100
200
300
400
500
600
700
800
900
1000

Figure B9. EDAX element maps for dolomite aggregate interior in durable Mar-Jo Hills quarry concrete. Note the euhedral illite inclusion, as shown by elevated Si, Al and K concentrations. Figure A7e shows corresponding SEM view.

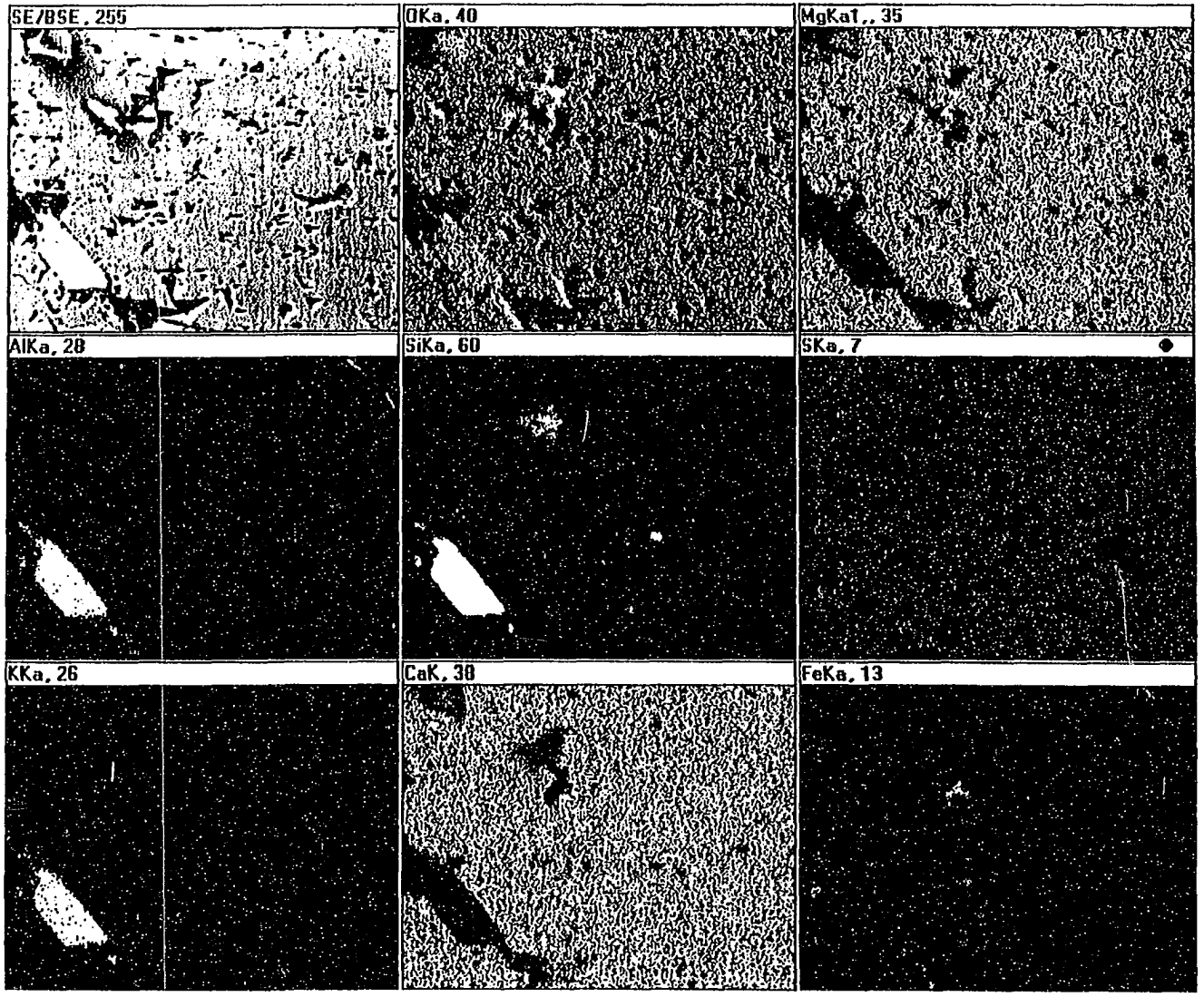
SE/BSE, 255
OKa, 40
MgKa1,, 35
AlKa, 28
SiKa, 60
SKa, 7
KKa, 26
CaK, 38
FeKa, 13

Figure B10. EDAX element maps for non-durable concrete containing Smith quarry aggregate. Note the anhedral illite inclusion in dolomite aggregate, as shown by localized Si, Al and K concentrations. The Mg- and O-rich dots in cement paste probably indicate brucite. Refer to Figure A7f for corresponding SEM view.

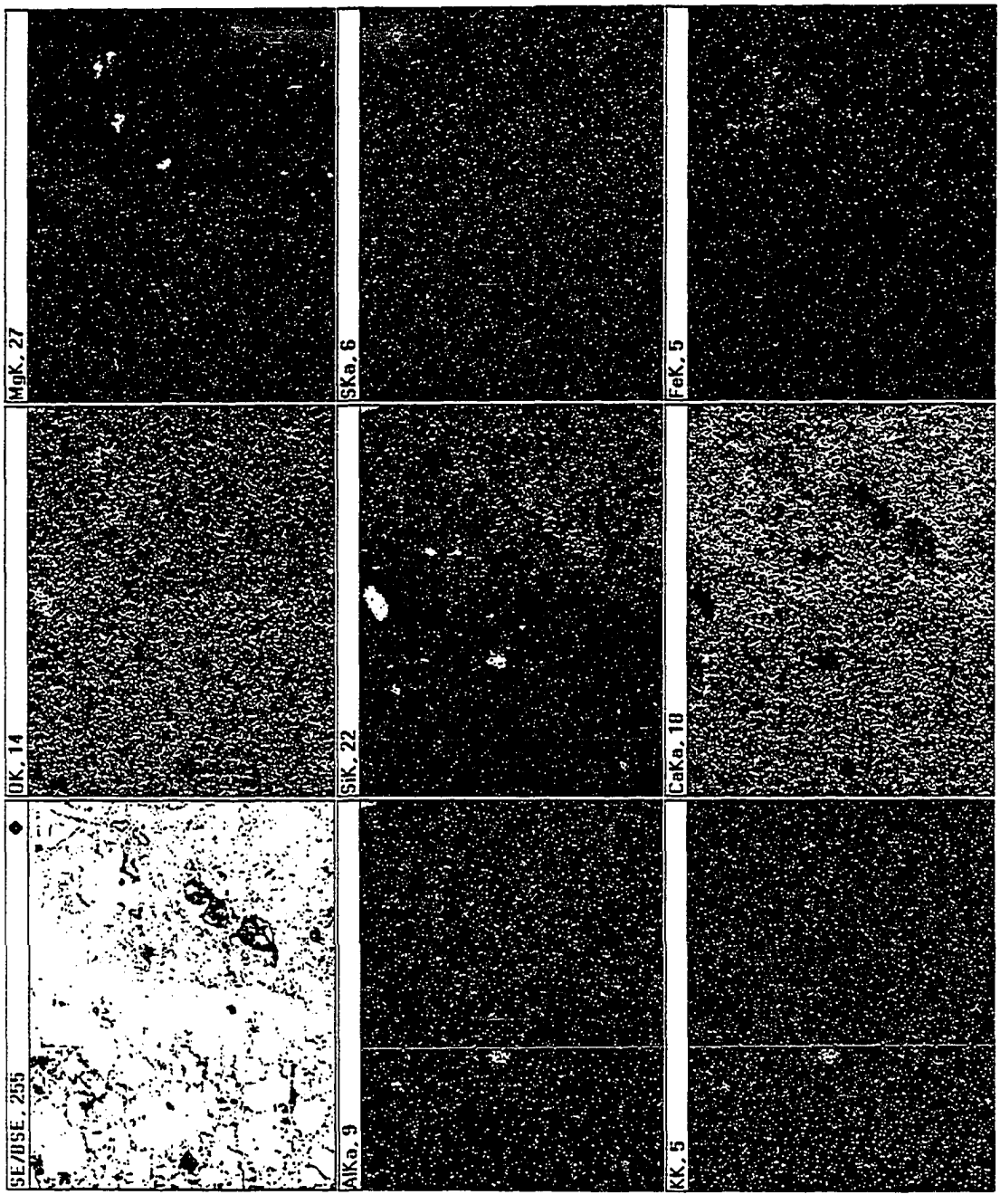
SE/DSE, 255
OK, 14
MgK, 27
AlKa, 9
SiK, 22
SKa, 6
KK, 5
CaKa, 18
FeK, 5

Figure B11. EDAX maps for non-durable Garrison quarry concrete after CaWD treatment. Cement paste shows severe cracking. Air-void-filling materials appear to show zonation: A very thin Ca-rich (calcite) film precipitated immediately adjacent to the void-wall, and Ca-, Cl-rich, and O-, Al-bearing phases (such as in void 2 and the upper portion of void 1) and Ca-, S-rich, and O-bearing phases (such as in the lower portion of void 1) precipitated on the calcite film. Crack-filling materials are Ca-rich (calcite ?) and sometimes, as indicated by arrows, Al-, and O-rich. Mg- and O-rich dots in cement paste probably indicate brucite. See Figure A10e for corresponding SEM photo.

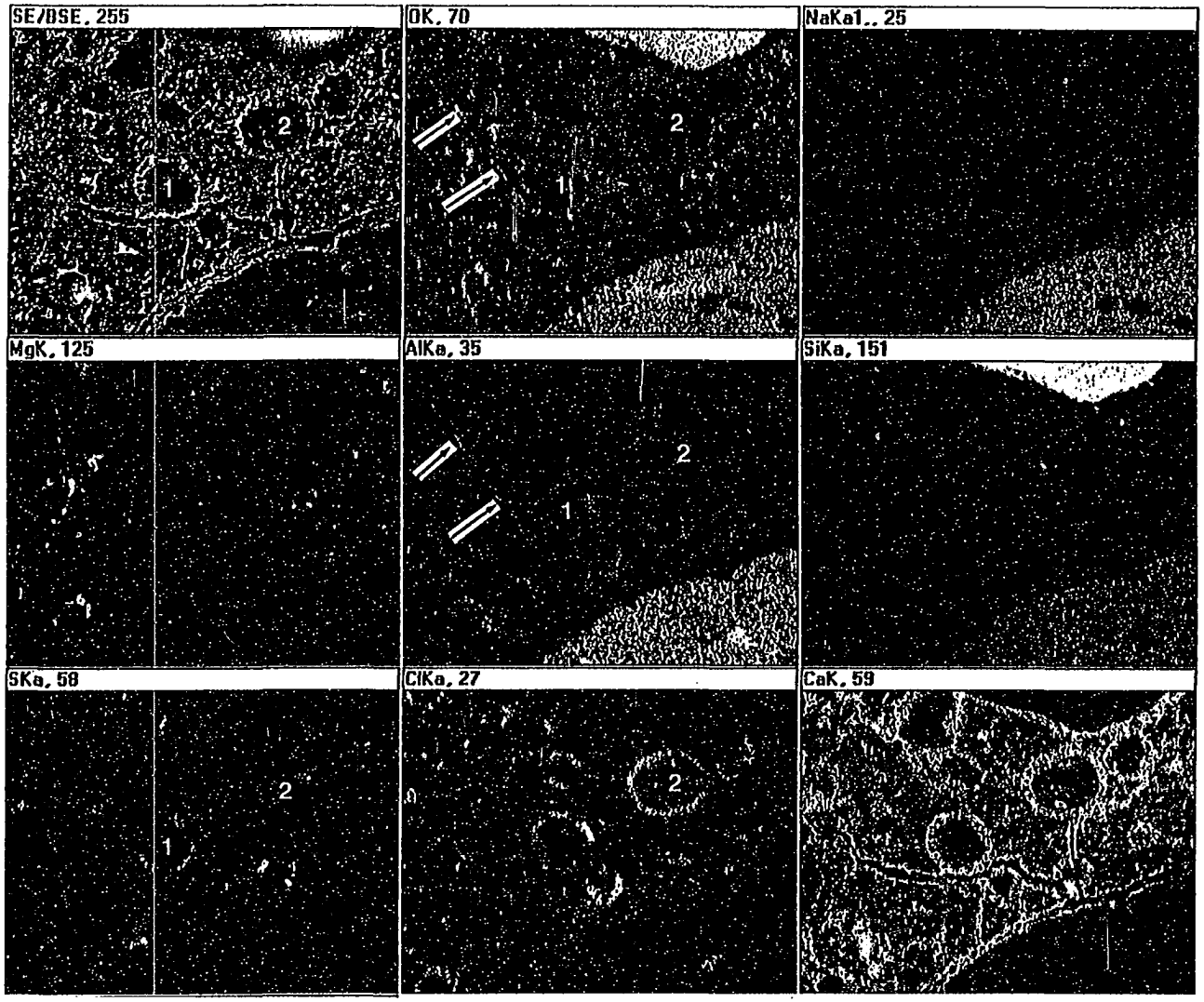
SE/BSE, 255
OK, 70
NaKa1., 25
MgK, 125
AlKa, 35
SiKa, 151
SKa, 58
ClKa, 27
CaK, 59
1
2

Figure B12. Electron microprobe traverse through non-durable Paralta quarry concrete after CaWD cycling.

a. CaO, MgO and SiO_2 traverse.
b. FeO and Al_2O_3 traverse.
c. K_2O and Na_2O traverse.

A slight but significant increase in MgO occurs in the light-colored dolomite rim, zone Ce, with a tiny decrease in CaO content. As expected, the $CaCl_2$-solution-treated cement paste shows a much higher CaO/SiO_2 ratio, compared to the untreated paste. The positive correlation between Al_2O_3, and between Na_2O and K_2O seem to have survived the experimental treatment. Refer to Figures A11a-b and Figure B13 for corresponding light micrographs and EDAX maps.

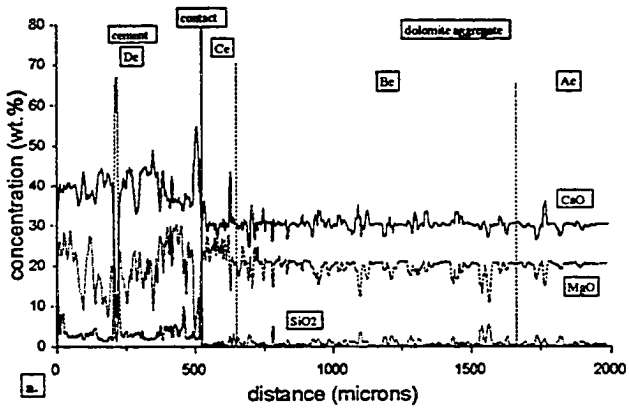
cement
contact
dolomite aggregate
De
Ce
Be
Ae
CaO
MgO
SiO2
concentration (wt.%)
distance (microns)
a.

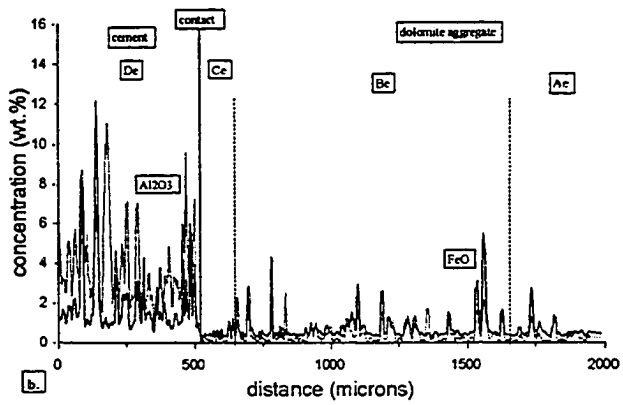
cement
contact
dolomite aggregate
De
Ce
Be
Ae
Al2O3
FeO
concentration (wt.%)
distance (microns)
b.

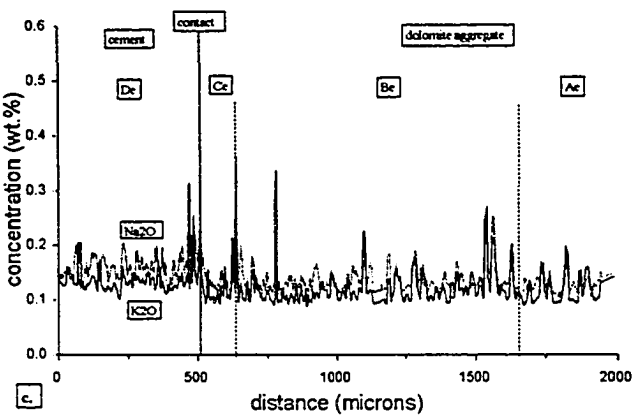
cement
contact
dolomite aggregate
De
Ce
Be
Ae
Na2O
K2O
concentration (wt.%)
distance (microns)
c.

Figure B13. EDAX maps for dolomite and paste rims in Paralta quarry concrete after CaWD treatment. Compared to zone Be, zone Ce contains much more abundant interstitial brucite and, possibly, calcite. Zone De contains abundant Ca-rich minerals and some Ca-, Al- and O-rich minerals. See the central part of Figure A11d for corresponding SEM view.

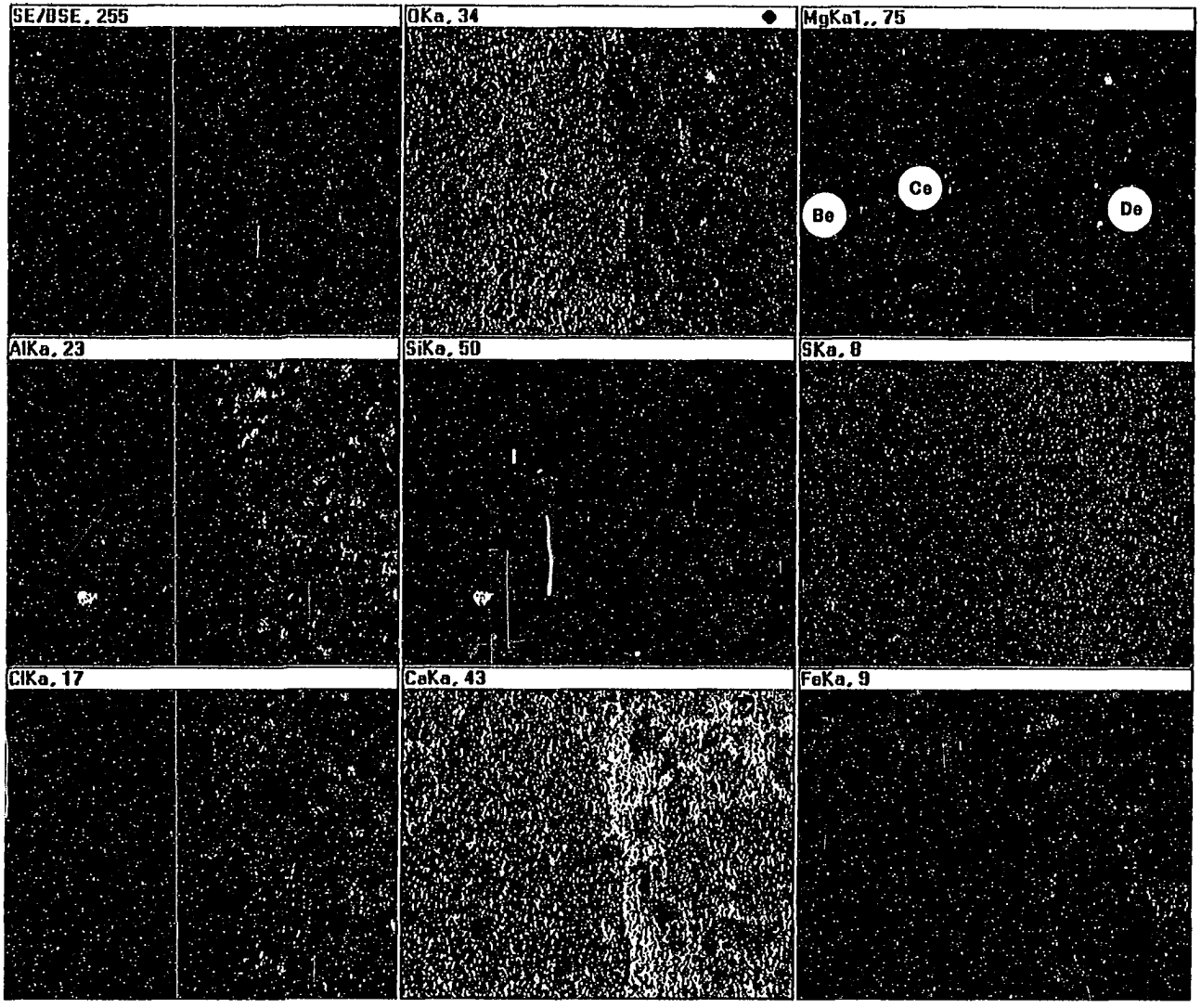
SE/BSE, 255
OKa, 34
MgKa1,, 75
Be
Ce
De
AlKa, 23
SiKa, 50
SKa, 8
ClKa, 17
CaKa, 43
FeKa, 9

Figure B14. Electron microprobe traverse through non-durable Paralta quarry concrete after freeze/thaw treatment in $CaCl_2$ solution.

a. CaO, MgO and SiO_2 traverse.
b. FeO and Al_2O_3 traverse.
c. K_2O and Na_2O traverse.

This traverse passed entirely through a small coarse aggregate particle and into paste on both sides. Compared to zone Ae, the aggregate interior, zone Be shows a slight increase in MgO and a decrease in CaO. More pronounced increase in MgO and decrease in CaO occur in zone Ce. Zone De is Ca-rich and Si- and Mg-poor. Refer to Figure A11e for corresponding light micrograph.

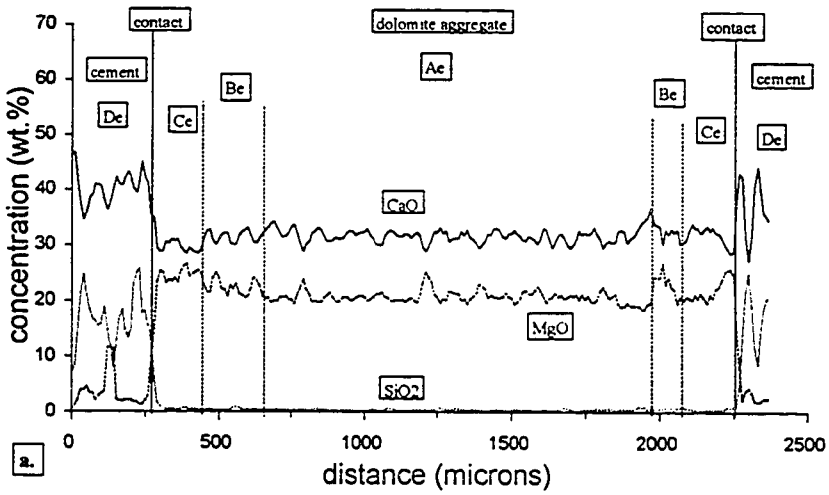
contact
dolomite aggregate
contact
cement
Ae
cement
Be
Be
De
Ce
Ce
De
CaO
MgO
SiO2
concentration (wt.%)
70
60
50
40
30
20
10
0
0
500
1000
1500
2000
2500
distance (microns)
a.

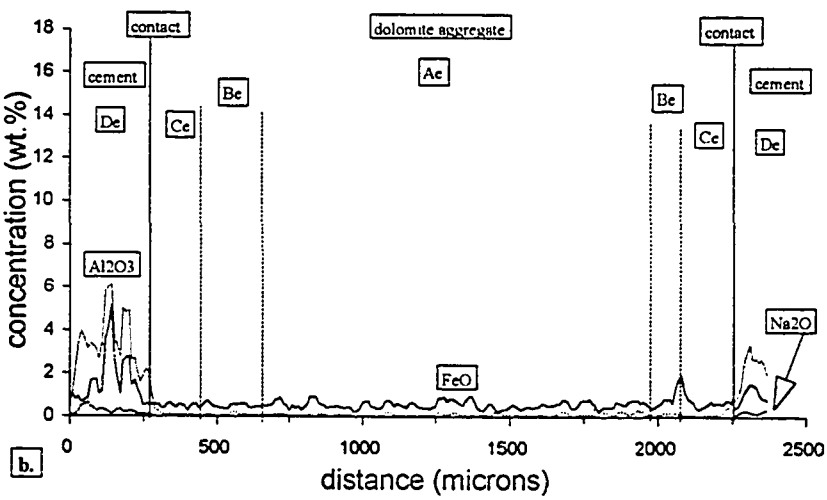
contact
dolomite aggregate
contact
cement
Ae
cement
Be
Be
De
Ce
Ce
De
Al2O3
Na2O
FeO
concentration (wt.%)
18
16
14
12
10
8
6
4
2
0
0
500
1000
1500
2000
2500
distance (microns)
b.

Figure B15. Electron microprobe traverse through non-durable Smith quarry concrete after wet/dry treatment in $CaCl_2$ solution.

a. CaO, MgO and SiO_2 traverse.
b. FeO and Al_2O_3 traverse.
c. K_2O and Na_2O traverse.

Unlike Figure B14, this traverse does not show increase in MgO and decrease in CaO in dolomite reaction rims. Zone De is Ca-rich and Si-poor. Figure A11f shows the light micrograph of this area.

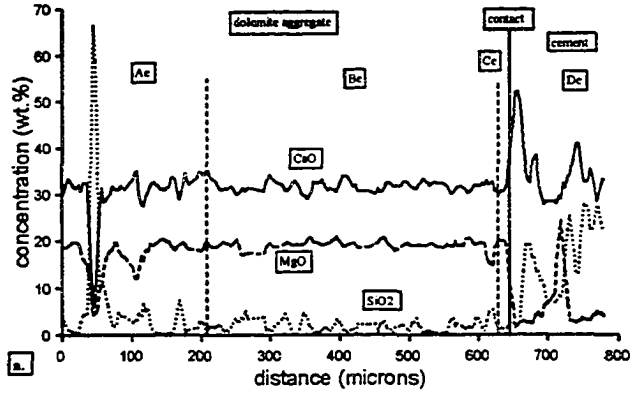
dolomite aggregate
contact
cement
Ae
Be
Ce
De
CaO
MgO
SiO2
concentration (wt.%)
distance (microns)
a.

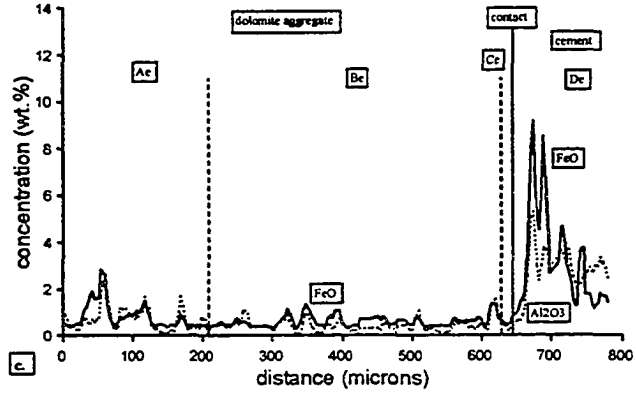
dolomite aggregate
contact
cement
Ae
Be
Ce
De
FeO
FeO
Al2O3
concentration (wt.%)
distance (microns)
c.

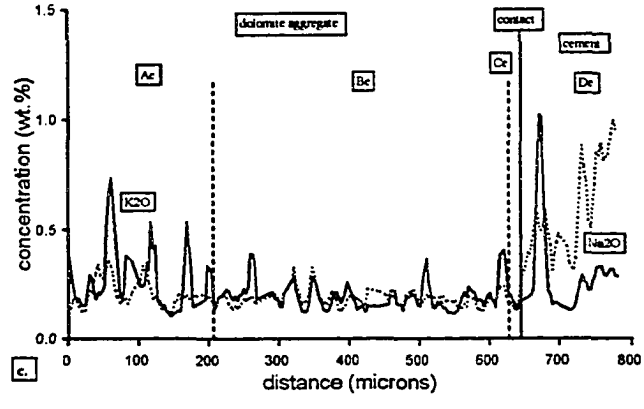
dolomite aggregate
contact
cement
Ae
Be
Ce
De
K2O
Na2O
concentration (wt.%)
distance (microns)
e.

Figure B16. Electron microprobe traverse through durable Mar-Jo Hills quarry concrete after wet/dry treatment in $CaCl_2$ solution.

a. CaO, MgO and SiO_2 traverse.
b. FeO and Al_2O_3 traverse.
c. K_2O and Na_2O traverse.

There is no rim development visible in dolomite aggregate or cement paste. The aggregate shows an uniform compositional pattern. The experimentally treated dark paste exhibits a much higher CaO/SiO_2 ratio than the untreated dark cement paste (c.f. Figure B6). See Figures A12a-b for light micrographs of this area.

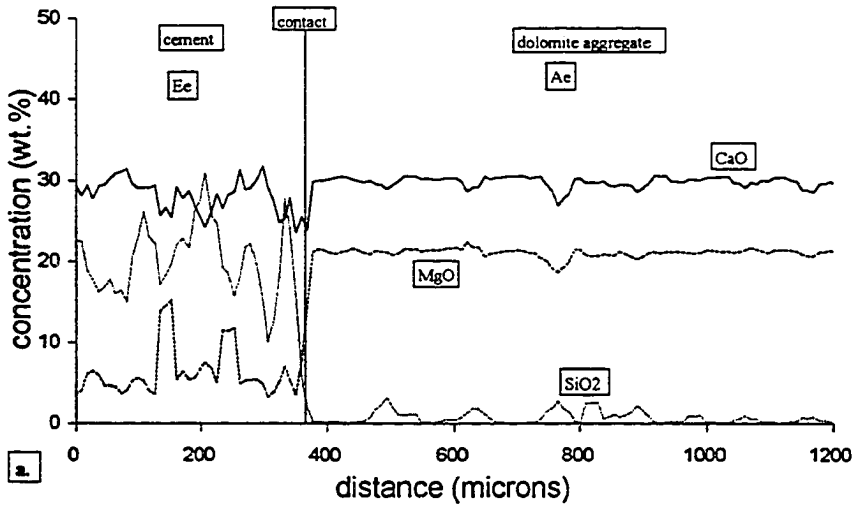
50
40
30
20
10
0
concentration (wt.%)
cement
Ee
contact
dolomite aggregate
Ae
CaO
MgO
SiO2
0
200
400
600
800
1000
1200
distance (microns)
a.

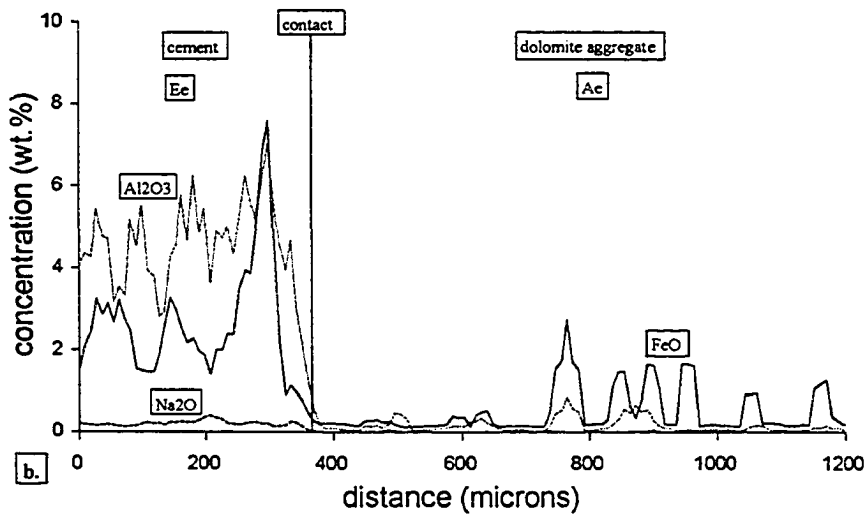
10
8
6
4
2
0
concentration (wt.%)
cement
Ee
contact
dolomite aggregate
Ae
Al2O3
Na2O
FeO
0
200
400
600
800
1000
1200
distance (microns)
b.

Figure B17. Electron microprobe traverse through durable Mar-Jo Hills quarry concrete after freeze/thaw treatment in $CaCl_2$ solution.

a. CaO, MgO and SiO_2 traverse.
b. FeO and Al_2O_3 traverse.
c. K_2O and Na_2O traverse.

This traverse shows very similar characteristics to Figure B16 -- no rim development visible in dolomite aggregate or cement paste, an uniform compositional pattern, and a much higher CaO/SiO_2 ratio in treated paste than the untreated dark cement paste (c.f. Figure B6). Refer to Figures A12c-d for light micrographs of this area.

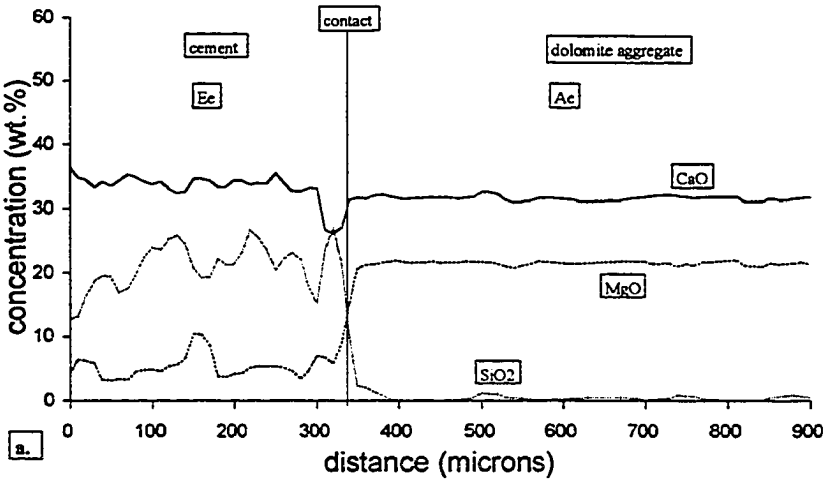
contact
cement
dolomite aggregate
Ee
Ac
CaO
MgO
SiO2
concentration (wt.%)
distance (microns)
a.

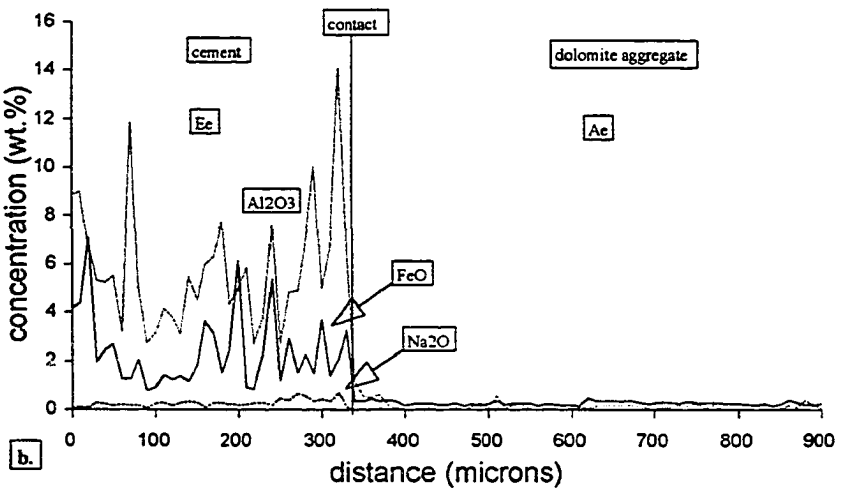
contact
cement
dolomite aggregate
Ee
Ae
Al2O3
FeO
Na2O
concentration (wt.%)
distance (microns)
b.

Figure B18. Electron microprobe traverse in Mar-Jo Hills quarry concrete after wet/dry treatment in $MgCl_2$ solution.

a. CaO, MgO and SiO_2 traverse.
b. FeO and Al_2O_3 traverse.
c. K_2O and Na_2O traverse.

The dolomite aggregate is relatively uniform in composition across the traverse except for the sharp CaO enrichment at the edge of aggregate particle. The oxide concentrations are close to zero at places where cement phases were decomposed. The strong positive correlation between Al_2O_3 and FeO survived the experimental treatment. Unlike the untreated cement paste, the treated paste shows elevated MgO concentration and reduced CaO content, and strong positive correlation between SiO_2 and MgO. Figures A12e-f show light micrographs of this area.

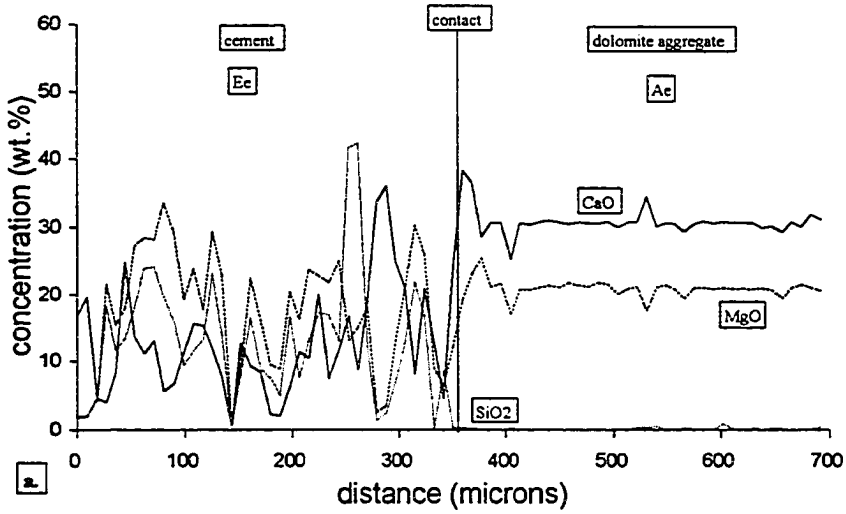
cement
Ec
contact
dolomite aggregate
Ae
CaO
MgO
SiO2
concentration (wt.%)
distance (microns)
a.

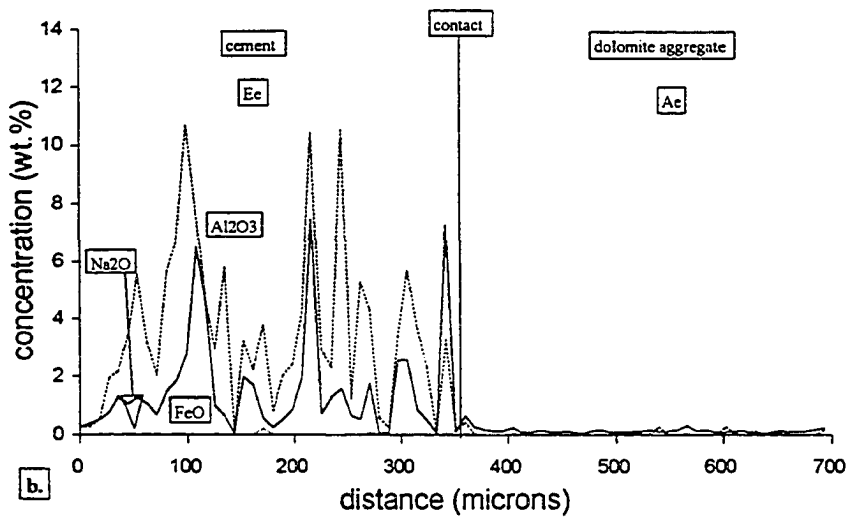
cement
Ec
contact
dolomite aggregate
Ae
Al2O3
Na2O
FeO
concentration (wt.%)
distance (microns)
b.

Figure B19. EDAX elemental maps showing experimental deterioration of Mar-Jo Hills quarry concrete after MgWD treatment. The crack-filling materials in dolomite aggregate are Ca-, O-rich (white, calcite), Mg-, Cl-rich (dark grey, Mg chloride or Mg chloride hydrate), and Mg-, O-rich (grey, brucite). The treated paste contains abundant Mg-, O-rich (grey, brucite) and Ca-, O-rich (white, calcite) phases. Crack- and void-filling materials in paste shows obvious zonation: Void walls are covered by a very thin layer of Ca-, O-rich white material (calcite); away from the Ca-rich film, there is a layer of materials consisting of grey Mg-, O-rich (brucite), dark-grey Mg-, Cl-rich or Mg-, O-, Cl-rich, and white Al-rich (gibbsite) phases; The very-fine-grained loose materials in the middle of cracks and voids contain Mg, Si, Cl, Fe, S, and show very complicated mineralogy. Refer to Figure A13a for corresponding SEM micrograph.

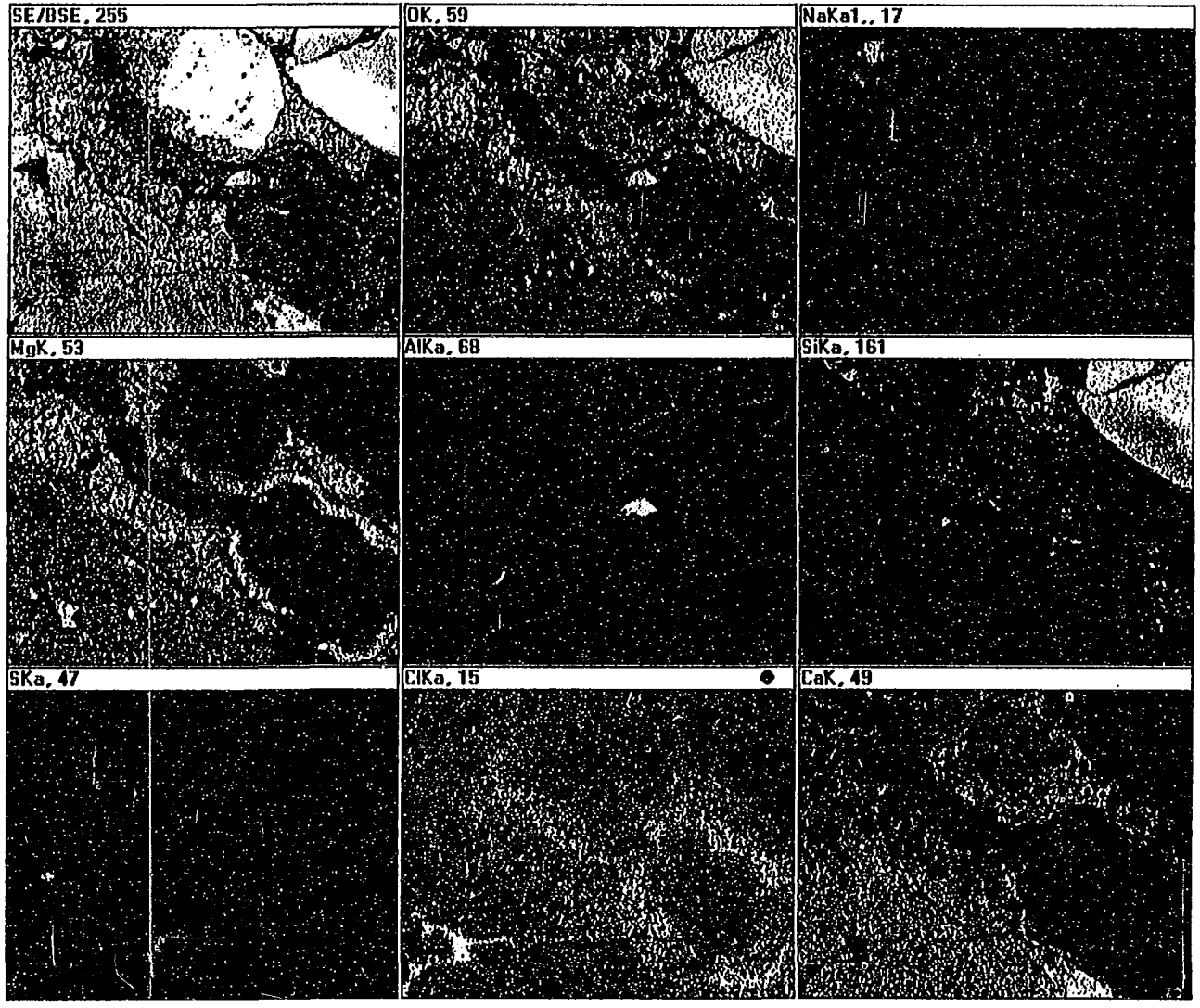
SE/BSE, 255
OK, 59
NaKa1,, 17
MgK, 53
AlKa, 68
SiKa, 161
SKa, 47
ClKa, 15
CaK, 49

Figure B20. EDAX elemental maps showing the central portion of Figure B19. These maps more clearly show the zonation of crack- and void-filling materials in cement paste. See Figure A13b for corresponding SEM micrograph.

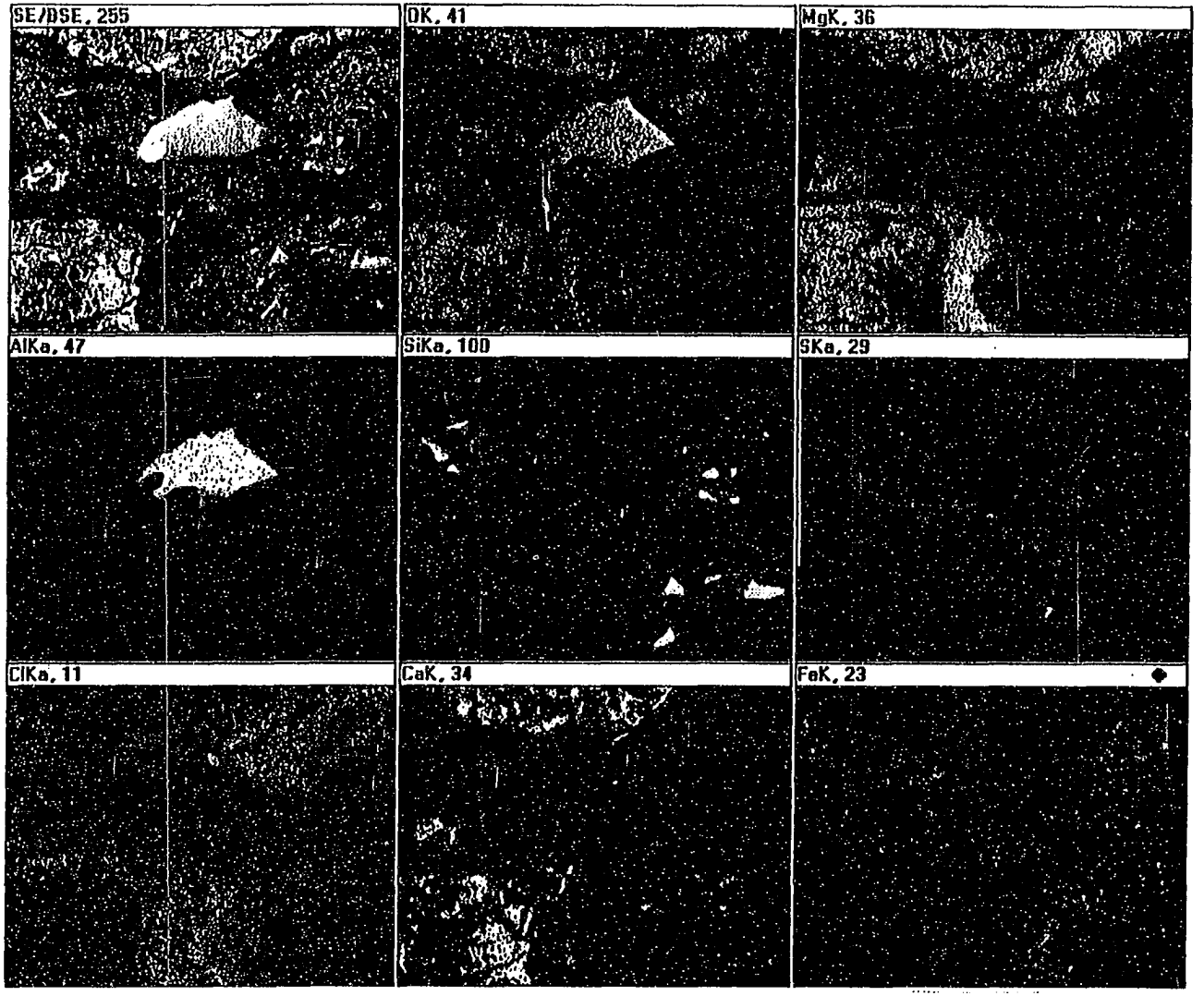
SE/BSE, 255
OK, 41
MgK, 36
AlKa, 47
SiKa, 100
SKa, 29
ClKa, 11
CaK, 34
FeK, 23

Figure B21. Electron microprobe traverse in Paralta quarry concrete after wet/dry treatment in $MgCl_2$ solution.

a. CaO, MgO and SiO_2 traverse.
b. FeO and Al_2O_3 traverse.
c. K_2O and Na_2O traverse.

Dolomite aggregate shows a relatively uniform composition across the traverse, except for a slight magnesium depletion in light-colored dolomite rim, zone Ce. There is little, if any, corresponding increase in calcium in this rim. As a result of the MgWD treatment, the paste shows a magnesium increase and a positive correlation between MgO and SiO_2 (cf. Figure B1). Like the untreated paste, the treated cement paste shows positive correlation between Al_2O_3 and FeO. Refer to Figures A14a-b for light micrograph of this area.

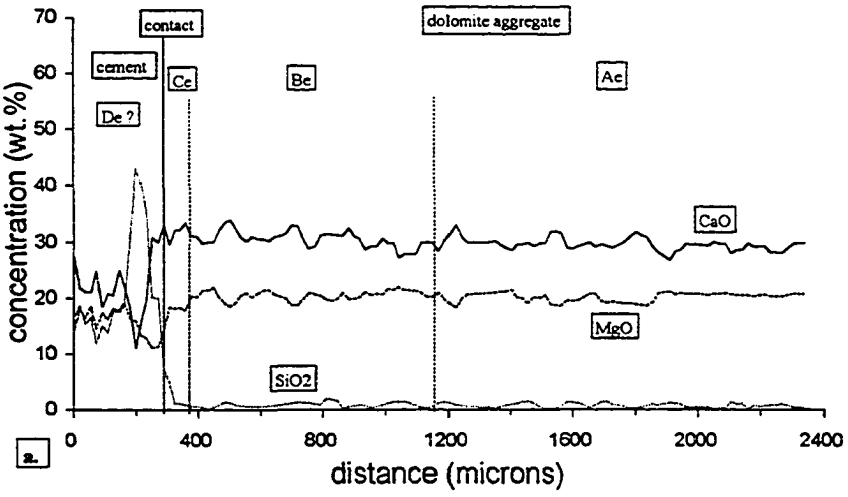
contact
dolomite aggregate
cement
Ce
Be
Ac
De ?
CaO
MgO
SiO2
concentration (wt.%)
distance (microns)
a.

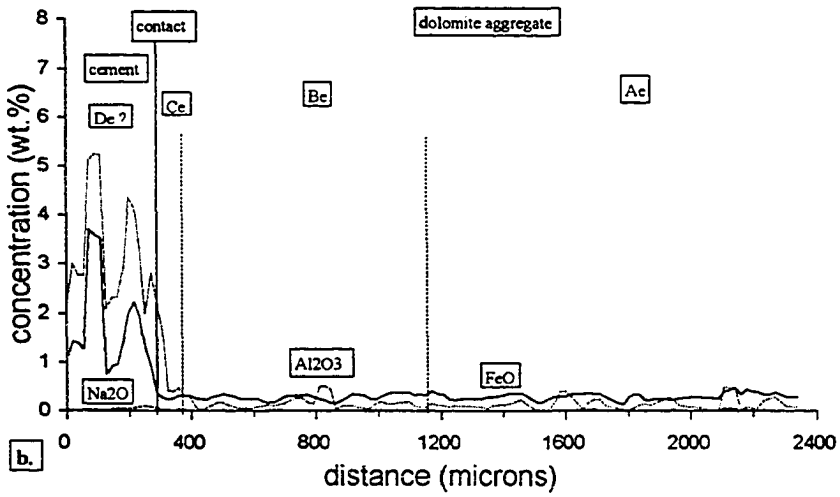
contact
dolomite aggregate
cement
Ce
Be
Ac
De ?
Al2O3
FeO
Na2O
concentration (wt.%)
distance (microns)
b.

Figure B22. EDAX elemental maps showing experimental deterioration of Garrison quarry concrete after MgWD treatment. Interstitial voids in dolomite aggregate are filled with grey Mg-, O-rich (brucite), white Ca-, O-rich (calcite) and dark grey Mg-, Cl-rich (Mg chloride or Mg chloride hydrate) phases. Voids and cracks in the severely deteriorated dark cement paste are filled with brucite, Mg chloride or Mg chloride hydrate, and possibly calcite. The less deteriorated paste rim is Ca-rich and contains some Cl. Figures A13c-d show light micrographs and A13e shows the corresponding SEM view.

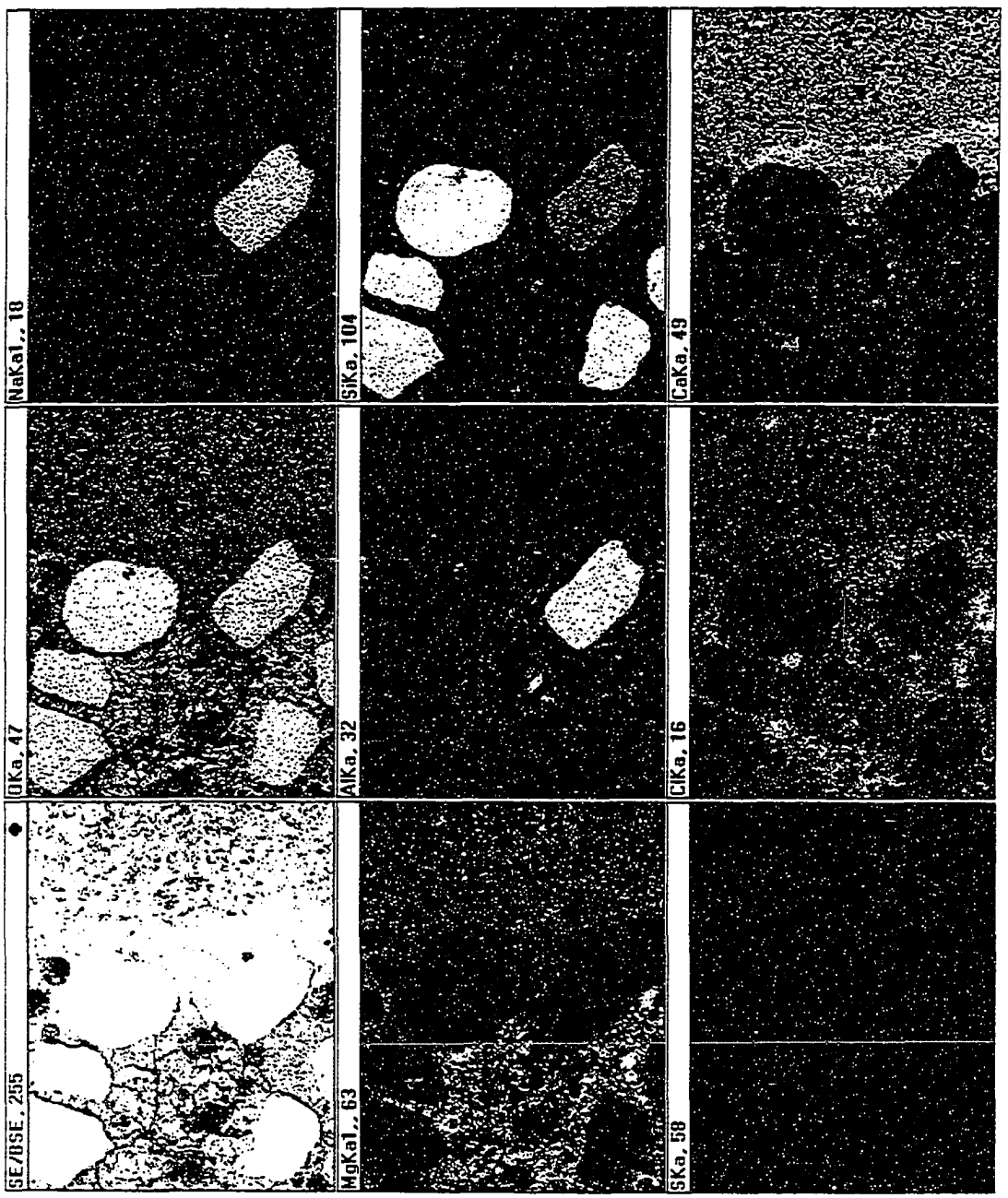
SE/BSE, 255
OKa, 47
NaKa1, 18
MgKa1, 63
AlKa, 32
SiKa, 104
SKa, 58
ClKa, 16
CaKa, 49

Figure B23. Electron microprobe traverse in Paralta quarry concrete after NaWD treatment.
a. CaO, MgO and SiO_2 traverse.
b. FeO and Al_2O_3 traverse.
c. K_2O and Na_2O traverse.

Dolomite aggregate has a relatively constant composition across the traverse except at the extreme outer edge of the dark dolomite rim, zone Be, where CaO increases at the expense of MgO. This rim-composition change probably was inherited from the untreated concrete. Like the light paste rim in untreated concrete (zone D), zone De is enriched in Ca and relatively poor in Si. The paste seems to show positive correlation between Al_2O_3 and FeO. as expected, Na_2O is enriched in the paste as a result of NaCl-solution treatment. Figures A14c-d give the light micrographs.

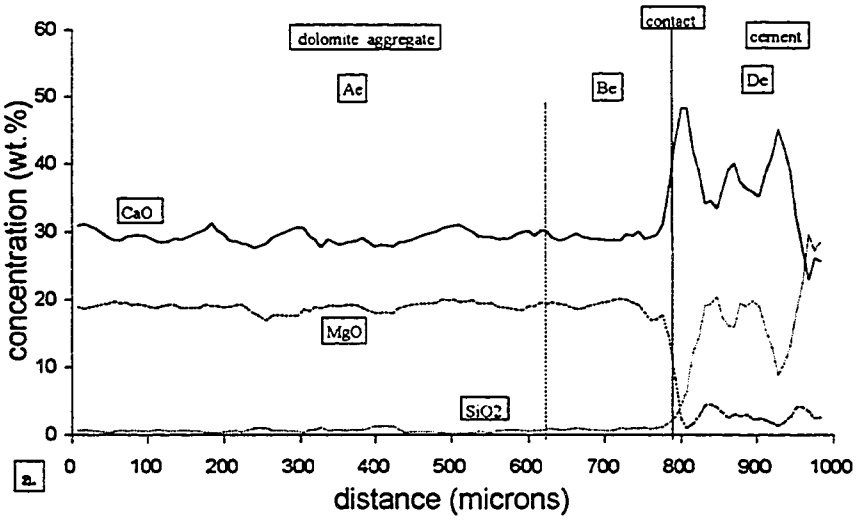
dolomite aggregate
contact
cement
Ae
Be
De
CaO
MgO
SiO2
concentration (wt.%)
distance (microns)
a.

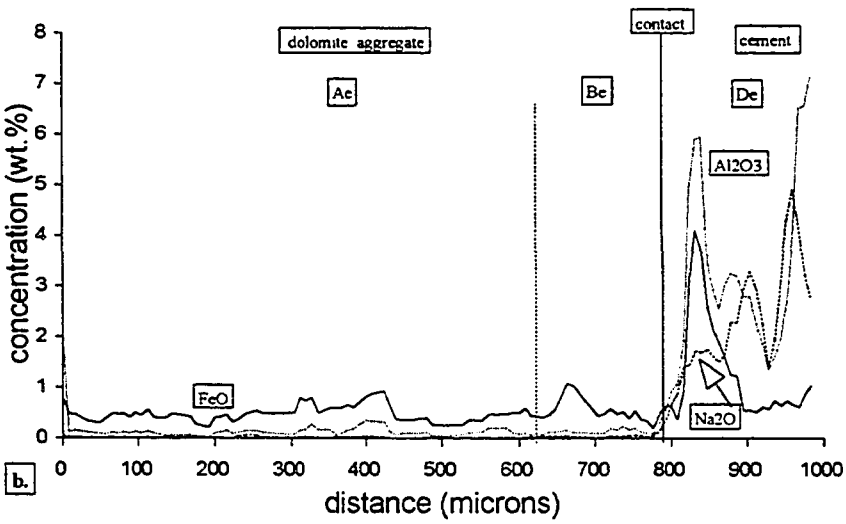
dolomite aggregate
contact
cement
Ae
Be
De
Al2O3
FeO
Na2O
concentration (wt.%)
distance (microns)
b.

Figure B24. EDAX elemental maps showing the interface in Paralta quarry concrete after NaWD treatment. Interstitial voids in dolomite aggregate are filled with Mg-, O-rich (brucite) and Ca-, O-rich (calcite) phases. The light-colored paste rim is strongly enriched in Ca. The experimentally treated cement paste contains brucite and some Cl (chloride). Figure A14f gives corresponding SEM view.

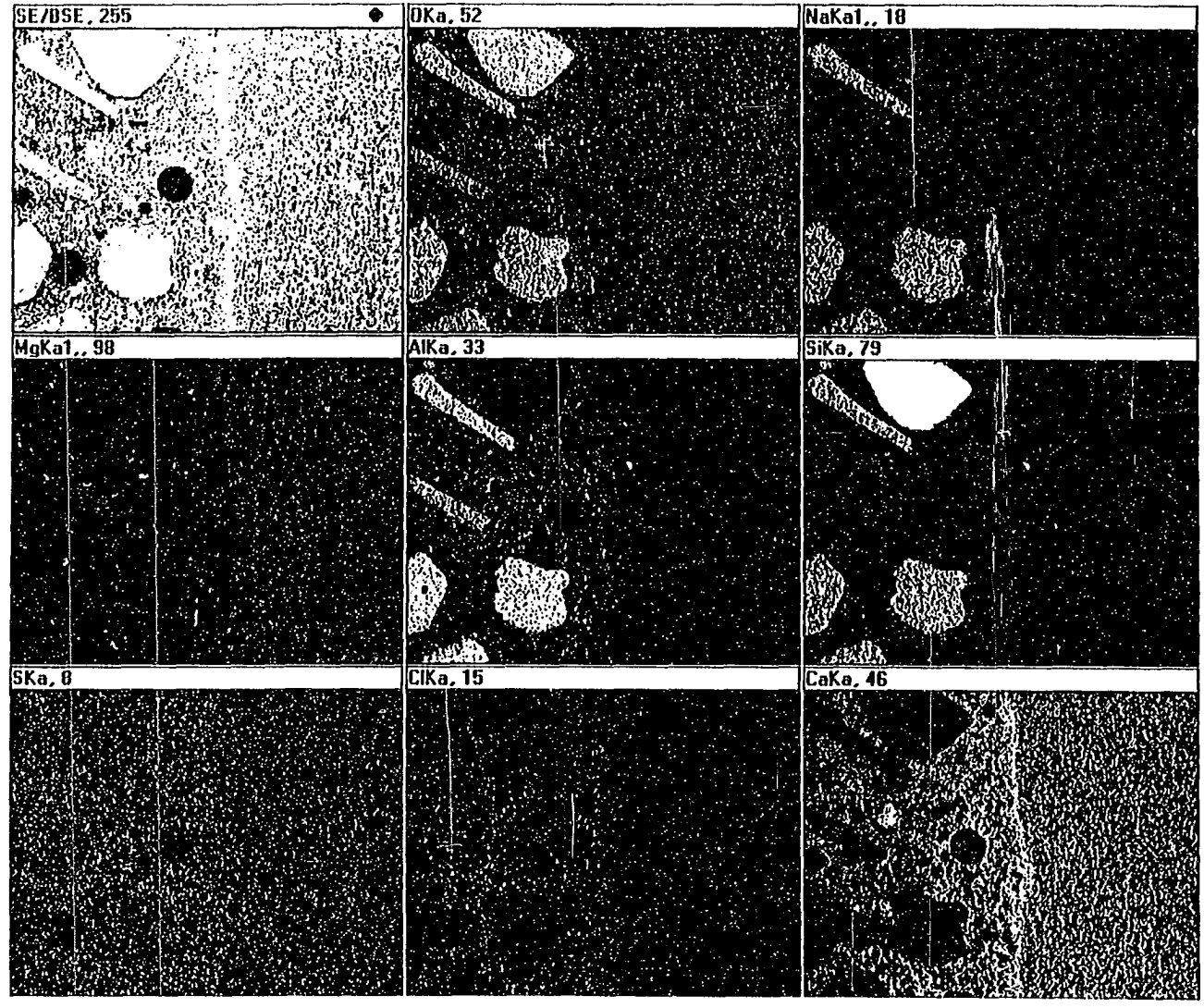
SE/BSE, 255
OKa, 52
NaKa1,, 18
MgKa1,, 98
AlKa, 33
SiKa, 79
SKa, 8
ClKa, 15
CaKa, 46